UNIVERSITY OF LATVIA
FACULTY OF PHYSICS AND MATHEMATICS

Jānis Cīmurs

Single-domain and superparamagnetic particle dynamics in time dependent magnetic fields

Doctoral Thesis

Submitted for the degree of Doctor of Physics
Subfield: Fluid and gas mechanics

Supervisor:
Prof. *Dr. habil. phys.* Andrejs Cēbers

Riga, 2015

Abstract

The work discusses single-domain ferromagnetic particles with uniaxial anisotropy in time dependent magnetic fields (rotating, precessing and crossed AC/DC). Particle motion regimes and their stability in dependence on the magnetic field strength and frequency are analytically obtained. The analytic expressions is experimentally verified. Thermal dissipation generated by viscous drag and magnetic moment jumps inside particle is calculated. It is shown how superparamagnetic rods can be used as a tool for microrheology. In addition, colloidal particle thermal relaxation in external magnetic field in viscoelastic fluid is simulated numerically, leading to nuclear magnetic resonance relaxation times in viscoelastic fluid.

Keywords: Single-domain particle, Magnetic anisotropy, Viscoelasticity, Microrheology, Thermal relaxation

Anotācija

Darbā tiek aplūkotas viendomēna feromagnētiskas daļiņas ar vienas ass anizotropiju mainīgā magnētiskajā laukā (rotējošā, precesējošā un krustotos AC/DC). Analītiski tiek iegūti daļiņas kustības režīmu un to stabilitātes atkarība no magnētiskā lauka stipruma un frekvences. Iegūtās analītiskās izteiksmes tiek eksperimentāli verificētas. Tiek aprēķināta termiskā disipācija, ko rada viskozā berze un magnētiskā momenta lēcieni daļiņas iekšienē. Tiek demonstrēts, kā superparamagnētisks stienītis var tikt izmatots mikroreoloģiskajos pētījumos. Papildus tam skaitliski tiek aplūkota koloidālu daļiņu termiskā relaksācija ārējā magnētiskajā laukā viskoelastīgā šķidrumā, kas dod iespēju iegūt kodolmagnētiskās rezonanses relaksācijas laikus viskoelastīgā šķidrumā.

Atslēgas vārdi: Viendomēna daļiņa, Magnētiskā anizotropija, Viskoelastība, Mikroreoloģija, Termiskā relaksācija

Contents

Chapter 1

Introduction

1.1 CGS and SI system of units

Historically *cgs-emu* (centimeter-gram-second electromagnetic units) system is used in theory of magnetism. Whereas SI (International System) or *mks* (meter-kilogram-second) is currently taught in all physics courses and is standard for scientific work throughout the world. It has not, however, been enthusiastically accepted by workers of magnetism. "Although both systems describe the same physical reality, they start from somewhat different ways of visualizing that reality" [32]. Brown, who spent long time developing magnetism theory, says that we should "bear in mind two principles: first, dimensions are the invention of man , and man is at liberty to assign them in any way he pleases, as long as he is consistent throughout any on interrelated set of calculations. Second, international committees arrive at their decisions by the same irrational procedures as do various IEEE committees that you have served on." [19].

The only "natural" system of units is the system, where speed of light $c = 1$ and Planck constant $\hbar = 1$ [74], but this system gives inappropriate (large or small) numbers for everyday use. In order not to mess with powers of ten, the SI system of units is used widely in physics. But "the designers of SI system left open the possibility of expressing some magnetic quantities in more than one way, which has not helping in speeding its adoption" [32]. Sivukhin [77] says that two units of magnetic (or electric) field: $\vec{H}$ and $\vec{B}$, is unnecessary and makes it harder to understand essence of the physical phenomena.

The SI system has a clear advantage to *cgs* when both electrical and magnetic behavior must be considered together, where *cgs* units gets messy. But in this work only magnetic behavior is examined and historically preferred *cgs-emu* system of units will be used through the work.

1.2 Single-domain grain

This work deals with a single-domain ferromagnetic grain, which can behave as rigid magnetic dipole or superparamagnetic particle or something in between. Difference between rigid magnetic dipole and superparamagnetic particle will be explained in sections 1.4 and 1.5. In this section the size of particle to be single-domain is discussed.

Differences in behaviour for magnetic particles of different sizes is explained by domain structure [17]: "whereas a ferromagnetic material in bulk (in zero applied field) possesses a domain structure so, that the specimen as whole has a magnetic moment considerably smaller than the saturation value, the same material in the form of a sufficiently fine particle is uniformly magnetized to (very near) the saturation value, or in other words consists of a single domain". Experimentally it is tested by Kittel et al.[50].

Brown [17] found lower bound (radius) for spherical particles to be in single domain phase:

$$R_{c_0} = \frac{1.017\sqrt{C}}{M_s}, \tag{1.1}$$

and two upper bounds (radii):

$$R_{c_1} = \frac{\frac{1.278\sqrt{C}}{M_s}}{\sqrt{1 - 0.4468\frac{|K_1|}{M_s^2}}} \tag{1.2}$$

$$R_{c_2} = \frac{3.1584\pi\sqrt{C(|K_1| + 19.739M_s^2}}{M_s^2} \tag{1.3}$$

where M_s is saturation magnetization, K_1 is first-order magnetocrystalline anisotropy constant and C is the exchange constant. The exchange constant is effect of electron spin interaction and describes the effect of aligning of individual spins in magnetic material. More about exchange interaction can be found in [40].

The lower bound is the radius of the particle below which the lowest energy for the magnetic moment in the particle is in the single-domain state. The upper bound is the radius of the particle above which the lowest energy of magnetic state is multi-domain. Two types of multi-domain configuration has been used by Brown, so he got two different upper bounds. As upper bound we use the lowest of two $\min(R_{c_1}, R_{c_2})$. The border between multi-domain and single-domain state should lie somewhere between lower and upper bounds.

It should be noted that the existence of a low-energy state does not guaranty that the state can be reached. Because of the hysteresis involved,

a real ferromagnet may sometimes be stuck in a high-energy state, without being able to switch into the low-energy one.

For example in the case of Fe particle the critical radius is between 8.46 and 11.0 nm [6]. Brown for the same material calculated lower bound at 16.7 nm [17]. The difference is because exchange constant C is not accurately known for any ferromagnet. Whereas pure nickel lower bound is 38.3 nm [17] and critical radius for Ni-Co alloy is between 20 and 25 nm [6]. It should be mentioned that these values is applicable only for spherical particles.

As stated by Aharoni [6] "the situation is different for two cases, for which the upper and the lower bounds are very far from each other, making them useless for estimating the actual critical size. One is hard ferromagnetic material, and the other is a collection of many adjacent, interacting particles of a soft material." Then he slightly modifies upper bound R_{c_1} (1.2), in order to reduce interval between lower and upper bound [6]. Generalization of the Brown's theory for ellipsoidal particle can be found in [34].

The largest single-domain particles can be found in magnetotactic bacteria. Each bacterium contains chain of single-domain particles inside itself. Particles mainly consists of magnetite, Fe_3O_4, or greigite, Fe_3S_4. These particles with their organic coating are called magnetosomes. The particle sizes range between 40 and 100 nm and always are within single-domain range [49]. The fact that particles are single-domain maximizes magnetic moment in defined volume. More about magnetotactic bacteria and magnetosomes can be found in [11].

1.3 Magnetic anisotropy

Some ferromagnetic materials form permanent magnets. These materials are magnetized even in zero applied field. That means that some direction in the space for the magnetic moment is more favourable than others. Therefore material is anisotropic. Favourable direction is called the easy axis of magnetic anisotropy. And not favourable directions are called the hard axes of magnetic anisotropy.

In this section energy density $w = \frac{E}{V}$, which is energy per unit volume, will be used. The most common anisotropy type is crystallographic anisotropy.

1.3.1 Crystallographic anisotropy

According to [7]: "The magnetocrystalline anisotropy energy is usually small compared with the exchange energy. The magnitude of magnetic moment is determined almost only by the exchange and the contribution of the anisotropy is negligible for almost all the known ferromagnetic materials.

But the direction of the magnetization is determined only by this anisotropy, because the exchange is indifferent to the direction in space"

Quantitative evaluation of the spin-orbit interaction from basic principles is possible [65], but the accuracy is inadequate. Therefore, anisotropy energies are always written as phenomenological expressions with power series, taking into account the crystal symmetry.

Uniaxial anisotropy

Uniaxial anisotropy means that anisotropy energy is function of only one parameter: the angle θ between anisotropy axis $\vec{n}$ and magnetic moment $\vec{m}$. Magnetic anisotropy axis $\vec{n}$ define direction to precision of sign so both directions $\vec{n}$ and $-\vec{n}$ are equally favourable. That means that Taylor expansion of anisotropy energy has only even powers of $\cos\theta$:

$$E_u = -\sum_{i=1}^{\infty} K_i V \cos^{2i}\theta = -\sum_{i=1}^{\infty} K_i V (\vec{n}\cdot\vec{e})^{2i} \text{ , where} \tag{1.4}$$

$\vec{e} = \dfrac{\vec{m}}{|\vec{m}|}$.

Usually higher terms in anisotropy are negligible comparing to the first and uniaxial anisotropy energy can be written in simple form:

$$E_u = -\frac{K_u V}{2}(\vec{n}\cdot\vec{e})^2 \text{ , where } K_u = 2K_1 \tag{1.5}$$

From crystallographic symmetry hexagonal and tetrahedral crystals have uniaxial magnetocrystalline anisotropy.

Usually K_u is positive for uniaxial crystallographic anisotropy, what means that anisotropy energy is minimal if magnetic moment is in the direction of the crystallographic anisotropy axis. The anisotropy axis than is called the easy axis. Without external magnetic field magnetic moment aligns along the easy axis. There are, however, materials with negative K_u and for them crystallographic anisotropy axis is hard axis. In these materials, without external magnetic field, magnetic moment stays somewhere in the plane orthogonal to anisotropy axis. In this situation the direction of magnetic moment is determined by anisotropy terms in the plane, which does not satisfy uniaxial symmetry (1.4).

Cubic anisotropy

For cubic crystals there are 3 equivalent orthogonal directions. They are along crystallographic axis and will be called x, y and z with unit vectors $\vec{n}_x$, $\vec{n}_y$ and $\vec{n}_z$. As in the uniaxial case, the direction is defined to precision of sign, so odd powers are ruled out and lowest-order combination which fits is $(\vec{e}\cdot\vec{n}_x)^2 + (\vec{e}\cdot\vec{n}_y)^2 + (\vec{e}\cdot\vec{n}_z)^2 = \vec{e}^2 = 1$, which is constant. Therefore, the

expansion starts with the fourth order. As in the uniaxial case higher terms are omitted and only one term in the expansion of cubic anisotropy energy is written

$$E_c = \frac{K_c V}{2}\left[(\vec{e}\cdot\vec{n}_x)^2(\vec{e}\cdot\vec{n}_y)^2 + (\vec{e}\cdot\vec{n}_y)^2(\vec{e}\cdot\vec{n}_z)^2 + (\vec{e}\cdot\vec{n}_x)^2(\vec{e}\cdot\vec{n}_z)^2\right] \quad (1.6)$$

For example for iron (Fe) ($K_c > 0$) there are 3 easy axis along crystallographic axis (100, 010, 001), while for nickel (Ni) ($K_c < 0$) there are 4 easy axis along crystallographic diagonals (111, 11-1,1-11,-111).

Magnetostriction

Ferromagnetic material can shrink or expand in the direction of the magnetization, when it is magnetized. This effect is called magnetostriction. Mathematically magnetostriction is extremely complicated [16] and have never been fully developed; not even for the case when the sample is magnetically saturated [60]. Large part of magnetostriction mathematically can be expressed in the same mathematical form as uniaxial or cubic magnetocrystalline anisotropy. That means when the anisotropy constants is measured, the magnetostriction is already included therefore no additional terms in anisotropy energy (1.5) and (1.6) should be added. It is therefore assumed in this work that all bodies are rigid and magnetoelastic effect will be ignored.

1.3.2 Shape anisotropy

Generally, the field inside a uniformly magnetized ferromagnetic body is not uniform. However, if and only if the surface of the body is of the second degree (in a Cartesian coordinate system satisfy an algebraic equation of degree two) [62], the internal field is uniform. The internal field is not necessarily in the same direction as external field. The ellipsoid is the only finite second degree surface, all other surfaces extend to infinity and cannot be realized in practice. So ellipsoidal particles are frequently used in precise investigations of magnetic materials.

The magnetostatic self-energy, which can be interpreted as anisotropy energy, of a uniformly magnetized ellipsoid is [78]

$$E_M = \frac{1}{2} V M_S^2 \left(N_x(\vec{e}\cdot\vec{n}_x)^2 + N_y(\vec{e}\cdot\vec{n}_y)^2 + N_z(\vec{e}\cdot\vec{n}_z)^2\right) , \quad (1.7)$$

where $V = \frac{4\pi}{3}abc$ is volume of the ellipsoidal particle with semi-axis of lengths a, b and c, M_S is saturation magnetization and $\vec{n}_x$, $\vec{n}_y$ and $\vec{n}_z$ are unit vectors in directions of ellipsoid principal axis a, b and c, and N_x, N_y and N_z are demagnetizing factors in directions $\vec{n}_x$, $\vec{n}_y$ and $\vec{n}_z$. These demagnetizing factors in general depend on $\frac{a}{c}$ and $\frac{b}{c}$ and can be calculated numerically [68,

78]. But there are analytic expression for ellipsoids of revolution (spheroids) [62, 68, 78]:

- For prolate spheroid ($a > b = c$):

$$N_{\parallel} = N_x = \frac{4\pi(1-\varepsilon^2)}{\varepsilon^2}\left[\frac{1}{2\varepsilon}\ln\left(\frac{1+\varepsilon}{1-\varepsilon}\right) - 1\right] , \tag{1.8}$$

  where $\varepsilon = \sqrt{1-\frac{b^2}{a^2}}$ is eccentricity of ellipse, which generated given spheroid.

- For oblate spheroid ($a < b = c$):

$$N_{\parallel} = N_x = \frac{4\pi}{\varepsilon^2}\left[1 - \frac{\sqrt{1-\varepsilon^2}}{\varepsilon}\arcsin\varepsilon\right] , \tag{1.9}$$

  where $\varepsilon = \sqrt{1-\frac{a^2}{b^2}}$

For prolate and oblate spheroids:

$$N_{\perp} = N_y = N_z = \frac{4\pi - N_{\parallel}}{2} \tag{1.10}$$

To express (1.7) in the form (1.5), the shape anisotropy constant for prolate and oblate spheroids can be introduced:

$$K_s = \left(N_{\perp} - N_{\parallel}\right) M_S^2 = \left(2\pi - \frac{3}{2}N_{\parallel}\right) M_S^2$$

For rod like particles ($a \gg b \approx c$)

$$N_{\parallel} = 0 \qquad N_{\perp} = 2\pi \qquad K_s = 2\pi M_S^2 \tag{1.11}$$

For plate like particles ($a \ll b \approx c$)

$$N_{\parallel} = 4\pi \qquad N_{\perp} = 0 \qquad K_s = -4\pi M_S^2 \tag{1.12}$$

1.3.3 Paramagnetic particle

Larger particle which consists of magnetic nanoparticles behave as paramagnetic particle. Estimate of susceptibility of such particles can be found in [12].

Susceptibility of small paramagnetic particles differ from bulk materials. For anisotropic particles susceptibility is direction dependent. If the material either is isotropic or has its principal axes of magnetic anisotropy along the

principal axes of the ellipsoid, then magnetic moment of the particle can be calculated as [68]:

$$m_i = \frac{\chi_i H_i}{1 + N_i \chi_i} V \ , \tag{1.13}$$

where m_i, H_i are magnetic moment $\vec{m}$ and magnetic field $\vec{H}$ components in the direction of the ellipsoid principal axes i (where $i \in \{a, b, c\}$) and χ_i, N_i are susceptibility and demagnetization factor in the direction i.

If the particle is spheroidal type (b=c), then we can introduce direction of anisotropy as $\vec{n} = \vec{n}_x$ and magnetic field $\vec{H}$ can be divided in parallel to anisotropy field $\vec{H}_\parallel = (\vec{H} \cdot \vec{n})\vec{n}$ and perpendicular to anisotropy field $\vec{H}_\perp = \vec{H} - \vec{H}_\parallel$. Magnetic moment $\vec{m}$ can also divided in parallel to anisotropy magnetic moment $\vec{m}_\parallel = (\vec{m} \cdot \vec{n})\vec{n}$ and perpendicular $\vec{m}_\perp = \vec{m} - \vec{m}_\parallel$. If the spheroidal particle is isotropic ($\chi_i = \chi$), then

$$m_\parallel = \frac{V \chi H_\parallel}{1 + N_\parallel \chi} \qquad m_\perp = \frac{V \chi H_\perp}{1 + N_\perp \chi}$$

In the vector form magnetic moment can be written as:

$$\vec{m} = \chi_\perp V \vec{H} + \Delta\chi V (\vec{H} \cdot \vec{n})\vec{n} \ , \tag{1.14}$$

where

$$\chi_\perp = \frac{\chi}{1 + N_\perp \chi} \qquad \chi_\parallel = \frac{\chi}{1 + N_\parallel \chi} \qquad \Delta\chi = \chi_\parallel - \chi_\perp$$

and $N_\parallel$ and $N_\perp$ is given by (1.8), (1.9) and (1.10).

The same equation (1.14) can be obtained for spherical particle with anisotropic susceptibility if anisotropy is uniaxial. But in this case

$$\chi_\perp = \frac{3\chi_z}{3 + 4\pi\chi_z} \qquad \chi_\parallel = \frac{3\chi_x}{3 + 4\pi\chi_x} \ ,$$

where χ_x is susceptibility in the direction $\vec{n}$ and χ_z is susceptibility orthogonal to $\vec{n}$

For long ($a \gg b \approx c$) isotropic ($\chi_i = \chi$) particle (1.13) can be rewritten in form:

$$m_\parallel = V \chi H_\parallel \qquad m_\perp = \frac{V \chi H_\perp}{1 + 2\pi\chi}$$

In the vector form (1.14) this can be written as:

$$\vec{m} = \frac{V\chi}{1 + 2\pi\chi} \vec{H} + \frac{2\pi\chi^2 V}{1 + 2\pi\chi} (\vec{H} \cdot \vec{n})\vec{n} \tag{1.15}$$

Similar for flat ($a \ll b \approx c$) isotropic particle (1.13) can be rewritten in form:

$$m_\parallel = \frac{V \chi H_\parallel}{1 + 4\pi\chi} \qquad m_\perp = V \chi H_\perp$$

In vector form (1.14) this can be written as:

$$\vec{m} = V\chi\vec{H} - \frac{4\pi\chi^2 V}{1 + 4\pi\chi} (\vec{H} \cdot \vec{n})\vec{n} \tag{1.16}$$

1.4 Superparamagnetic particles

An uniaxial anisotropic magnetic particle with magnetic moment $\vec{m} = m\vec{e}$ has anisotropy energy (1.5)

$$E_u = -\frac{K_u V}{2}(\vec{n} \cdot \vec{e})^2 \ ,$$

which has two minimums $E_{min} = -\frac{K_u V}{2}$ at $\vec{n} \cdot \vec{e} = 1$ and $\vec{n} \cdot \vec{e} = -1$ and maximum $E_{max} = 0$ at $\vec{n} \cdot \vec{e} = 0$ ($K_u > 0$). If the particle is large enough in the thermal equilibrium magnetic moment will tend to be in the vicinity of one of these minimums, that is in the direction of anisotropy axis or opposite to it.

If particle is small then energy barrier $\Delta E = E_{max} - E_{min}$ becomes comparable to thermal energy $E_T = k_B T$, where $k_B = 1.3806 \cdot 10^{-16} \frac{erg}{K}$ is Boltzmann constant and T is temperature. Roughly it can be assumed that magnetic moment spends all its time in one of the directions of energy minimums which are separated by energy barrier ΔE, and no time at all other directions. In that case average time it takes magnetic moment to jump from one minimum to the other is function only of the height of the energy barrier ΔE. This time is called relaxation time τ and is proportional to inverse of probability of spontaneous magnetic moment jumps per unit time which can be calculated using Boltzmann distribution.

$$\tau = \tau_0 \exp\left(\frac{\Delta E}{k_B T}\right) \ , \tag{1.17}$$

where τ_0 is a constant that has dimension of time. Neel [67] estimated this constant $\tau_0 \approx 10^{-9} s$. Of course, this constant is not necessarily the same for different ferromagnetic material.

The material is called superparamagnetic if in the characteristic time of the experiment magnetic moment jumps many times from one minimum to other. Therefore observable mean magnetic moment of the particle is zero. In the external magnetic field relaxation times τ can be different for different directions, which give observable magnetization of the particle. The magnetization dependence is similar to paramagnetic materials discussed in section 1.3.3, but with higher susceptibilities.

For typical ferromagnetic materials $K_u \approx 10^5 \frac{erg}{cm^3}$, therefore typical ferromagnetic particles becomes superparamagnetic if their size is less than $11\,nm$ (for experimental times larger than $\tau = 1\,ms$). This size is close to single-domain grain size discussed in section 1.2, therefore there is narrow size range of particles in single-domain state with frozen in magnetic moment (rigid dipole).

There was made assumption that energy minimums are narrow and magnetization is always in one of the two minimums and spend no time at any

other direction. In any realistic case, there is a finite probability of spending some of the time in the vicinity of either minimum, in which case coefficient τ_0 is function of temperature. Brown [15] tried to solve the problem with real-sized minimums. He showed that this is random walk problem and wrote a differential equation to describe it. He did not solve his differential equation, just found some asymptotic expression. Later [18] he improved it and concluded that for a uniaxial anisotropy the exact solution would not be drastically different from (1.17) with constant coefficient τ_0 in the range of values of the physical parameters for which this theory is usually applied. Numerically it is proved in zero [2] and non-zero [3] applied field. For more precise result several easy-to-use approximations can be used [27].

Situation with combination of crystalographic and shape anisotropy is explained in [5].

For cubic anisotropy in zero field situation is very similar to (1.17), with the only difference that K_u is replaced by $\frac{K_c}{4}$. However, in this case τ_0 it is not constant, because there are more minimums and subsequently more possibilities of wiggling around before jumping to other minimum. Numerically it is studied in [4, 8]. More about cubic anisotropy effects can be found in [54, 32]

1.5 Dynamic equations of magnetic particle

1.5.1 Magnetic relaxation

Usually torque $\vec{M}$ on magnetic moment $\vec{m} = m\vec{e}$ in effective magnetic field $\vec{H}_{eff}$ are written as [44]

$$\vec{M} = [\vec{m} \times \vec{H}_{eff}] \ .$$

Using gyromagnetic ratio γ, in static particle this equation can be rewritten

$$\frac{d\vec{e}}{dt} = \gamma[\vec{e} \times \vec{H}_{eff}] \ .$$

This equation gives infinity long precession of magnetic moment around magnetic field $\vec{H}_{eff}$ with Larmor (angular) frequency $\omega_L = \gamma|\vec{H}_{eff}|$. It is known from experiments, that magnetic moment approaches direction of effective field, so additional damping should be included. This damping first was introduced by Landau and Lifshitz [53] and then written in mathematically equivalent form by Gilbert [39]. The Gilbert form of Landau-Lifshitz equation is called Landau-Lifshitz-Gilbert equation:

$$\frac{d\vec{e}}{dt} = -\vec{e} \times \left(\gamma \vec{H}_{eff} - \alpha_{mag} \frac{d\vec{e}}{dt} \right) \ , \tag{1.18}$$

where α_{mag} is phenomenological damping parameter. Landau-Lifshitz-Gilbert equation instead of Landau-Lifshitz is used because it gives physically acceptable result , when damping is infinitely large [58, 48].

Effective field can be calculated from magnetic energy $\vec{H}_{eff} = -\frac{\partial E}{\partial \vec{m}}$, where magnetic energy is sum of anisotropy energy (1.5) and energy of magnetic moment in the field $\vec{H}$:

$$E = -mH\vec{e}\cdot\vec{h} - \frac{KV}{2}(\vec{e}\cdot\vec{n})^2 \ . \tag{1.19}$$

Then $\vec{H}_{eff} = \vec{H} + \vec{H}_a$, where $\vec{H}_a = \frac{KV}{m}(\vec{e}\cdot\vec{n})\vec{n}$ is anisotropy field.

After some calculations the Landau-Lifshitz-Gilbert equation (1.18) can be written in form:

$$\begin{aligned} \frac{d\vec{e}}{dt} &= \vec{\omega}_{\vec{e}} \times \vec{e} = (\vec{\omega}_L + \vec{\omega}_R) \times \vec{e} \\ \vec{\omega}_L &= \frac{\gamma}{1+\alpha_{mag}^2}\vec{H}_{eff} \\ \vec{\omega}_R &= \alpha_{mag}\vec{e} \times \vec{\omega}_L \end{aligned} \quad , \tag{1.20}$$

where $\vec{\omega}_L$ is Larmor frequency and $\vec{\omega}_R$ is relaxation frequency. Using effective field and rotation operator $\vec{J}_{\vec{e}} = \vec{e} \times \frac{\partial}{\partial \vec{e}}$ it can be written:

$$-\xi_{mag}\vec{\omega}_R = \vec{J}_{\vec{e}}E \ , \tag{1.21}$$

where $\xi_{mag} = \frac{m(1+\alpha_{mag}^2)}{\gamma\alpha_{mag}}$. Landau-Lifshitz-Gilbert equation is written for stationary particle. To calculate dynamic of particle the egg-yolk model [76, 75] should be used, where (1.21) is rewritten:

$$-\xi_{mag}(\vec{\omega}_R - \vec{\omega}_{\vec{n}}) = \vec{J}_{\vec{e}}E \ , \tag{1.22}$$

where $\vec{\omega}_{\vec{n}}$ is angular frequency of magnetic particle. Using balance of viscous torque inside and outside of the magnetic particle equation of the motion of the particle can be written in non-rotating fluid [76]:

$$\xi\vec{\omega}_{\vec{n}} + \vec{J}_{\vec{e}}E + \vec{J}_{\vec{n}}E = 0 \ , \tag{1.23}$$

where ξ is rotational drag coefficient.

In this work spheroidal particles will be examined. Rotational drag coefficient ξ for spheroidal particles is derived in [70, 71, 52]. In general there are two rotational drag coefficients for a general spheroid, one for a rotation about the axial semiaxis (hydrodynamic anisotropy axis) and other for a rotation about one of the equatorial semiaxes. We will use that hydrodynamic anisotropy axis coincide with magnetic anisotropy axis, therefore magnetic torque is applied perpendicular to hydrodynamic anisotropy axis and only rotational drag coefficient for rotation about the equatorial semiaxes should be used.

Here will be used form of ξ (for rotation about the equatorial semiaxes) given in [82]

$$\xi = 8\pi\eta V\Gamma \ , \tag{1.24}$$

where η is dynamic viscosity of the particle surrounding fluid, V is volume of the particle and Γ is geometric factor which depends on spheroid semi-axis a and b:

$$\Gamma = \frac{a^2 + b^2}{a^2 N_{\parallel} + b^2 N_{\perp}} \ , \tag{1.25}$$

where $N_{\parallel}$ and $N_{\perp}$ are demagnetization factors (1.8), (1.9), (1.10). For rod-like particles ($a \gg b$)

$$\Gamma = \frac{a^2}{b^2\left[4\pi \ln\left(2\frac{a}{b}\right) - 2\pi\right]}$$

and for plate like particles ($a \ll b$)

$$\Gamma = \frac{b}{a\pi^2}$$

Here more terms in expansion of $N_{\parallel}$ (1.8), (1.9) were used.

Before we proceed some assumptions about relaxation times should be made. The gyromagnetic ratio can be expressed as $\gamma = \frac{g|e|}{2m_e c} = \frac{g\mu_B}{\hbar}$, where g is 'Landé g-factor' (for electron $g \approx 2$), e is electron charge, m_e is electron mass, c is speed of light, $\hbar$ is Planck constant and μ_B is Bohr magnetron. Typical magnetic relaxation time is of order $\tau_{mag} = \frac{\xi_{mag}}{mH} \leq \frac{1+\alpha_{mag}^2}{H_a \gamma \alpha_{mag}}$. Smallest possible effective magnetic field is anisotropy field $H_a = \frac{KV}{m}$. For single domain particles magnetic moment can be calculated using saturation magnetization M_S ($m = M_S V$). So $H_a = \frac{K}{M_S}$. Magnetocrystalline anisotropy is of order $K \approx 10^5 \frac{erg}{cm^3}$ [32], saturation magnetization is of order $M_S \approx 10^3 \frac{G}{cm^3}$ [32] and gyromagnetic ratio is of order $\gamma \approx 10^7 \frac{1}{s \cdot G}$. If it will be assumed that $\frac{1+\alpha_{mag}^2}{\alpha_{mag}} < 1000$, than magnetic relaxation time would be $\tau_{mag} < 10^{-6} s$ which is approximately equal to smallest particle relaxation time $\tau_p = \frac{\xi}{KV} = \frac{8\pi\eta\Gamma}{K} \approx 10^{-6} s$ for sphere ($\Gamma = \frac{3}{4\pi}$), where $\Gamma \geq \frac{3}{4\pi}$ is form-factor (1.25) and η is viscosity (for water $\eta \approx 10^{-2} \frac{erg \cdot s}{cm^3}$). In the magnetic field τ_{mag} would decrease. And if the particle is not spherical then τ_p would increase. If the magnetic particle is coated to prevent agglutination of the particles, than magnetic volume is smaller than hydrodynamic volume which again increase τ_p. In most physically observed cases $\tau_p \gg \tau_{mag}$

Further it will be assumed that magnetic moment relaxation is much faster than particle movement ($\xi \gg \xi_{mag}$). Therefore magnetic moment

movement can be separated from particle movement, and magnetic moment relaxation can be assumed infinitely fast. So magnetic moment always is aligned with effective magnetic field

$$\vec{H}_{eff} \times \vec{e} = \vec{J}_{\vec{e}} E = 0 \tag{1.26}$$

Then equation of particle motion (1.23) can be rewritten in form:

$$\xi \vec{\omega}_{\vec{n}} + \vec{J}_{\vec{n}} E = 0 \tag{1.27}$$

1.5.2 Stoner-Wohlfarth model

The magnetic moment movement in particle with uniaxial anisotropy, which is small enough to be single domain and which is large enough that all time-effects described in section 1.4 are negligible, is known as Stoner-Wohlfarth model [79].

To find the direction of magnetic moment the minimums of energy (1.19) should be found. Minimums can be found by equation (1.26) or using angles in equation(1.19):

$$E = -\frac{KV}{2} \cos^2 \theta - mH \cos(\phi - \theta) \ , \tag{1.28}$$

where ϕ is angle between magnetic field and particle anisotropy axis and θ is angle between magnetic moment and particle anisotropy axis (angles shown in figure 1.1). Further will be used technique from [54].

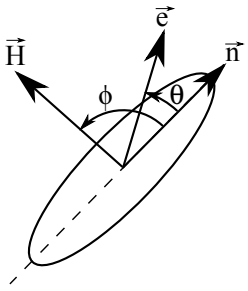

Figure 1.1: Scheme of used angles in equation (1.28)

The extremes of energy (1.28) are given by equilibrium condition $\frac{\partial E}{\partial \theta} = 0$, whence

$$\frac{H_a}{H} \sin\theta \cos\theta = \sin(\phi - \theta) \ . \tag{1.29}$$

This equation can be written as fourth degree equation for $x = \cos\theta$:

$$\left(\frac{H_a}{H} x + \cos\phi \right)^2 (1 - x^2) = x^2 \sin^2 \phi \ . \tag{1.30}$$

This equation has either two or four real roots (all less than unity). Since all four roots correspond to extrema of energy, it is clear that, energy (1.28) has one minimum and one maximum (when 2 roots) or two minimums and two maximums (when 4 roots). In other words , the number of possible directions of magnetization $\vec{e}$ for given field $\vec{H}$ depends on its angle with particle anisotropy axis.

The number of extremes change when maximum annihilates with minimum and at that point also is inflection point $\frac{\partial^2 E}{\partial \theta^2} = 0$. It can be found that graph separating regions with one and two minimums (two and four extremes) is (fig. 1.2)

$$\left(\frac{H}{H_a}\cos\phi\right)^{\frac{2}{3}} + \left(\frac{H}{H_a}\sin\phi\right)^{\frac{2}{3}} = 1 \ . \tag{1.31}$$

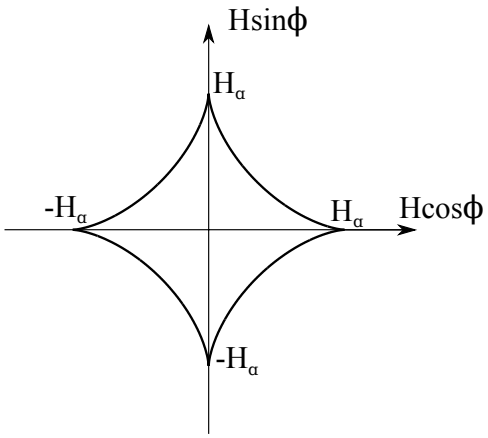

Figure 1.2: The graph separating inner region with two minimum (four extremes) from outer region with one minimums (two extremes)

In the inner region of fig. 1.2, where $|\vec{H}|$ is small, E has two minimums and outside of this region, where $|\vec{H}|$ is large, E has only one minimum. In which of the two minimums will "sit" the magnetic moment depends on the history. A solution which starts from a particular branch cannot be allowed to jump into another branch spontaneously. The jump must be at a field value at which there is no energy barrier between these branches. This feature is the basis of the hysteresis. Further analysis can be found in chapter 2.

The case of a cubic, instead of a uniaxial, anisotropy has also been worked out [56] in detail. In this case there are more branches than in the uniaxial case, which makes it sometimes more difficult to decide into which branch to jump.

1.6 Viscoelastic fluid models

We will use linear viscoelasticity, which satisfies Boltzmann superposition, which can be stated as: "The creep in a specimen is a function of entire loading history and each increment of load makes an independent and additive contribution to the total deformation" [83]. This gives that:

$$\epsilon_{ij}(t) = \int_0^\infty \sigma_{kl}(t-s)\, dJ_{ijkl}(s) \ ,$$

where ϵ_{ij} is strain tensor component, σ_{ij} is stress tensor component and the integration function comprise a forth order tensor $J_{ijkl}(t)$. Similar expression should hold for inverse statement:

$$\sigma_{ij}(t) = \int_0^\infty \epsilon_{kl}(t-s)\, dG_{ijkl}(s) \ ,$$

where G_{ijkl} is another forth order tensor. After partial integration and change of variables this can be written in form:

$$\sigma_{ij}(t) = \int_{-\infty}^t G_{ijkl}(t-\tau)\frac{d\epsilon_{kl}(\tau)}{d\tau}\, d\tau \ , \tag{1.32}$$

where it is assumed that infinity long ago material had no strain $\epsilon_{lk}(-\infty) = 0$ and material deformation is continuous $G_{ijkl}(0) = 0$.

In isotropic case G_{ijkl} has only two independent components and can be written in form [25]:

$$G_{ijkl}(t) = \frac{1}{3}[G_2(t) - G_1(t)]\delta_{ij}\delta_{kl} + \frac{1}{2}G_1(t)[\delta_{ik}\delta_{jl} + \delta_{il}\delta_{jk}] \ ,$$

where $G_1(t)$ and $G_2(t)$ are independent relaxation functions and δ_{ij} is the Kronecker delta symbol. For the isotropic, incompressible ($\frac{d\epsilon_{ii}}{dt} = 0$) fluid, using symmetry of σ_{ij} or ϵ_{ij}, equation (1.32) can be written in form:

$$\sigma_{ij}(t) = \int_{-\infty}^t G(t-\tau)\frac{d\epsilon_{ij}(\tau)}{d\tau}\, d\tau \ , \tag{1.33}$$

where $G(t) = G_1(t)$ will be called memory kernel.

Since $G(t)$ is independent of coordinate, then rotational drag in low Reynolds in viscoelastic fluid should be calculated similar to viscous fluid giving:

$$\vec{M}_{drag}(t) = -\int_{-\infty}^t \xi'(t-\tau)\vec{\omega}(\tau)\, d\tau \ , \tag{1.34}$$

where $\xi'(t) = 8\pi G(t)V\Gamma$ and Γ is defined in (1.25).

In viscous fluid $\vec{M}_{drag}(t) = -\xi\vec{\omega}(t)$ and equation (1.34) is kept right if $\xi'(t) = \xi\delta(t)$, therefore $G(t) = \eta\delta(t)$. Further some simple linear viscoelastic fluid models will be shown.

1.6.1 Maxwell model

Probably the simplest way of expressing mechanic model of viscoelastic fluid is using springs (elastic elements) and dashpots (viscous elements). For spring $\sigma_i = E_j\epsilon_i$ and for dashpot $\sigma_i = \eta_j\frac{d\epsilon_i}{dt}$.

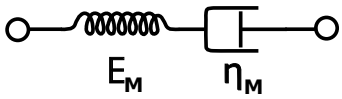

Figure 1.3: Simple spring-dashpot model of the Maxwell fluid

Maxwell model consists of one spring and one dashpot connected in series (fig. 1.3). Then total stress at the point of fluid is equal to the stresses on each of the element $\sigma = \sigma_1 = \sigma_2$ and total strain at the point of fluid is sum of the both strains $\epsilon = \epsilon_1 + \epsilon_2$. From these conditions equation for Maxwell fluid can be derived [83]:

$$\frac{1}{E_M}\frac{d\sigma}{dt} + \frac{\sigma}{\eta_M} = \frac{d\epsilon}{dt}\ , \tag{1.35}$$

where E_M is Young's modulus of the spring and η_M is viscosity of the dashpot. Sudden strain ($\epsilon(t < 0) = 0$ and $\epsilon(t > 0) = \epsilon_0$) gives stress relaxation of the Maxwell fluid as:

$$\sigma(t) = \sigma_0 \exp\left(-\frac{t}{\tau_M}\right)$$

for $t > 0$, where $\tau_M = \frac{\eta_M}{E_M}$ and $\sigma_0 = E_M\epsilon_0$. Comparing it with (1.33) gives that $G(t) = E_M \exp\left(-\frac{t}{\tau_M}\right)$ for Maxwell model.

Sudden stress ($\sigma(t < 0) = 0$ and $\sigma(t > 0) = \sigma_0$) gives change of strain as:

$$\epsilon(t) = \frac{\sigma_0}{\eta_M}t + \frac{\sigma_0}{E_M}\ ,$$

where second term of the right hand side comes from spring element, but first term from dashpot. The jump in strain is undesirable for modeling viscoelastic materials in thermal movement, therefore other models are introduced. The problems with Brownian motion in frame of Maxwell model are discussed also in [73]. Simple situation, where the Maxwell model gives unphysical result, is shown in appendix A.1.

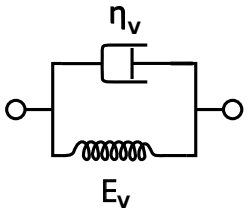

Figure 1.4: Simple spring-dashpot model of the Voigt-Kelvin fluid

1.6.2 Voigt-Kelvin model

Another model consisting of only one dashpot and one spring is Voigt-Kelvin model, where these elements are connected parallel to each other (fig. 1.4). In this case total stress is sum of stresses of each element $\sigma = \sigma_1 + \sigma_2$ and total strain is equal to the strain of each element $\epsilon = \epsilon_1 = \epsilon_2$, what gives equation of Voigt-Kelvin model:

$$\sigma = E_V \epsilon + \eta_V \frac{d\epsilon}{dt} \tag{1.36}$$

Sudden strain ($\epsilon(t < 0) = 0$ and $\epsilon(t > 0) = \epsilon_0$) gives equation for stress:

$$\sigma(t) = E_V \epsilon_0$$

for $t > 0$. This gives that, when the stress is kept constant, strain also stays unchanged, what is more suitable for plastic solids than for fluids. therefore more complicated spring-dashpot model should be chosen.

1.6.3 Jeffreys model

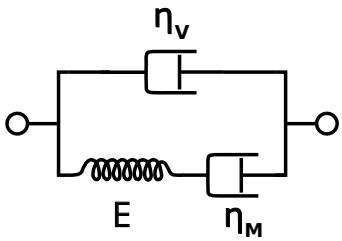

Figure 1.5: Simple spring-dashpot model of the Jeffrey fluid

The next simplest spring-dashpot fluid model is the Jeffrey model [72] shown in fig. 1.5, which is called also Oldroid-B model [38]. Jeffrey model is similar to standard linear solid model [63], which is the simplest model giving adequate description of the behaviour of some Earth materials. And Jeffrey model is the simplest model for adequate description of fluid with elastic behaviour. Jeffrey model consists of Maxwell element connected parallel to

dashpot (fig. 1.5). Similar model can be obtained connecting dashpot with Voigt-Kelvin element in series [72], what gives the same physical equation of motion just with different unknown parameters.

In Jeffrey model total strain is equal to the strain of Maxwell element and single dashpot $\epsilon = \epsilon_V = \epsilon_M$, but total stress is sum of both stresses $\sigma = \sigma_M + \sigma_V$. This gives equation of Jeffrey fluid:

$$\frac{d\sigma}{dt} + \frac{\sigma}{\tau_M} = \frac{\eta_V + \eta_M}{\tau_M}\frac{d\epsilon}{dt} + \eta_V \frac{d^2\epsilon}{dt^2} \ , \tag{1.37}$$

where $\tau_M = \frac{\eta_M}{E}$. Sudden strain ($\epsilon(t<0) = 0$ and $\epsilon(t>0) = \epsilon_0$) gives stress relaxation in Jeffrey fluid:

$$\sigma(t) = \sigma_0 \exp\left(-\frac{t}{\tau_M}\right)$$

for $t > 0$, where $\sigma_0 = \frac{\eta_V+\eta_M}{\tau_M}\epsilon_0$. The difference in $G(t)$ from Maxwell fluid is addition of Dirac delta function for Jeffrey fluid $G(t) = \eta_V\delta(t) + E\exp\left(-\frac{t}{\tau_M}\right)$, where first term comes from single dashpot element and second term comes from Maxwell element.

Sudden stress ($\sigma(t<0) = 0$ and $\sigma(t>0) = \sigma_0$) gives strain change without jump:

$$\epsilon(t) = \frac{\sigma_0}{\eta_M + \eta_V}t + \frac{\sigma_0\eta_M\tau_M}{(\eta_V+\eta_M)^2}\left[1 - \exp\left(-\frac{t}{\tau_J}\right)\right] \tag{1.38}$$

for $t > 0$, where $\tau_J = \frac{\tau_M\eta_V}{\eta_V+\eta_M}$ is Jeffrey relaxation time.

1.7 Thermal fluctuation effects

If the particle is so small that magnetic energy becomes comparable to thermal energy, the particle thermal fluctuations becomes significant. Single-domain grain above superparamagnetic limit has magnetic moment $m = M_S V$ and its magnetic energy is of order mH, where H is external magnetic field strength. In room temperature thermal energy is around $k_B T = 4 \cdot 10^{-14}\, erg$. In the magnetic resonance imaging typical field is $1.5 \cdot 10^4\, Oe$ [84], what gives that thermal energy becomes comparable to magnetic energy of the magnetic grain with saturation magnetization $M_s \approx 10^3 \frac{G}{cm^3}$ [32] if grain size is less than $70\, nm$. This value is above single-domain particle size limit discussed in section 1.2, therefore single thermal fluctuations of the particle gives significant influence.

In this work special interest is about particle rotation in viscous and viscoelastic fluid, therefore thermal effects of particle rotation in these fluids will be discussed.

Equipartition theorem states that translation degrees of freedom is equal to rotation degrees of freedom, therefore similar equation can be used for rotation as is used for translation motion. From fluctuation-dissipation theorem is known that fluctuation is connected with dissipative element (dashpot), where for viscous fluid [22]:

$$\xi\omega = \zeta(t) \ ,$$

where $\zeta(t)$ is white noise therm with $\langle\zeta(t)\rangle = 0$ and $\langle\zeta(t)\zeta(t')\rangle = 2\xi k_B T\delta(t-t')$, where ξ is drag of the particle (1.24) and averaging $\langle\rangle$ is over large ensemble of particle which is equal to average of one particle over infinity long time interval. In the viscoelastic fluid we get similar equation, but, because more than one damping element is possible, the noise is coloured with corresponding memory kernel [36]:

$$\int_{-\infty}^{t} \xi'(t-\tau)\vec{\omega}(\tau)\, d\tau = \vec{\zeta}(t) \ , \tag{1.39}$$

where for each component of noise vector $\vec{\zeta}$ the mean value is $\langle\zeta_i(t)\rangle = 0$ and components is identical and independent with variance $\langle\zeta_i(t)\zeta_k(t')\rangle = 2\delta_{ik}\xi'(t-t')k_B T$, where $\xi'(t)$ defines appropriate viscoelastic model, e.g. for Jeffrey model:

$$\xi'(t) = 8\pi V\Gamma G(t) = 8\pi V\Gamma\left[\eta_V\delta(t) + E\exp\left(-\frac{t}{\tau_M}\right)\right] \tag{1.40}$$

In the numerical experiments it is more convenient to use white (not coloured) noise. The coloured noise in viscoelastic fluid is obtained from spring-dashpot model with white noise, where white noise comes from dashpots [28]. Equation with white noise for Jeffrey fluid will be found in chapter 5.

1.8 Objective of the work

Since magnetic particles are used in different applications and many features of their behaviour are not well understood the objective of the present work is to develop the understanding of their behaviour in time dependent magnetic fields. To achieve the objective the following problems will be solved:

- Find all possible stable regimes of uniaxial single-domain particle in rotating magnetic field and calculate corresponding phase diagram.
- Compare dissipation due to viscous drag with dissipation of magnetic moment movement inside particle for uniaxial single-domain particle in rotating magnetic field

- Calculate stability of synchronous with the precessing magnetic field regime of the superparamagnetic particle and draw corresponding phase diagram.
- Find mean angular velocity of the superparamagnetic particle which moves asynchronously with the precessing field.
- Derive algorithm for measuring form-factor of the superparamagnetic particle using crossed alternating and constant fields.
- Find the way to use the superparamagnetic particle to measure viscoelastic properties of the fluid.
- Compare nuclear magnetic resonance relaxation times in viscous and viscoelastic fluids.

Chapter 2

Dynamics of single-domain particle with uniaxial anisotropy in rotating magnetic field

2.1 Motivation and contents

In paper [33] is mentioned that magnetotactic bacterium in rotating magnetic field should escape form the plane of rotating magnetic field for high field frequencies. In [33] is calculated some trajectories of the bacterium, but full analysis about stability of the possible regimes is not made.

Available work of C. Caroli and P. Pincus [21] tries to find possible regimes of magnetic grain in rotating magnetic field and gives some insight in stability of the regimes. But C. Caroli and P. Pincus work [21] does not solve stability problem in general case and, as will be shown in this work, they did not found all possible regimes. Asynchronous rotation was not mentioned in [21].

In hypothermia description usually energy dissipation due to magnetic moment movement is considered [43, 46]. In rotating field some energy is dissipated due to viscous drag, which is not taken into account. In this work dissipated energy in stable regimes will be calculated. It will be checked for what parameters the assumption that viscous dissipation can be neglected is valid.

In this chapter possible stable regimes of a magnetic particle with finite energy of magnetic anisotropy in a rotating magnetic field will be found. The stability of these regimes will be examined and stable regimes in dependence of magnetic field strength and frequency will be shown. Dissipated energy in each stable regime will be calculated. The dissipation due to viscous drag will be compared to dissipation of magnetic moment movement.

2.2 Model

The dynamics of the single-domain particle with uniaxial anisotropy in rotating magnetic field will be examined using equations (1.26) and (1.27) where energy is given by (1.19). As stated by (1.26) magnetic moment is in the direction of effective magnetic field

$$\vec{H}_{eff} = -\frac{\partial E}{m\partial \vec{e}} = H\vec{h} + \frac{KV}{m}(\vec{n}\cdot\vec{e})\vec{n}$$

Equation for anisotropy axis is found from (1.27) with assumption (1.26):

$$\xi\vec{\omega}_{\vec{n}} = KV(\vec{e}\cdot\vec{n})[\vec{n}\times\vec{e}] = mH\vec{e}\times\vec{h} \tag{2.1}$$

Where $\vec{\omega}_{\vec{n}}$ is angular velocity of anisotropy axis and

$$\frac{d\vec{n}}{dt} = \vec{\omega}_{\vec{n}}\times\vec{n} \tag{2.2}$$

Introducing anisotropy frequency $\omega_a = \dfrac{KV}{\xi}$ and anisotropy field $H_a = \dfrac{KV}{m}$ the equation of magnetic moment can be written in form:

$$\vec{e} = \frac{\vec{H}_{eff}}{H_{eff}} = \frac{H\vec{h} + H_a(\vec{e}\cdot\vec{n})\vec{n}}{H_{eff}}\ , \tag{2.3}$$

where $H_{eff} = |\vec{H}_{eff}| = H(\vec{h}\cdot\vec{e}) + H_a(\vec{e}\cdot\vec{n})^2$.

Using that H_{eff} can be expressed as $H_{eff} = \dfrac{\vec{H}_{eff}\cdot\vec{n}}{\vec{e}\cdot\vec{n}}$ and equations (2.1) and (2.3) the equation of anisotropy axis movement (2.2) can be written in form

$$\frac{d\vec{n}}{dt} = \omega_a f\left(\vec{n}\cdot\vec{h}, \frac{H_a}{H}\right)[\vec{h} - \vec{n}(\vec{n}\cdot\vec{h})]\ , \tag{2.4}$$

where the function

$$f\left(\vec{n}\cdot\vec{h}, \frac{H_a}{H}\right) = \frac{(\vec{e}\cdot\vec{n})^2}{\vec{n}\cdot\vec{h} + \frac{H_a}{H}(\vec{e}\cdot\vec{n})} = \frac{H(\vec{e}\cdot\vec{n})}{H_{eff}} \tag{2.5}$$

in general depends on the history of $(\vec{e}\cdot\vec{n})$. f is two argument function, where third argument $(\vec{e}\cdot\vec{n})$ can be found as energy minimum of equation (1.19). In the region, where two different values of $\vec{e}$ are possible, the closest to previous in time value of $\vec{e}$ should be chosen, therefore it is history dependent.

2.3 Synchronous with field regimes

Magnetic field $H\vec{h}$ rotates with angular velocity $\vec{\omega}_H = \omega_H \vec{e}_H$, where $\vec{e}_H$ is unit vector in the direction of $\vec{\omega}_H$. Magnetic field is called rotating if $\vec{h} \perp \vec{\omega}_H$. Rotation of particle is called synchronous with the field (stationary) if angles between introduced unit vector $\vec{h}$, $\vec{n}$, $\vec{e}$ and $\vec{e}_H$ does not change and all of them rotates as one with angular velocity $\vec{\omega}_H$. Than it can be written that $\dfrac{d(\vec{e}_H \cdot \vec{n})}{dt} = \vec{e}_H \cdot \dfrac{d\vec{n}}{dt} = 0$. Using equation (2.4) it transforms in

$$\frac{(\vec{e}_H \cdot \vec{n})(\vec{n} \cdot \vec{h})(\vec{e} \cdot \vec{n})^2}{\vec{n} \cdot \vec{h} + \frac{H_a}{H}(\vec{e} \cdot \vec{n})} = 0 \tag{2.6}$$

From (2.6) three synchronous with the field regimes can be found. They will be called:

- **Planar regime**, when particle (anisotropy axis) rotates in the same plane as magnetic field. Than $\vec{n} \perp \vec{e}_H$ and $\vec{e}_H \cdot \vec{n} = 0$
- **Precession regime**, when particle (anisotropy axis) rotates around cone. In this regime $\vec{n} \cdot \vec{h} = 0$ so $\vec{n} \perp \vec{h}$.
- **Stationary regime**, when particle (anisotropy axis) stays in the direction of rotation $\vec{e}_H$ and rotates only magnetic moment inside the particle $\vec{e}$. In this regime $\vec{e} \perp \vec{n}$ and $\vec{n} \cdot \vec{e} = 0$.

Further we look closer to all three regimes.

2.3.1 Planar regime

In the synchronous planar regime it can be written that $\vec{\omega}_{\vec{n}} = \vec{\omega}_H$. From (2.1) it follows that:

$$\vec{e}_H = \frac{\omega_a}{\omega_H}(\vec{e} \cdot \vec{n})[\vec{n} \times \vec{e}] = \frac{\omega_a}{\omega_H}\frac{H}{H_a}\vec{e} \times \vec{h} \tag{2.7}$$

Using angles introduced in section 1.5.2 it can be written that $\vec{e} \cdot \vec{n} = \cos\theta$, $\vec{n} \times \vec{e} = \sin\theta\, \vec{e}_H$ and $\vec{e} \times \vec{h} = \sin(\phi - \theta)\, \vec{e}_H$ and equation (2.7) change into:

$$\sin(2\theta) = 2\frac{\omega_H}{\omega_a} \qquad \& \qquad \sin(\phi - \theta) = \frac{\omega_H}{\omega_a}\frac{H_a}{H} \tag{2.8}$$

Since sin function is bounded by 1 it can be found that planar regime exists in region:

$$\begin{cases} \omega_H < \omega_a \dfrac{H}{H_a} & \text{if } H < \dfrac{H_a}{2} \\ \omega_H < \dfrac{\omega_a}{2} & \text{if } H > \dfrac{H_a}{2} \end{cases} \tag{2.9}$$

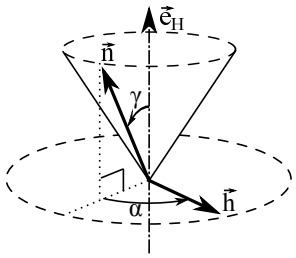

Figure 2.1: Definition of the angles α and γ.

Existence of regime does not ensure physical appearance of the regime. Only stable regimes physically remains after some time, so stability of the regimes should be examined.

Planar regime in angle representation (shown in fig. 2.1) can be expressed as $\gamma = \frac{\pi}{2}$ or $\cos\gamma = 0$ and $\sin\gamma = 1$. In planar regime we can write that $\alpha = \phi$ and $\vec{n}\cdot\vec{h} = \cos\alpha$. Planar regime would be stable if small variance from γ namely γ' would decrease with time.

For small variance γ' (2.18) is written as:

$$\dot{\gamma}' = -\omega_a f\left(\cos\alpha, \frac{H_a}{H}\right)\cos\alpha\sin\gamma\,\gamma'$$

And we see that regime is stable if $\cos\alpha > 0$. So stability changes at $\cos\alpha = \cos\phi = 0$. From equations (2.8) it can be found that stability changes at $\cos\theta = \frac{\omega_H}{\omega_a}\frac{H_a}{H}$ and $\sin\theta = \frac{H}{H_a}$. By eliminating θ it is found that stability of regime changes on line

$$\omega_H = \omega_a \frac{H}{H_a}\sqrt{1 - \left(\frac{H}{H_a}\right)^2} \tag{2.10}$$

In figure 2.2 is shown boundary of existence of stationary planar regime and boundary at which stability of regime changes. Neutral curve of stability divides existence region in three disjoint regions I, II and III. Point where both curves (existence and stability) touch is $\frac{H}{H_a} = \frac{\sqrt{2}}{2}$ and $\frac{\omega_H}{\omega_a} = \frac{1}{2}$.

In each region stability of the regime does not change so it is sufficient to calculate stability only at one point at each region in order to define stability of all region. To find stability (2.8) and stability criterion $\cos\alpha = \cos\phi > 0$ will be used.

- In region I we will choose point $\frac{H}{H_a} = \frac{1}{2}$ and $\frac{\omega_H}{\omega_a} = \frac{1}{2}$. And we obtain that $\theta = \frac{\pi}{4}$ and $\cos\alpha = \cos\frac{3\pi}{4} = -\frac{\sqrt{2}}{2} < 0$ what means that synchronous planar regime is unstable in fig. 2.2 region I.

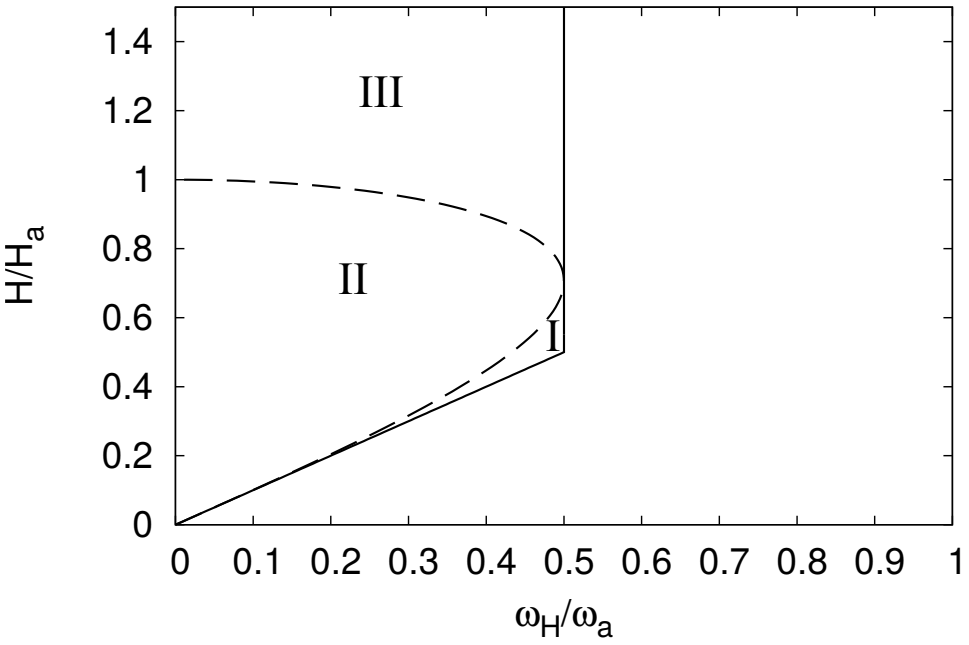

Figure 2.2: Existence region of synchronous planar regime divided by neutral curve of stability into disjoint regions I, II and III. The solid line is the boundary of existence of synchronous planar regime defined in (2.9); the dashed line is the neutral curve of stability of synchronous planar regime defined in (2.10). Synchronous planar regime is stable in region II ∪ III and unstable in region I.

- In regions II and III we will choose point $\frac{H}{H_a} = \frac{\sqrt{3}}{2}$ and $\frac{\omega_H}{\omega_a} = \frac{\sqrt{3}}{4}$ which is on the boundary of both regions. And we obtain that $\theta = \frac{\pi}{6}$ and $\cos\alpha = \cos\frac{\pi}{3} = \frac{1}{2}$ or $\theta = \frac{\pi}{3}$ and $\cos\alpha = \cos\frac{\pi}{2} = 0$. There is possible more values of α, but $\alpha = \pi$ and $\alpha = \frac{7\pi}{6}$ corresponds to maximums not minimums of the energy (1.28), and other values of θ corresponds to reversed particle. It can be seen that in both regions there is at least one stable state (at chosen point it is state where $\cos\alpha = \frac{1}{2}$) and the other state changes its stability. So we can say that there exist stable synchronous planar regime in both fig. 2.2 regions II and III.

From numerical calculations it is found that in region II fig. 2.2 there are one stable and one unstable point in the frame rotating with angular velocity ω_H, in region I - one stable and one saddle point, and in region III - one unstable and one saddle point. Saddle point emerges from pitchfork bifurcation, where node is divided in saddle point and two nodes. These two new nodes correspond to precession regime.

2.3.2 Precession regime

In order to find existence region of precession regime equation (1.30) will be used, which in limit $\phi = \frac{\pi}{2}$ (which is equal to limit $\vec{h} \cdot \vec{n} = 0$) gives:

$$(\vec{e} \cdot \vec{n})^2 = \cos^2\theta = 1 - \left(\frac{H}{H_a}\right)^2 , \tag{2.11}$$

which implies that precession regime is possible if $H < H_a$. With condition $\vec{h} \cdot \vec{n} = 0$ (2.5) transform into $f\left(0, \frac{H_a}{H}\right) = \frac{H}{H_a}(\vec{n} \cdot \vec{e})$, what gives that equation of motion of particle (2.4) is written as:

$$\vec{\omega}_H \times \vec{n} = \omega_a \frac{H}{H_a}(\vec{n} \cdot \vec{e})\vec{h}$$

Square of this equation gives

$$\sin^2\gamma = \left(\frac{\omega_a}{\omega_H}\right)^2 \left(\frac{H}{H_a}\right)^2 \left[1 - \left(\frac{H}{H_a}\right)^2\right] , \tag{2.12}$$

where γ is angle between anisotropy axis $\vec{n}$ and direction of rotation $\vec{e}_H$. Since $\cos\gamma \neq 0$ particle precesses around direction $\vec{e}_H$ with precession angle γ shown in fig. 2.1. Equations (2.11) and (2.12) give two existence conditions:

$$\omega_H > \omega_a \frac{H}{H_a}\sqrt{1 - \left(\frac{H}{H_a}\right)^2} \qquad \& \qquad H < H_a \tag{2.13}$$

In order to find stability of precession regime small perturbation to $\vec{n}$ in (2.4) should be added which gives in situation where $\vec{n} \cdot \vec{h} = 0$:

$$\frac{d\vec{n}'}{dt} = \omega_a f' \vec{h} - \omega_a f (\vec{n} \cdot \vec{h})' \vec{n} , \tag{2.14}$$

where $f = f\left(0, \frac{H_a}{H}\right) = \frac{H}{H_a}(\vec{e} \cdot \vec{n})$ and

$$f' = \frac{H}{H_a}(\vec{e} \cdot \vec{n})' - \left(\frac{H}{H_a}\right)^2 (\vec{n} \cdot \vec{h})' \tag{2.15}$$

And $(\vec{e} \cdot \vec{n})'$ in dependence on $(\vec{n} \cdot \vec{h})'$ is calculated according to equation (1.30), which using conditions (2.11) and $\vec{n} \cdot \vec{h} = 0$ gives:

$$(\vec{e} \cdot \vec{n})' = -\frac{H}{H_a} \frac{1}{\left[1 - \left(\frac{H_a}{H}\right)^2\right]} (\vec{n} \cdot \vec{h})'$$

so (2.15) can be written

$$f' = \frac{1 - 2\left(\frac{H}{H_a}\right)^2}{1 - \left(\frac{H_a}{H}\right)^2}(\vec{n}\cdot\vec{h})'$$

and as a result

$$\frac{d\vec{n}'}{dt} = \omega_a(\vec{n}\cdot\vec{h})'\left[\frac{1 - 2\left(\frac{H}{H_a}\right)^2}{1 - \left(\frac{H_a}{H}\right)^2}\vec{h} - \frac{H}{H_a}\sqrt{1 - \left(\frac{H}{H_a}\right)^2}\vec{n}\right] . \tag{2.16}$$

Since length of $\vec{n}$ does not change, stability is determined by $\vec{n}'$ change in direction $\vec{h}$ as can be seen in (2.16) and precession regime is stable if $\vec{n}'$ decreases which is ensured by condition

$$\frac{1 - 2\left(\frac{H}{H_a}\right)^2}{1 - \left(\frac{H_a}{H}\right)^2} < 0$$

which gives

$$H < \frac{H_a}{\sqrt{2}} \qquad \text{or} \qquad H > H_a \ ,$$

but $H > H_a$ is outside existence region (2.13) of precession regime. That leaves us with only one stability condition:

$$H < \frac{H_a}{\sqrt{2}} \tag{2.17}$$

Visualization of found results can be found in figure 2.3, where in region I regime is unstable and in region II regime is stable.

2.3.3 Stationary regime

If particle stands perpendicular to the plane, where magnetic field rotates, than this regime will be called stationary ($\vec{n}\|\vec{e}_H$ and $\vec{n} \perp \vec{h}$). This regime will be stationary ($\frac{d\vec{n}}{dt} = 0$) only if $f(0, \frac{H}{H_a}) = 0$, because $(\vec{n}\cdot\vec{h}) = 0$ in (2.4). Equation (2.5) shows that this is possible only if $\vec{e} \perp \vec{n}$. Energy minimum therefore is when $\vec{e} = \vec{h}$. In the case $\vec{n}\cdot\vec{h} = 0$ energy (1.28) has minimum at $\vec{e} \perp \vec{n}$ only if (1.28) has two minimums, which is found from (1.31). Therefore stationary regime can exist only if $\dfrac{H}{H_a} > 1$.

To find stability of this regime small perturbation $\vec{n}'$ of the vector $\vec{n}$ is introduced. Equation (1.29) in the limit $(\vec{n}\cdot\vec{e}) \approx (\vec{h}\cdot\vec{n}) \to 0$ gives:

$$(\vec{n}\cdot\vec{h}) = \left(1 - \frac{H_a}{H}\right)(\vec{e}\cdot\vec{n}) \quad \Rightarrow \quad (\vec{n}\cdot\vec{h})' = \left(1 - \frac{H_a}{H}\right)(\vec{e}\cdot\vec{n})' \ ,$$

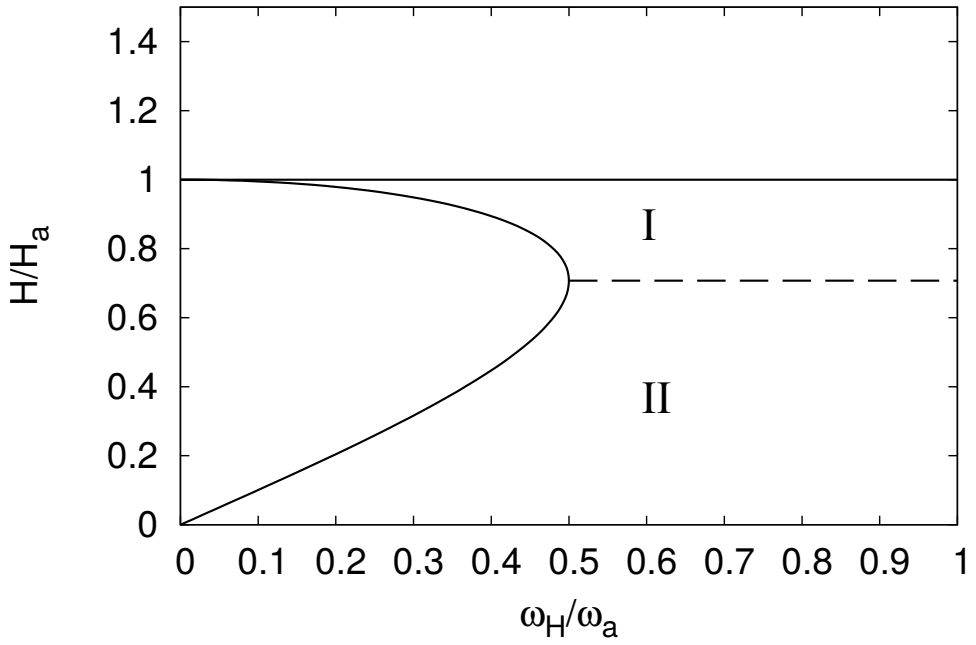

Figure 2.3: Existence region of synchronous precession regime divided by neutral curve of stability into disjoint regions I and II. The solid lines are the boundary of existence of precession regime defined in (2.13); the dashed line is the neutral curve of stability of precession regime, where stable regime is defined in (2.17). Precession regime is stable in region II and unstable in region I.

It can be calculated that $H_{eff} = H$ and

$$f' = (\vec{n}\cdot\vec{e})' - (\vec{n}\cdot\vec{h})' + \frac{(\vec{n}\cdot\vec{h})}{(\vec{n}\cdot\vec{e})}(\vec{n}\cdot\vec{e})' = \frac{(\vec{n}\cdot\vec{h})'}{1-\frac{H_a}{H}}$$

and

$$\frac{d\vec{n}'}{dt} = \omega_a f'\vec{h} = \frac{\omega_a(\vec{n}\cdot\vec{h})'}{1-\frac{H_a}{H}}\vec{h}$$

which gives that $\vec{n}'$ increases for all values of $H > H_a$. It follows that stationary regime is unstable in all values H from the region of existence of the regime.

2.4 Asynchronous planar regime

In the region $H > \dfrac{H_a}{\sqrt{2}}$ and $\omega_H > \dfrac{\omega_a}{2}$ should be some asynchronous regime, because none of the synchronous regimes is stable in this region. From numerical calculations it is found that in selected region stable is asynchronous

planar regime ($\vec{n} \perp \vec{e}_H$). The existence region of asynchronous planar regime is all region of parameters where synchronous planar regime can not exist.

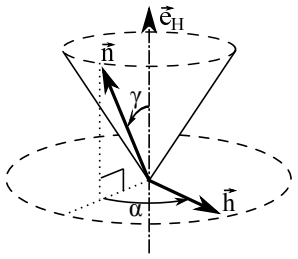

Figure 2.4: Definition of the angles α and γ used in (2.18)

To find stability of this regime the angle representation will be used with angles $\alpha \in [0, 2\pi)$ and $\gamma \in [0, \pi]$. In angle representation $\vec{h} = (\cos\omega_H t, \sin\omega_H t, 0)$ and $\vec{n} = (\cos[\omega_H t - \alpha]\sin\gamma, \sin[\omega_H t - \alpha]\sin\gamma, \cos\gamma)$. The defined angles is shown in figure 2.4. In angle representation $\vec{n}\cdot\vec{h} = \cos\alpha\sin\gamma$. Using angles equation (2.4) can be written as:

$$\begin{cases} \dot{\alpha} = \omega_H - \omega_a f\left(\vec{n}\cdot\vec{h}, \dfrac{H_a}{H}\right)\dfrac{\sin\alpha}{\sin\gamma} \\ \dot{\gamma} = \omega_a f\left(\vec{n}\cdot\vec{h}, \dfrac{H_a}{H}\right)\cos\alpha\cos\gamma \end{cases} \tag{2.18}$$

We should bear in mind that $f\left(\vec{n}\cdot\vec{h}, \dfrac{H_a}{H}\right)$ is history dependent and for some values it can have two values, where the value which will be chosen depends on the history of value of $f\left(\vec{n}\cdot\vec{h}, \dfrac{H_a}{H}\right)$.

In planar regime $\gamma = \frac{\pi}{2}$ and $\dot{\gamma} = 0$. From equation of $\dot{\alpha}$ it can be found that

$$dt = \frac{d\alpha}{\omega_a\left[\frac{\omega_H}{\omega_a} - f(\cos\alpha, \frac{H_a}{H})\sin\alpha\right]} \tag{2.19}$$

Considering small perturbation γ' of the angle γ around value $\gamma = \frac{\pi}{2}$ gives

$$\dot{\gamma}' = -\omega_a f\left(\cos\alpha, \frac{H_a}{H}\right)\cos\alpha\gamma'$$

In order to find average dynamics of γ' the Floquet multiplier λ_F will be used, where $\alpha'(t+T) = \lambda_F\alpha'(t)$ and T is the period. Floquet multiplier can be calculated as

$$\lambda_F = \exp\left[-\int_t^{t+T}\omega_a f\left(\cos\alpha, \frac{H_a}{H}\right)\cos\alpha\, dt\right]$$

It can be seen that stability of the asynchronous planar regime is determined by the sign of the integral

$$I_0\left(\frac{\omega_H}{\omega_a}, \frac{H}{H_a}\right) = \int_t^{t+T} \omega_a f\left(\cos\alpha, \frac{H_a}{H}\right)\cos\alpha\, dt$$

Using equation (2.19) it can be rewritten as

$$I_0\left(\frac{\omega_H}{\omega_a}, \frac{H}{H_a}\right) = \int_{\alpha_0}^{\alpha_0+2\pi} \frac{f\left(\cos\alpha, \frac{H_a}{H}\right)\cos\alpha\, d\alpha}{\frac{\omega_H}{\omega_a} - f(\cos\alpha, \frac{H_a}{H})\sin\alpha} \tag{2.20}$$

From equation (1.31) it can be found that in the region $H < \frac{H_a}{2}$ direction of magnetic moment "stuck" around one of the directions of magnetic anisotropy therefore $f(-\cos\alpha, \frac{H_a}{H}) \neq -f(\cos\alpha, \frac{H_a}{H})$ and I_0 should be calculated according to (2.20). In the region $H > \frac{H_a}{2}$ magnetic moment $\vec{e}$ spend some time near both directions $-\vec{n}$ and $\vec{n}$ when $\vec{n}\cdot\vec{h}$ continuously changes. Since both directions coaxial with anisotropy axis is equal the integral can be divided into two equal integrals about half period, because $f(-\cos\alpha, \frac{H_a}{H}) = -f(\cos\alpha, \frac{H_a}{H})$. In this case:

$$I_0\left(\frac{\omega_H}{\omega_a}, \frac{H}{H_a}\right) = 2\int_{\alpha_0}^{\alpha_0+\pi} \frac{f\left(\cos\alpha, \frac{H_a}{H}\right)\cos\alpha\, d\alpha}{\frac{\omega_H}{\omega_a} - f(\cos\alpha, \frac{H_a}{H})\sin\alpha} \tag{2.21}$$

From equation (1.31) it can be found that in the region $\frac{H_a}{2} < H < H_a$ irreversible jumps can take place if angle $\alpha = \phi$ between $\vec{n}$ and $\vec{h}$ changes. Because integral I_0 is independent of α_0 it is better to take α_0 so that invertible "jumps" are on the boundary of the integral and integration is made over continuous function, because numerical integration can fail on discontinuities. α_0 is found from (1.31).

$I_0\left(\frac{\omega_H}{\omega_a}, \frac{H}{H_a}\right)$ in dependence of $\frac{\omega_H}{\omega_a}$ for some values of $\frac{H}{H_a}$ is shown in fig. 2.5.

In the limit $H \to \frac{H_a}{2}$ it is possible to have two noticeably different regimes. Limit from the top $H > \frac{H_a}{2}$ gives situation where the "jumps" of magnetic moment is possible, but limit form bottom $H < \frac{H_a}{2}$ gives situation where magnetic moment "stuck" near direction of anisotropy axis $\vec{n}$ (or opposite to it). $\lim\limits_{H\to\frac{H_a}{2}+0} I_0\left(\frac{\omega_H}{\omega_a}, \frac{H}{H_a}\right)$ is shown in fig.2.5 by long dashed line and $\lim\limits_{H\to\frac{H_a}{2}-0} I_0\left(\frac{\omega_H}{\omega_a}, \frac{H}{H_a}\right)$ by solid line.

In section 2.3.1 we found that synchronous planar regime stability changes when $f\left(\cos\alpha, \frac{H}{H_a}\right)\cos\alpha$ changes sign. Same is valid for asynchronous planar regime near boundary between synchronous and asynchronous planar

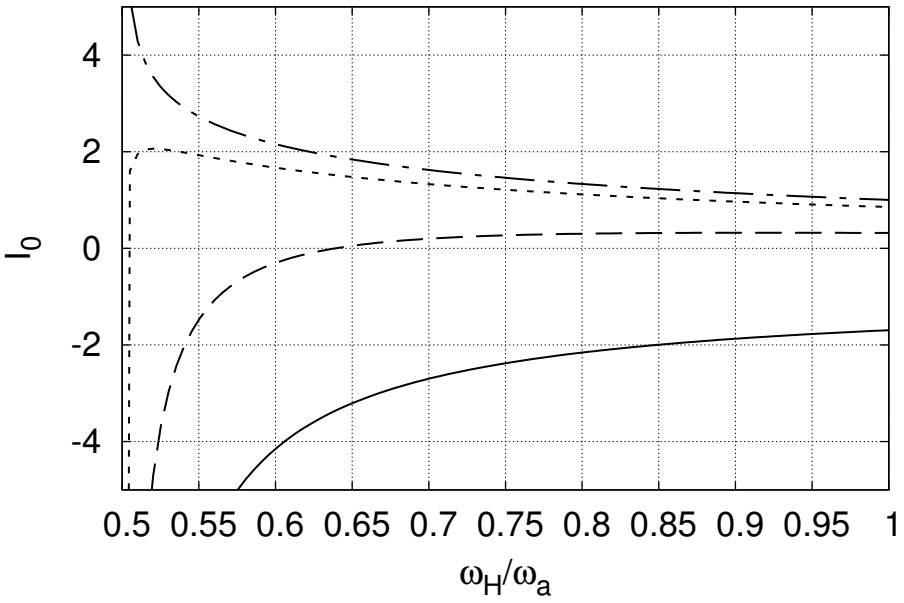

Figure 2.5: Power of Floquet multiplier I_0 as function of rotating field frequency ω_H for magnetic field strength $\frac{H}{H_a}$ = 0.5-0 (without jumps); 0.5+0 (with jumps); 0.65; 0.8. Field is increasing in upwards direction.

regimes, because near this boundary $I_0\left(\frac{\omega_H}{\omega_a}, \frac{H}{H_a}\right)$ is dominated by value of numerator $f\left(\cos\alpha, \frac{H}{H_a}\right)\cos\alpha$ where denominator $\frac{\omega_H}{\omega_a} - f(\cos\alpha, \frac{H_a}{H})\sin\alpha \to +0$ (2.21). Therefore at the boundary dividing existence regions of planar synchronous and asynchronous regimes stability of planar regime does not change.

On the other hand at $\omega_H \gg \omega_a$ it can be seen that (2.20) transforms into

$$I_0\left(\frac{\omega_H}{\omega_a}, \frac{H}{H_a}\right) = \frac{\omega_a}{\omega_H}\int\limits_{\alpha_0}^{\alpha_0+2\pi} f\left(\cos\alpha, \frac{H_a}{H}\right)\cos\alpha\, d\alpha$$

The values of I_0 at large frequency ω_H in the dependence of magnetic field H is shown in fig. 2.6.

From numerical calculations it can be found that in the region $H < \frac{H_a}{2}$, where magnetic moment always has two possible stable positions and no "jumps" of magnetic moment occur, $I_0 < 0$ for all possible values of $\frac{\omega_H}{\omega_a}$ and asynchronous planar regime is unstable. If the field is large enough $H > \frac{H_a}{\sqrt{2}}$, than $I_0 > 0$ for all possible value of $\frac{\omega_H}{\omega_a}$ and asynchronous planar regime is stable. In region in between $\frac{H_a}{2} < H < \frac{H_a}{\sqrt{2}}$, stability of the asynchronous

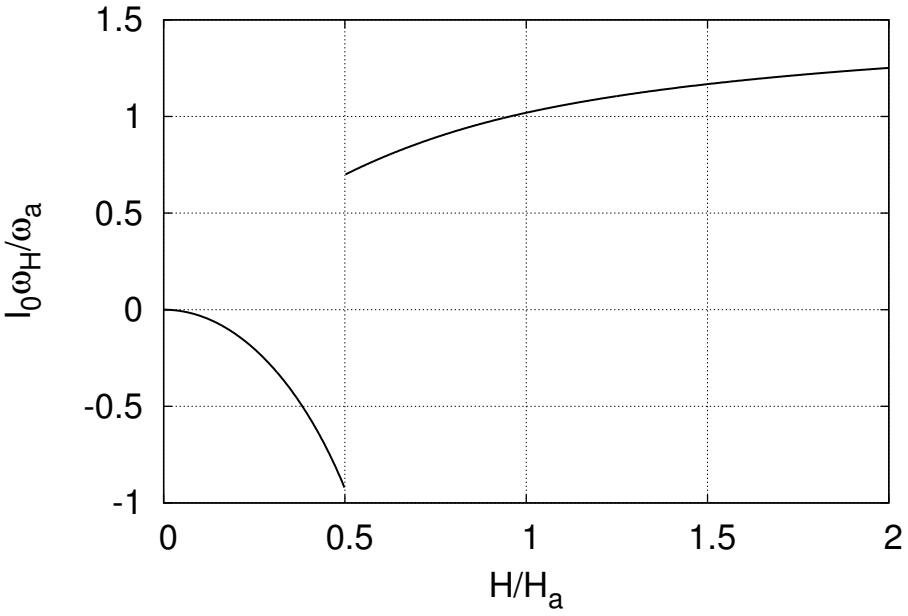

Figure 2.6: Power of Floquet multiplier I_0 at large field frequency $\omega_H \gg \omega_a$ in dependence of magnetic field strength H

planar regime change at some ω_H value, because in this region $I_0 < 0$, when $\omega_H \to \frac{\omega_a}{2}$, and $I_0 > 0$, when $\omega_H \to \infty$. The Octave code for calculation of zero stability line ($I_0 = 0$) is shown in appendix C.1.

Visualization of stability region of asynchronous planar regime can be found in fig. 2.7, where regime is stable in region I and unstable in region II. Solving equation $I_0\left(\frac{\omega_H}{\omega_a}, \frac{H}{H_a}\right) = 0$ for minimal possible value of $H = \frac{H_a}{2}$ in the region with magnetic moment "jumps", it can be found that for $\omega_H > 0.63881\omega_a$ stability changes at line $H = \frac{H_a}{2}$.

Before we go further we should summarize results obtained in sections 2.3.1, 2.3.2, 2.3.3 and 2.4 and draw phase diagram showing only stable regimes. All possible stable regimes is illustrated in fig. 2.8. In regions I, II and III only one of the regimes is stable, but is region IV fig. 2.8 both synchronous precession and asynchronous planar regime are stable. Therefore in region IV both regimes can coexist and which of the regimes will particle approach depends on initial conditions. The dependence on initial condition is shown in fig, 2.9.

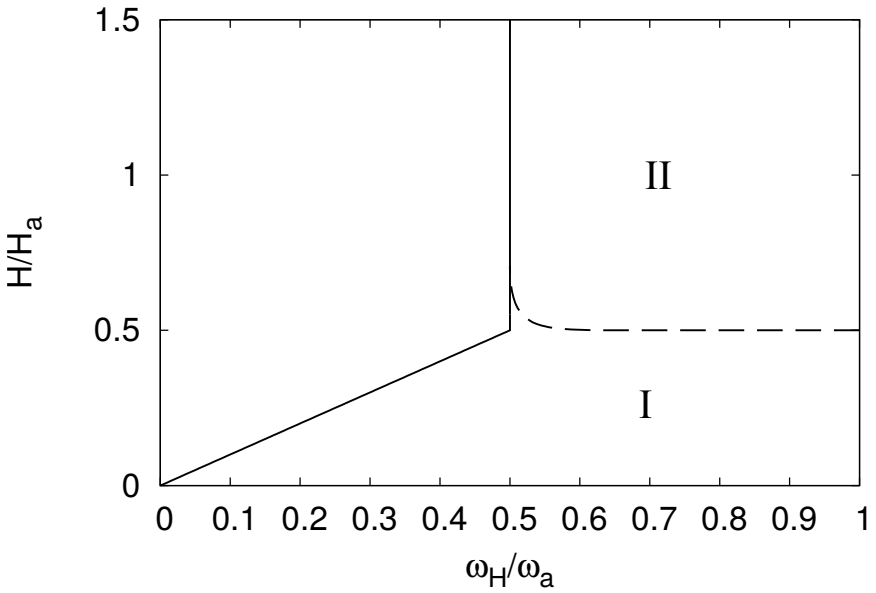

Figure 2.7: Existence region of asynchronous planar regime divided by neutral curve of stability into disjoint regions I and II. The solid line is the boundary of existence of asynchronous planar regime defined; the dashed line is the neutral curve of stability of precession regime defined by sign of I_0 (2.20). Asynchronous planar regime is stable in region II and unstable in region I.

2.5 Special cases

2.5.1 Rigid dipole

If the magnetic field strength is small $H \ll H_a$ then magnetic moment is "frozen" in magnetic particle and rotates with it. Behaviour of such particle can be described by rigid dipole approximation [33]. In the dipole approximation $\vec{e} \| \vec{n}$ and

$$\frac{d\vec{n}}{dt} = \omega_a \frac{H}{H_a}[\vec{h} - \vec{n}(\vec{n} \cdot \vec{h})]$$

These particles have two stable regimes: synchronous planar regime for the slow rotation of magnetic field $\omega_H < \omega_a \frac{H}{H_a} = \frac{mH}{\xi}$ and synchronous precession regime for the fast rotation of magnetic field $\omega_H > \omega_a \frac{H}{H_a}$. For small field strength $H \ll H_a$ stability of precession regime is weak ($\vec{n}'$ decreases with speed $\propto \left(\frac{H}{H_a}\right)^2$, when other variables change with speed $\propto \frac{H}{H_a}$), which means that it takes long time for the particle to get to the stable state.

For rigid dipole in section 2.3.2 found stable solution is center, which means that it is not attractive and not repulsive, but our calculations show

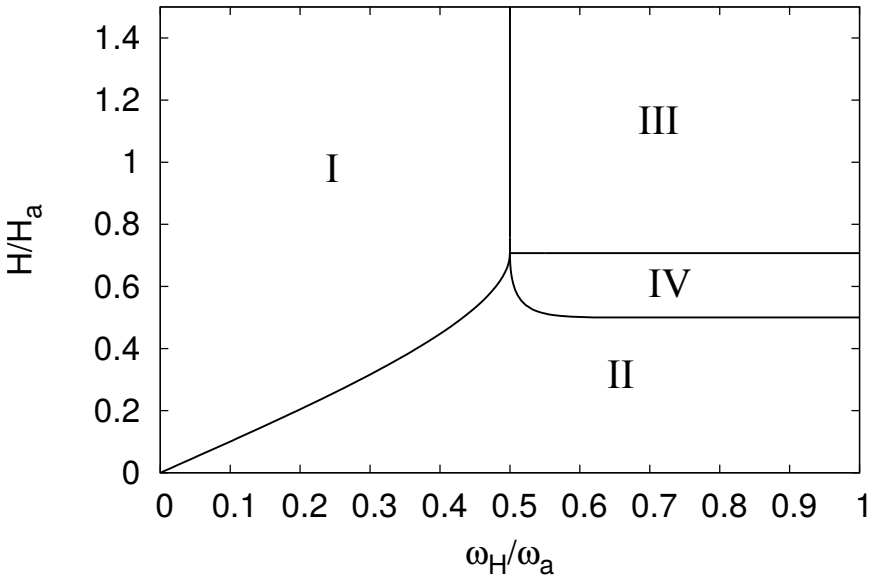

Figure 2.8: Phase diagram. In region I only synchronous planar regime is stable (section 2.3.1), in region II the only stable regime is synchronous precession regime (section 2.3.2), in region III only asynchronous planar regime is stable (section 2.4) and in region IV both synchronous precession and asynchronous planar regime are stable.

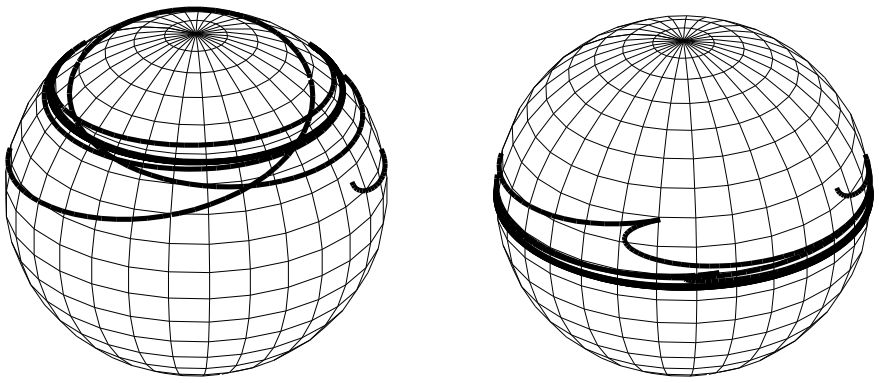

(a) $(\vec{n} \cdot \vec{h}) = 0.939$ and solution approaches the precession regime.

(b) $(\vec{n} \cdot \vec{h}) = 0.943$ and solution approaches the asynchronous planar regime

Figure 2.9: Trajectory of anisotropy axis $\vec{n}$ at $\omega_H = 0.58\,\omega_a$ and $H = 0.52\,H_a$ with starting conditions $\vec{n} \times \vec{h} \perp \vec{e}_H$ and two different $(\vec{n} \cdot \vec{h})$ values.

that, if the anisotropy constant is finite (but not infinite as in rigid dipole model), then center becomes (weakly) attractive.

2.5.2 Superparamagnetic particle

Superparamagnetic particle dynamics is similar to anisotropic particle in the case where $H \gg H_a$. To fit superparamagnetic particle with uniaxial symmetry in our model of single-domain uniaxial anisotropic particle we should use (1.14), from which we can find that torque on magnetic particle is:

$$\vec{M}_m = \vec{m} \times \vec{H} = V\Delta\chi(\vec{H} \cdot \vec{n})[\vec{n} \times \vec{H}] \tag{2.22}$$

It is similar to (2.1) with $\vec{e} \approx \vec{h}$ and $K = \Delta\chi H^2$ (In (2.1) $mH[\vec{e} \times \vec{h}]$ gives uncertainty $\infty \cdot 0$, therefore only first part of the equation should be taken into account). If the dynamic equations are equal then all conclusions made for particle with finite anisotropy energy in high field strength $H \gg H_a$ are applicable for superparamagnetic particle despite that magnetic moments differ.

Superparamagnetic particles have two planar regimes: synchronous with the field if the field frequency is small $\omega_H < \dfrac{\omega_a}{2} = \dfrac{\Delta\chi V H^2}{2\xi}$, where $\Delta\chi = \dfrac{2\pi\chi^2}{1+2\pi\chi}$, and asynchronous with the field if the field frequency is large $\omega_H > \dfrac{\omega_a}{2}$.

More about superparamagnetic particles can be found in chapter 3.

2.6 Energy dissipation

The calculated dynamics of the regimes gives us possibility to calculate dissipated energy and torque on the suspension of ferromagnetic particles in rotating field due to the viscous friction and irreversible "jumps" of the magnetic moment. The energy (1.19) change in time can be calculated as:

$$\frac{dE}{dt} = -mH\frac{d\vec{e}}{dt} \cdot \vec{h} - mH\frac{d\vec{h}}{dt} \cdot \vec{e} - KV(\vec{e} \cdot \vec{n})\frac{d\vec{e}}{dt} \cdot \vec{n} - KV(\vec{e} \cdot \vec{n})\frac{d\vec{n}}{dt} \cdot \vec{e}$$

Using equations (2.1) and (2.2) this equation transforms into

$$\frac{dE}{dt} = -mH\frac{d\vec{e}}{dt} \cdot \left(\vec{h} + \frac{H_a}{H}(\vec{e} \cdot \vec{n})\vec{n}\right) - mH\frac{d\vec{h}}{dt} \cdot \vec{e} - \xi\vec{\omega}_{\vec{n}}^2 \tag{2.23}$$

The first term on the right hand side is energy dissipated due to movement of magnetic moment. Why this is called energy dissipation due magnetic moment movement is explained in appendix A.3. The first term of (2.23) is zero for quasi- static $\frac{d\vec{e}}{dt} = 0$ movement of the magnetic moment in the particle, and gives finite contribution for its irreversible "jumps". The second term of (2.23) is energy supplied by the field to the system and the third term is energy dissipated due to viscous drag. The mean dissipated energy

per unit time can be calculated by averaging over period T (after period system goes to its initial position therefore $\langle \frac{dE}{dt} \rangle = 0$) [54]:

$$Q = \left\langle -mH \frac{d\vec{h}}{dt} \cdot \vec{e} \right\rangle = \xi \langle \vec{\omega}_{\vec{n}}^2 \rangle + \frac{n\Delta E}{T} \ , \tag{2.24}$$

where n is the number of irreversible "jumps" per period (0 or 2) and $\Delta E > 0$ is energy dissipated in the irreversible "jump" of magnetic moment in the particle. $\Delta E = E_1 - E_2$, where E_1 is energy before "jump" and E_2 is energy after "jump". Brackets $\langle\rangle$ defines averaging over period $\langle x(t) \rangle = \frac{1}{T} \int_t^{t+T} x(s)ds$. Here average dissipated energy per unit time Q is introduced.

2.6.1 Synchronous regimes

For the synchronous with the field regimes $\frac{d\vec{h}}{dt} \cdot \vec{e}$ and $\vec{\omega}_{\vec{n}}^2$ are constants and no magnetic moment jumps occur therefore averaging in (2.24) can be omitted and

$$Q = -mH\omega_H(\vec{e}_H \cdot [\vec{h} \times \vec{e}]) = \xi \vec{\omega}_{\vec{n}}^2$$

For synchronous planar regime ($\vec{\omega}_{\vec{n}} = \vec{\omega}_H$)

$$Q = \xi \omega_H^2 \tag{2.25}$$

Using equations (2.1) and (2.11) can be found expression for precession regime:

$$Q = \xi \omega_a^2 \left(\frac{H}{H_a} \right)^2 \left[1 - \left(\frac{H}{H_a} \right)^2 \right] \tag{2.26}$$

2.6.2 Asynchronous regime

From (2.1) in the planar asynchronous case we get

$$\omega_H - \frac{d\alpha}{dt} = \frac{mH}{\xi} (\vec{e} \cdot [\vec{h} \times \vec{e}_H]) \ ,$$

where particle does not rotate with field frequency ω_H but lags a bit in asynchronous regime. From this the mean dissipated energy (2.24) is

$$Q = \left\langle -mH(\vec{\omega}_H \cdot [\vec{h} \times \vec{e}]) \right\rangle = \xi \omega_H^2 \left(1 - \frac{2\pi}{\omega_H T} \right) \ , \tag{2.27}$$

where period T is time in which particle lags behind magnetic field $\vec{h}$ one full cycle ($\alpha(t+T) = \alpha(t) + 2\pi$) therefore $\langle \frac{d\alpha}{dt} \rangle = \frac{2\pi}{T}$. The period is calculated numerically integrating equation (2.19):

$$T = 2 \int_{\alpha_0}^{\alpha_0 + \pi} \frac{d\alpha}{\omega_a \left[\frac{\omega_H}{\omega_a} - f(\cos\alpha, \frac{H_a}{H}) \sin\alpha \right]} \ ,$$

where integral is taken only on the half period, because substitution $\alpha \to \alpha + \pi$ does not change function under integral sign in the region $H > \frac{H_a}{2}$. Similar to (2.21) it is better to take α_0 so that invertible "jumps" of the magnetic moment are on the boundary of the integral and integration is made over continuous function, because numerical integration can fail on discontinuities.

In the region $H > H_a$, where no magnetic moment "jumps" occur, period T can be calculated similar to rotational period of superparamagnetic particle [47], [13]:

$$T = \frac{2\pi}{\sqrt{\omega_H^2 - \left(\frac{\omega_a}{2}\right)^2}} \tag{2.28}$$

therefore

$$Q = \xi\omega_H^2 \left[1 - \sqrt{1 - \left(\frac{\omega_a}{2\omega_H}\right)^2}\right] \tag{2.29}$$

In the region $\frac{H_a}{2} < H < H_a$, where magnetic moment "jumps" in the particle occur, dissipated energy can be analytically calculated [47] but the result is hard to interpret so in this work period T is found numerically. But in this region dissipated energy can be divided into two parts: $Q = Q_v + Q_m$, where

$$Q_v = \xi \left\langle \vec{\omega}_{\vec{n}}^2 \right\rangle$$

is energy dissipated by viscous drag and

$$Q_m = \frac{2\Delta E}{T} \tag{2.30}$$

is energy dissipated by magnetic moment "jumps".

2.6.3 Numerical results and asymptotes

To express Q_v in form for numerical calculations we use (2.18), where $|\vec{\omega}_{\vec{n}}| = \omega_H - \dot{\alpha}$ and in planar regime it can be calculated as $|\vec{\omega}_{\vec{n}}| = \omega_a f(\cos\alpha, \frac{H_a}{H}) \sin\alpha$ therefore:

$$\begin{aligned} Q_v &= \frac{2\xi\omega_a^2}{T} \int_{\alpha_0}^{\alpha_0+\pi} \frac{f^2\left(\cos\alpha, \frac{H_a}{H}\right)\sin^2\alpha}{1 - f\left(\cos\alpha, \frac{H_a}{H}\right)\sin\alpha} d\alpha = \\ &= \xi\omega_a^2 \left(1 - \frac{2\pi}{T} + \frac{2}{T} \int_{\alpha_0}^{\alpha_0+\pi} f\left(\cos\alpha, \frac{H_a}{H}\right)\sin\alpha \, d\alpha\right) \end{aligned}, \tag{2.31}$$

where the last term on the right hand side is not zero only in the region where magnetic moment "jumps" occur ($\frac{H_a}{2} < H < H_a$). Period T is calculated from (2.28).

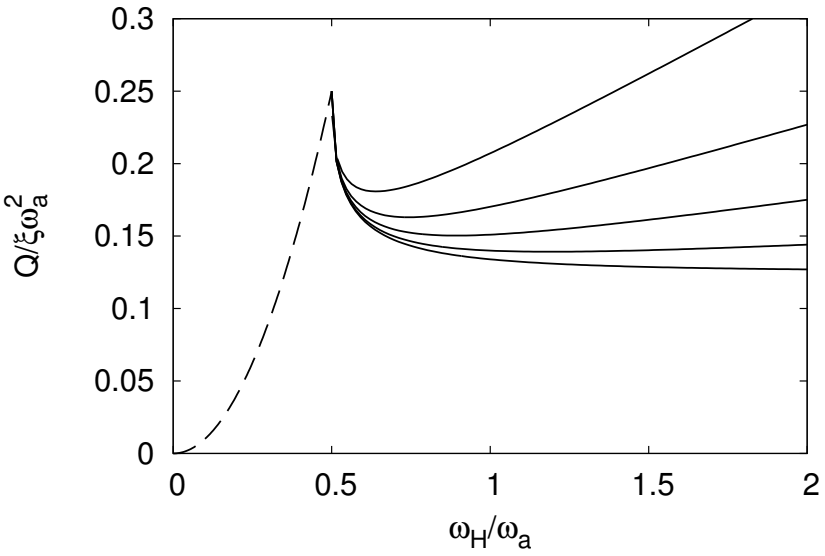

Figure 2.10: Average dissipated energy in synchronous and asynchronous planar regime per unit time in dependence of field frequency for field strength $\frac{H}{H_a}$ 0.55; 0.65; 0.75; 0.85; 1. Field strength is increasing in downward direction. Solid line is dissipated energy in asynchronous planar regime and dashed line - in synchronous planar regime.

According to [13] in the region $\frac{H_a}{2} < H < H_a$, where magnetic moment "jumps" occur, at the limit $\omega_H \gg \omega_a$ the rotational period can be calculated as:

$$T = \frac{2\pi}{\omega_H} + \frac{2\Delta E}{\xi \omega_H^2}$$

Putting this in (2.27) gives:

$$Q = \frac{\omega_H \Delta E}{\pi} = \frac{2\Delta E}{T_H} \tag{2.32}$$

which means that main dissipation in limit $\omega_H \gg \omega_a$ is due to magnetic moment "jumps". Here T_H is period of rotating magnetic field and ΔE is dissipated energy in one magnetic moment "jump". This result can be seen in figure 2.10, where graphs look linear for high $\frac{\omega_H}{\omega_a}$.

In the asynchronous planar region without magnetic moment "jumps" ($H > H_a$) in the limit $\omega_H \gg \omega_a$ equation (2.29) changes into

$$Q = \frac{\xi \omega_a^2}{8} \tag{2.33}$$

which also can be seen in figure 2.10 for $H = H_a$. This dissipation is due to viscous drag, because no magnetic moment "jumps" occur in region $H > H_a$

and no other dissipation is available. It should be reminded that we assumed that drag on magnetic moment inside particle is negligible, which makes it possible to separate magnetic moment movement from particle movement. If the rotational frequency becomes too large, relaxation of magnetic moment inside particle becomes comparable to particle speed therefore our model is not usable for very high frequencies.

If H is less but close to H_a as seen from fig. 2.10 dissipated energy is close to (2.29), where $H > H_a$ and all dissipated energy is due to viscous drag. This is because in limit $H \to H_a - 0$ energy difference ΔE before and after magnetic moment "jump" becomes small. If $H = H_a$ energy difference $\Delta E = 0$ and no magnetic moment "jumps" occur. For $H > H_a$ dissipated energy does not depend on magnetic field (2.29).

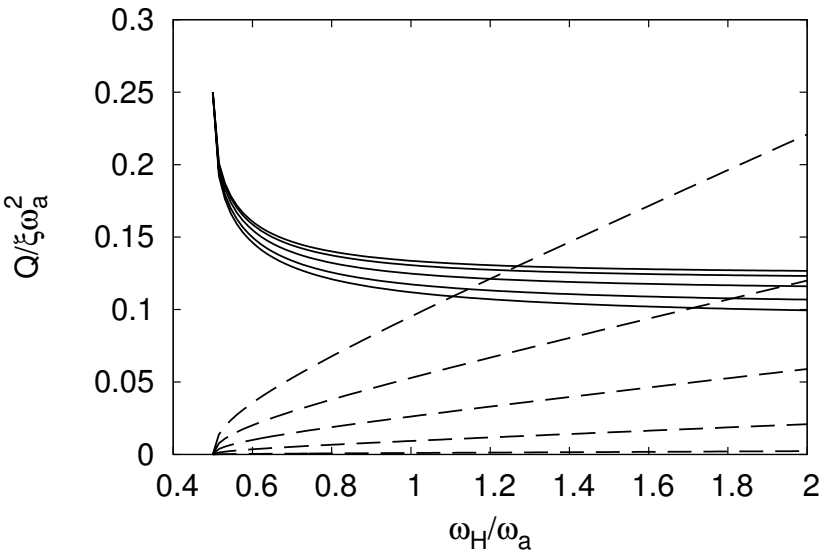

Figure 2.11: Comparison of average dissipated energy in asynchronous planar regime per unit time in dependence of field frequency for field strength $\frac{H}{H_a}$ 0.55; 0.65; 0.75; 0.85; 0.95. Solid line is dissipated energy by viscous drag (2.31) and field strength is increasing in upward direction. Dashed line is dissipated energy in magnetic moment "jumps" inside the particle (2.30) and magnetic field strength is increasing in downward direction.

In synchronous regimes all dissipated energy is due to viscous drag, but in asynchronous regime if the field strength is in range $\frac{H_a}{2} < H < H_a$, part of the energy is dissipated inside the particle due to magnetic moment "jumps". As can be seen in fig. 2.11 average dissipated energy by viscous drag in asynchronous planar regime does not change a lot in dependence of magnetic field, just increase a bit if the field strength increases. This is because

magnetic moment jumps only slightly effects particle movement. Whereas dissipated energy by magnetic moment "jumps" dramatically decrease with increase of magnetic field strength. This is because of decrease of energy "barrier" with increase of magnetic field. On the one hand if the magnetic field strength is higher than anisotropy field H_a the "barrier" disappears and no magnetic moment "jumps" are possible. On the other hand if the magnetic field strength is below limit $\frac{H_a}{2}$ the energy "barrier" is so high that magnetic moment stays in one of the minimums and magnetic field can not decrease it low enough to make magnetic moment to "jump" to second minimum.

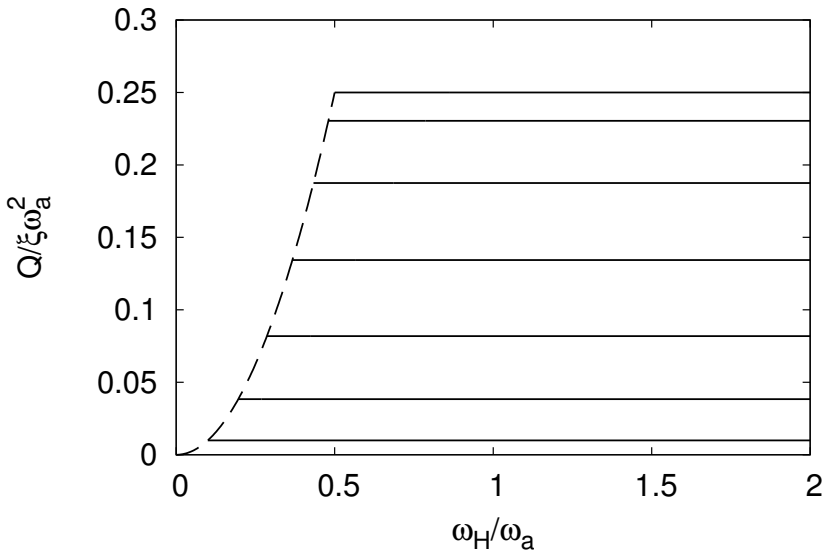

Figure 2.12: Average dissipated energy in synchronous planar and precession regime per unit time in dependence of field frequency for field strength $\frac{H}{H_a}$ 0.1; 0.2; 0.3; 0.4; 0.5; 0.6; 0.7. Field strength is increasing in upward direction. Solid line is dissipated energy in synchronous precession regime and dashed line - in synchronous planar regime.

If $H < \frac{H_a}{\sqrt{2}}$ besides asynchronous planar regime synchronous precession regime is possible. It can be seen in fig. 2.12 and from (2.26) that dissipation per unit time in precession regime does not depend on frequency, but depends only on magnetic field strength H.

Overview of possible dissipation graphs in dependence of field frequency is shown in fig. 2.13. If the field strength $H < \frac{H_a}{2}$ only synchronous planar and precession regime is stable. If the field strength $H > \frac{H_a}{\sqrt{2}}$ only synchronous and asynchronous planar regimes are stable, where in the region $\frac{H_a}{\sqrt{2}} < H < H_a$ magnetic moment "jumps" are possible and dissipated energy

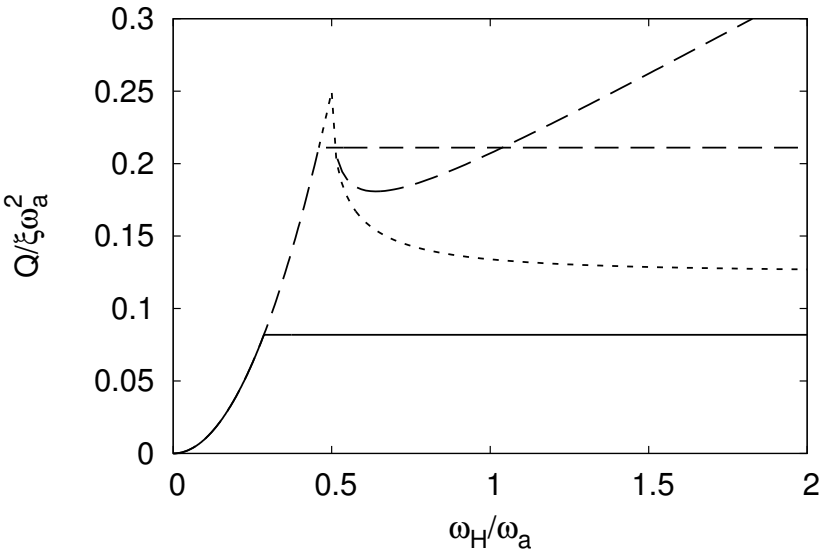

Figure 2.13: Average dissipated energy per unit time for stable states in the dependence of field frequency for some field strengths. Solid line - field strength $H = 0.3H_a$; short dashed line -field strength $H \geq H_a$; long dashed line - field strength $H = 0.55H_a$. In the range $\frac{\omega_H}{\omega_a} > 0.52$ two long dashed lines is depicted because there precession and asynchronous planar regimes coexist.

increases with the field frequency (for large frequencies), but if $H \geq H_a$ only short dashed graph of fig. 2.13 is possible and dissipated energy is independent of magnetic field strength.

In the region $\frac{H_a}{2} < H < \frac{H_a}{\sqrt{2}}$ all three stable regimes in dependence of the frequency are possible (long dashed line in fig. 2.13). For small frequencies synchronous planar regime. When synchronous planar regime becomes unstable, precession regime becomes stable and for higher frequencies $\omega_H > \omega_H^*$, where ω_H^* is given by neutral curve of stability of asynchronous planar regime, asynchronous planar regime becomes stable without destroying stability of precession regime. That is why two long dashed lines are shown in fig. 2.13.

Similar graphs for field strength H is shown in fig. 2.14. In region $\omega_H^* < \omega_H < \frac{\omega_a}{\sqrt{2}}$ asynchronous planar and precession regimes coexist and dissipated energies differ in both regimes (ω_H^* is given by line $I_0\left(\frac{\omega_H}{\omega_a}, \frac{H}{H_a}\right) = 0$ (2.21)). Which of the regimes will be obtained mainly depends on the particle position in the moment, when given parameter combination is set. If the magnetic field strength increases keeping field frequency constant, then particle will stay in precession regime while $\omega_H < \frac{\omega_a}{\sqrt{2}}$. Sometimes we

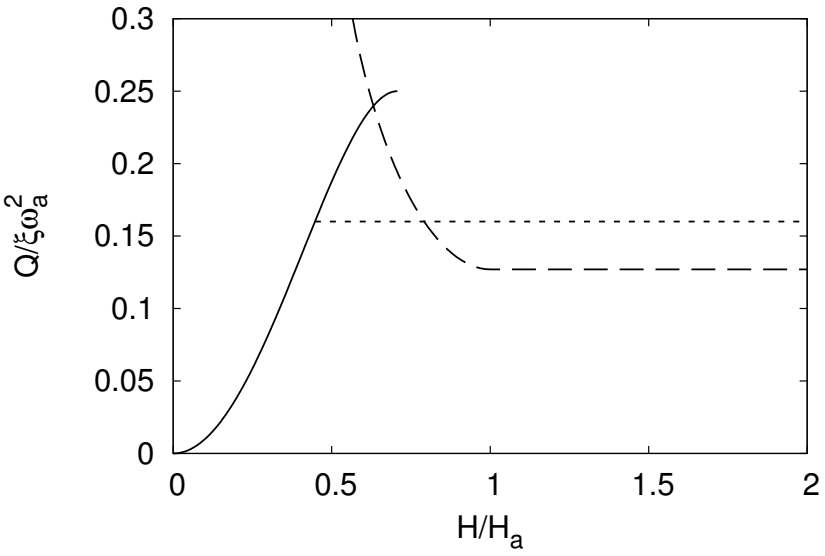

Figure 2.14: Average dissipated energy per unit time for stable states in the dependence of field strength for two different frequencies. Solid line is dissipated energy in precession regime (independent of frequency); long dashed line is dissipated energy in asynchronous planar regime for $\omega_H = 2\,\omega_a$; short dashed line is dissipated energy in synchronous planar regime for $\omega_H = 0.4\,\omega_a$.

want to increase dissipation. This can be achieved by getting particle to asynchronous planar regime and then to the region with magnetic moment "jumps" ($\frac{H_a}{2} < H < H_a$). The calculation of time, how long particle will stay in the regime with higher dissipation, depends on thermal fluctuations and is outside the scope of this work.

2.6.4 Comparison with experiment

In experiments dissipated energy and the rotational hysteresis usually are studied by measurements of the torque on a suspension as a function of the rotating field strength [45]. Average torque $\langle\tau\rangle$ is related to average dissipated energy per unit time Q by relation:

$$Q = \langle\tau\rangle\omega_H$$

In fig. 2.15 is shown comparison of theoretical results shown in fig. 2.14 with experimental results of $0.1\,\mu m$ $\gamma{-}Fe_2O_3$ particles found in [41, 42]. In fig. 2.15 it can be seen that torque curve for small fields in [41, 42] can be very well fitted by the dissipated energy in precession regime. While high field strength limit fits badly to the experiment. This could

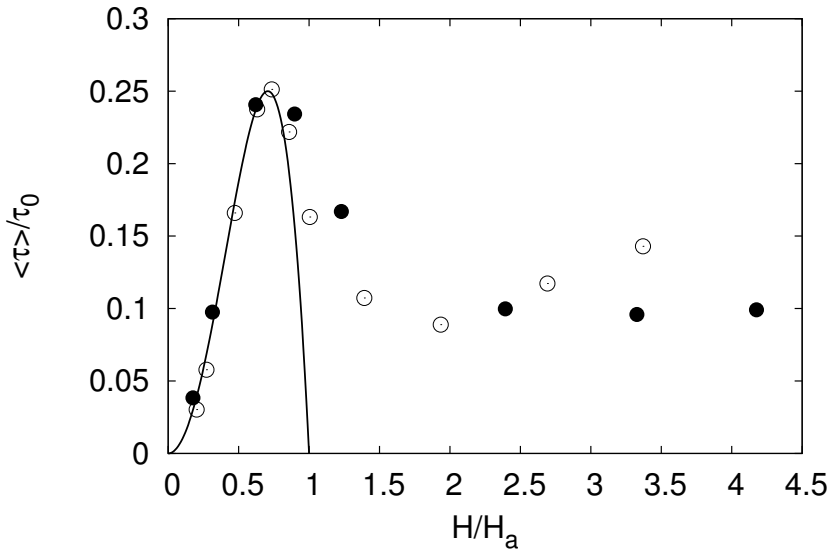

Figure 2.15: Average torque of suspension of 0.1 μm size $\gamma-Fe_2O_3$ particles dependence on magnetic field strength at field frequency $\omega_H = 26.2 \frac{rad}{s}$. Particle volume concentration is 10%. Experimental results shown as open circles [60] and full circles [61]. Solid line - torque on particles in precession regime (2.26).

be because all particles is not identical therefore not all particles are single domain. As shown by Butler and Banerjee [20] the size limit of single-domain state is narrow for cubic particles and becomes larger only for elongated particles. Therefore it is possible that in [41, 42] one part of the particles is multi domain, one part is superparamagnetic and one part is single-domain particles. In this work only single-domain and superparamagnetic particles are studied. The behaviour of multi domain particle is outside the scope of this work.

Approximating experimental data with dissipated energy in precession regime (2.26) gives that maximum is at $H \approx 0.7\, H_a$, what gives $H_a \approx 1.1\, kOe$ for [42] and $H_a \approx 0.9\, kOe$ for [41]. From [32] we get $M_S = 390 \frac{G}{cm^3}$ and, if particle is rod like, then $H_a = \frac{K}{M_S} = 2\pi M_S = 2.4\, kOe$, where K is taken from (1.11). Theoretical result is more than 2 times larger than experimentally observed what means that some effects related to experiment are not accounted for theoretical model.

In experiments [41, 42] the maximum of torque curve of liquid suspension is found at approximately the same value of magnetic field strength as for the solidified suspension what gives evidence that the maximum is due to the magnetic moment "jumps" inside the particle. Maximum of the torque curve due to magnetic moment "jumps" from theory is at $H = 0.5\, H_a$, what

gives $H_a \approx 1.5\,kOe$ for [42] and $H_a \approx 1.3\,kOe$ for [41]. These values is closer to theoretical $H_a = 2.4\,kOe$ but still smaller.

Chapter 3

Dynamics of superparamagnetic particle in precessing magnetic field

3.1 Motivation and contents

Recent advances in anisotropic magnetic particle colloids [81] shows that superparamagnetic particles are widely used and their dynamics in different magnetic field configurations have interest by scientists. Mainly theoretical dynamics of the superparamagnetic particle in precessing field are calculated numerically [85] and only in few papers analytic calculations of the dynamics of superparamagnetic particle in precessing field can be found [82, 29]. But analytic results found in [82] and [29] can be noticeably improved.

In this chapter stability of synchronous with the precessing magnetic field regimes of the superparamagnetic particle will be calculated. It will be shown what is common and what is different for prolate and oblate spheroidal superparamagnetic particles. Analytic equation of the mean angular velocity of the particle in asynchronous regime will be shown, which includes solutions of cubic equation. The visible length of the particle in synchronous regime will be calculated. Experimentally observable results will be compared to theoretical and form-factor of the particles will be calculated.

3.2 Model

Superparamagnetic particle with uniaxial symmetry has magnetic moment (1.14) $\vec{m} = V\chi_\perp \vec{H} + V\Delta\chi(\vec{H}\cdot\vec{n})\vec{n}$ in external magnetic field $\vec{H} = H\vec{h}$. Then magnetic torque which works on superparamagnetic particle is

$$\vec{\tau}_M = \vec{m} \times \vec{H} = VH^2\Delta\chi(\vec{n}\cdot\vec{h})\,\vec{n}\times\vec{h}$$

In the inertialess limit magnetic torque should be compensated by viscous drag $\vec{\tau}_v = -\xi\omega_{\vec{n}}$. Using relation $\dot{\vec{n}} = \omega_{\vec{n}} \times \vec{n}$ the equation of motion can be written as:

$$\frac{d\vec{n}}{dt} = \omega_a(\vec{n}\cdot\vec{h})\left[\vec{h} - (\vec{n}\cdot\vec{h})\vec{n}\right] \ , \tag{3.1}$$

where $\omega_a = \dfrac{V\Delta\chi H^2}{\xi}$ same as in section 2.5.2. Equation (3.1) is equivalent to (2.4) in high field limit $H \gg H_a$ as mentioned in section 2.5.2.

The sign of ω_a is determined by the sign of $\Delta\chi = \chi_\parallel - \chi_\perp$. For prolate particles $\Delta\chi > 0$ (1.15) and $\omega_a > 0$ but for oblate particles $\Delta\chi < 0$ (1.16) and $\omega_a < 0$. The equations does not change with the change of the sign of ω_a, but some conclusions will differ between prolate and oblate particles and will be mentioned further.

In this chapter $\vec{h}$ precesses around direction $\vec{e}_H$ with angular velocity ω_H ($\dot{\vec{h}} = \omega_H\vec{e}_H \times \vec{h}$) and precessing angle is ϑ ($\vec{e}_H \cdot \vec{h} = \cos\vartheta$). In precessing magnetic field superparamagnetic particle can move synchronously and asynchronously with the field in the dependence of field frequency $\frac{\omega_H}{\omega_a}$ and precessing angle ϑ. Further the parameters and stability of synchronous regime will be found.

3.3 Synchronous with the field regime

Particle will rotate synchronously with the field if it has the same angular frequency $\dot{\vec{n}} = \omega_H\vec{e}_H \times \vec{n}$. Therefore synchronous regime should satisfy:

$$\omega_H[\vec{e}_H \times \vec{n}] = \omega_a(\vec{n}\cdot\vec{h})[\vec{h} - (\vec{n}\cdot\vec{h})\vec{n}] \tag{3.2}$$

Scalar multiplication of (3.2) by $\vec{e}_H$, $\vec{h}$ and $[\vec{e}_H \times \vec{n}]$ gives consequently:

$$\vec{h}\cdot\vec{e}_H = (\vec{n}\cdot\vec{h})(\vec{n}\cdot\vec{e}_H) \tag{3.3}$$

$$\vec{e}_H\cdot[\vec{n}\times\vec{h}] = \frac{\omega_a}{\omega_H}(\vec{n}\cdot\vec{h})\left[1 - (\vec{n}\cdot\vec{h})^2\right] \tag{3.4}$$

$$1 - (\vec{n}\cdot\vec{e}_H)^2 = \frac{\omega_a}{\omega_H}(\vec{n}\cdot\vec{h})(\vec{e}_H\cdot[\vec{n}\times\vec{h}]) \ . \tag{3.5}$$

By eliminating $(\vec{e}_H\cdot[\vec{n}\times\vec{h}])$ and $\vec{n}\cdot\vec{e}_H$ from (3.3), (3.4) and (3.5) we get bi-cubic equation for $\vec{n}\cdot\vec{h}$:

$$(\vec{n}\cdot\vec{h})^6 - (\vec{n}\cdot\vec{h})^4 + \frac{\omega_H^2}{\omega_a^2}(\vec{n}\cdot\vec{h})^2 - \frac{\omega_H^2}{\omega_a^2}(\vec{h}\cdot\vec{e}_H)^2 = 0 \tag{3.6}$$

For simplicity parameters $y = (\vec{n}\cdot\vec{h})^2$, $\omega = \dfrac{\omega_H}{\omega_a}$ and $\sigma = \vec{h}\cdot\vec{e}_H$ are introduced. Further the cubic equation

$$f(y) = y^3 - y^2 + \omega^2 y - \omega^2\sigma^2 = 0 \tag{3.7}$$

will be examined.

The last term of left hand side of (3.7) is negative, what means that product of all roots is positive [1], therefore at least one root is positive (if the other two roots is complex then they are complex conjugate to each other and their product is positive). Therefore bi-cubic equation (3.6) has solution for all ω_H and ϑ.

Equation (3.6) does not change if the sign of the ω_a is changed, what gives that equal synchronous with the field states exist for prolate ($\omega_a > 0$) and oblate ($\omega_a < 0$) particles. The only difference is stability of these states, which should depend on ω_a.

3.4 Stability of the synchronous regime

In order to investigate stability of synchronous regime we introduce small perturbation $\vec{\varepsilon}$ from the synchronous state $\vec{n}$. Since $\vec{n}$ is unit vector and its length can not change $\vec{\varepsilon}$ should be perpendicular to $\vec{n}$ and can be written in form:

$$\vec{\varepsilon} = \varepsilon_1[\vec{n} \times \vec{h}] + \varepsilon_2[\vec{e}_H \times \vec{n}] \ , \tag{3.8}$$

where ε_1 and ε_2 are small perturbations in two non-collinear directions.

After some arithmetical manipulations shown in appendix A.4 we can find time dependence of $\vec{\varepsilon}$ (A.10)

$$\begin{cases} \dfrac{d\varepsilon_1}{dt} = -\omega_a(\vec{n}\cdot\vec{h})^2\varepsilon_1 - \omega_a(\vec{e}_H\cdot\vec{n})(\vec{n}\cdot\vec{h})\varepsilon_2 \\ \dfrac{d\varepsilon_2}{dt} = \dfrac{\omega_H^2}{\omega_a}\dfrac{(\vec{e}_H\cdot\vec{n})}{(\vec{n}\cdot\vec{h})}\varepsilon_1 + \omega_a\left(2-(\vec{n}\cdot\vec{h})^2\right)\varepsilon_2 \end{cases} \tag{3.9}$$

The stability of the regime is determined by eigenvalues of Jacobi matrix J [80], where J is found in (3.9)

$$\begin{pmatrix} \dot{\varepsilon}_1 \\ \dot{\varepsilon}_2 \end{pmatrix} = J \begin{pmatrix} \varepsilon_1 \\ \varepsilon_2 \end{pmatrix}$$

The eigenvalues of Jacobi matrix are:

$$\lambda_{1,2} = \omega_a \frac{\tau \pm \sqrt{\tau^2 - 4\Delta}}{2} \ , \tag{3.10}$$

where

$$\tau = 1 - 3(\vec{n}\cdot\vec{h})^2 \tag{3.11}$$

is trace of J divided by ω_a and

$$\Delta = \left(\frac{\omega_H}{\omega_a}\right)^2 - 2(\vec{n}\cdot\vec{h})^2 + 3(\vec{n}\cdot\vec{h})^4 \tag{3.12}$$

is determinant of J divided by ω_a^2, where $(\vec{e}_H \cdot \vec{n})$ is excluded using (3.4) and (3.5).

It can be seen from (3.10) that stability of stationary nodes changes as changes the sign of ω_a. Therefore if the state is stable for prolate particle ($\omega_a > 0$) then it is unstable for oblate particle ($\omega_a < 0$) and if the state is stable for oblate particle then it is unstable for prolate particle. The opposite is not always true, because (unstable) saddle points stay saddle points when sign of ω_a is changed.

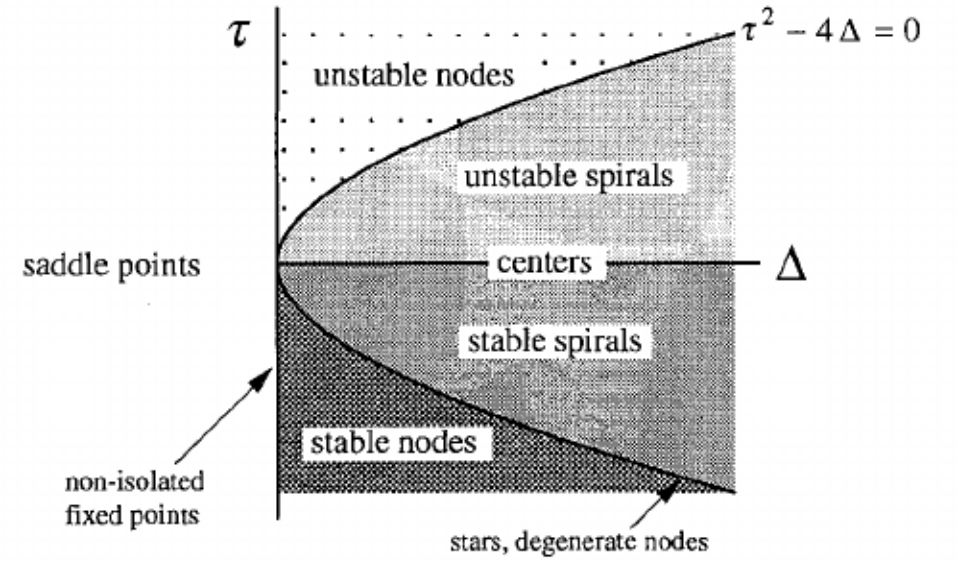

Figure 3.1: Stability of prolate particle in dependence of τ and Δ. Depicted from [67].

Before we continue we will compare found values of τ (3.11) and Δ (3.12) with properties of cubic equation.

The derivative of $f(y)$ (3.7) looks equal to Δ (3.12):

$$\frac{df(y)}{dy} = \omega^2 - 2y + 3y^2 = \Delta$$

Similarly can be found that τ (3.11) is equal to second derivative of $f(y)$ (3.7) with precision to constant:

$$\tau = 1 - 3y = -\frac{1}{2}\frac{d^2 f(y)}{dy^2}$$

therefore it is sufficient to look at first and second derivative of function $f(y)$ (3.7) at its roots $f(y) = 0$ to examine the stability of synchronous state and synchronous regime (which consists of all possible states). The possibilities of τ and Δ and consequences of the state $f(y) = 0$ are following:

- If $\tau < 0$ ($\frac{d^2f}{dy^2} > 0$) and $\Delta > 0$ ($\frac{df}{dy} > 0$), then $\frac{\lambda_1}{\omega_a} < 0$ and $\frac{\lambda_2}{\omega_a} < 0$ (3.10), therefore prolate particle ($\omega_a > 0$) is stable in this state, but oblate particle ($\omega_a < 0$) is unstable in this state.

- If $\tau > 0$ ($\frac{d^2f}{dy^2} < 0$) and $\Delta > 0$ ($\frac{df}{dy} > 0$), then $\frac{\lambda_1}{\omega_a} > 0$ and $\frac{\lambda_2}{\omega_a} > 0$ (3.10), therefore prolate particle ($\omega_a > 0$) is unstable in this state, but oblate particle ($\omega_a < 0$) is stable in this state.

- If $\Delta < 0$ ($\frac{df}{dy} < 0$), then $\frac{\lambda_1}{\omega_a} > 0$ and $\frac{\lambda_2}{\omega_a} < 0$ (3.10) and it is saddle point, therefore both prolate particle ($\omega_a > 0$) and oblate particle ($\omega_a < 0$) are unstable in this state.

These results can be summarized in fig. 3.1 for prolate particle. For oblate particle the sign of τ changes, because ω_a is taken out from τ in (3.10).

The coefficient at y^3 term (3.7) is positive, therefore $f(y)$ is mainly increasing and if there is only one root of $f(y) = 0$, then $\frac{df}{dy} > 0$ at this root. Then the stability of the only root is determined by $\frac{d^2f}{dy^2}$ and stability changes at $\frac{d^2f}{dy^2} = 0$, which gives $y = (\vec{n} \cdot \vec{h})^2 = \frac{1}{3}$. Putting this in $f(y) = 0$ (3.7) gives condition of neutral stability curve:

$$\omega^2 = \left(\frac{\omega_H}{\omega_a}\right)^2 = \frac{2}{9\left(1 - 3(\vec{h} \cdot \vec{e}_H)^2\right)} \tag{3.13}$$

It can be seen that (3.13) has solution only if $\vec{h} \cdot \vec{e}_H = \sigma < \frac{1}{\sqrt{3}}$. If $\sigma > \frac{1}{\sqrt{3}}$ then $f(y) = 0$ (3.7) has one root with $\frac{d^2f}{dy^2} > 0$, what means that prolate particle ($\omega_a > 0$) is stable and oblate particle ($\omega_a < 0$) is unstable.

If the equation $f(y) = 0$ has 3 roots, then between these 3 real roots one must have $\frac{df}{dy} > 0$ and $\frac{d^2f}{dy^2} < 0$, one must have $\frac{df}{dy} > 0$ and $\frac{d^2f}{dy^2} > 0$ and one must have $\frac{df}{dy} < 0$, which are between first two. therefore both particles prolate $\omega_a > 0$ and oblate $\omega_a < 0$ have one stable state if $f(y) = 0$ has 3 real roots. The equation (3.7) has 3 real solution if [1]:

$$18\omega^4\sigma^2 - 4\omega^2\sigma^2 + \omega^4 - 4\omega^6 - 27\omega^4\sigma^4 > 0$$

Which gives quadratic inequality for ω^2 (because $\omega^2 > 0$):

$$4\omega^4 - \omega^2(1 + 18\sigma^2 - 27\sigma^4) + 4\sigma^2 < 0 \tag{3.14}$$

This inequality has solution only if

$$(1 + 18\sigma^2 - 27\sigma^4)^2 - 64\sigma^2 = (1 - 9\sigma^2)^3(1 - \sigma^2) > 0$$

or simply

$$\cos\vartheta = (\vec{h} \cdot \vec{e}_H) = \sigma < \frac{1}{3} , \tag{3.15}$$

because $\sigma < 1$ and $(\sigma^2 - 1) < 0$. If $0 < \sigma^2 < \frac{1}{9}$ we can check that $1 + 18\sigma^2 - 27\sigma^4 > 0$ (3.14) has two positive roots. Therefore (3.7) has three solutions if $0 < \sigma < \frac{1}{3}$ and $\omega_1(\sigma) < \omega < \omega_2(\sigma)$, where

$$\omega_{1,2}(\sigma) = \sqrt{\frac{1 + 18\sigma^2 - 27\sigma^4 \pm \sqrt{(1 - 9\sigma^2)^3(1 - \sigma^2)}}{8}} , \tag{3.16}$$

where ω_1 has minus sign and ω_2 has plus sign in $\pm$ (3.16).

3.5 Phase diagram

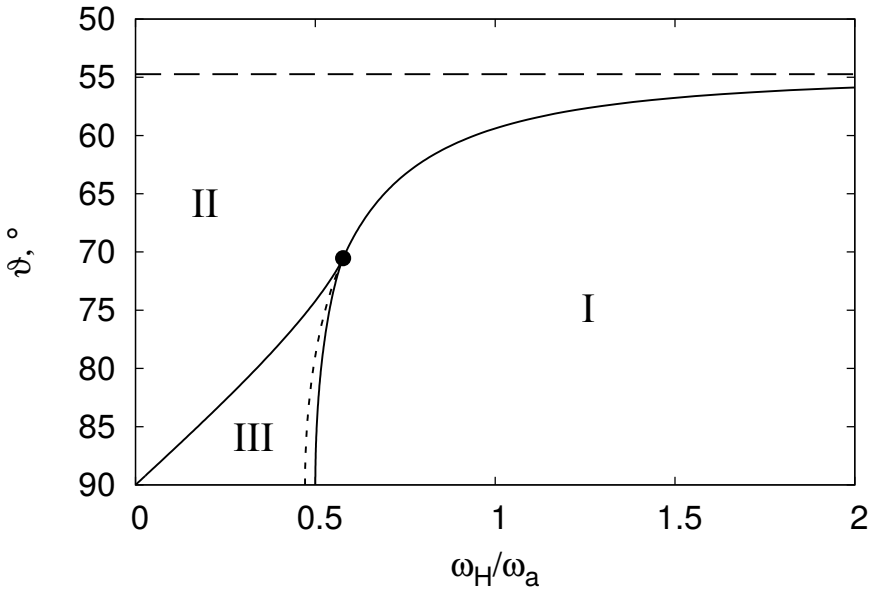

Figure 3.2: Phase diagram. The prolate particle has a stable synchronous regime in region $II \bigcup III$, and the oblate particle in region $I \bigcup III$. The regions is divided by the neutral stability (solid) line. Long dashed line is asymptote at $\frac{\omega_H}{\omega_a} \to \infty$ and short dashed line is extension of line (3.13) in the region where equation $f(y) = 0$ has three real roots. The point shows a codimension-2 bifurcation point.

To summarize obtained results the phase diagram is drawn in fig. 3.2. In the region II prolate particle has stable synchronous with the field state

and oblate particle does not, therefore oblate particle moves asynchronously in this region. In region I oblate particle moves synchronously and prolate particle moves asynchronously. In the region III both particles has stable synchronous states, therefore both particles moves synchronously with the field. The region II is extended above long dashed line fig. 3.2 till $\vartheta = 0$.

Long dashed line in fig. 3.2 is asymptote $\vartheta = \arccos\frac{1}{\sqrt{3}} \approx 54.7^o$ above which prolate particle has synchronous regime for all values of ω_H and oblate particle moves asynchronously for all values of ω_H.

Short dashed line in fig. 3.2 is extension of line (3.13) in the region where equation $f(y) = 0$ has three roots. As can be seen this line is close to prolate particle neutral stability line. If too high accuracy is not necessary it is sufficient to use (3.13) for prolate particle for all ϑ range (at $\cos\vartheta = 0$ (3.13) gives neutral point at $\frac{\omega_H}{\omega_a} = \frac{\sqrt{2}}{3}$, which is close to true value $\frac{\omega_H}{\omega_a} = 0.5$ (3.16)).

The dark point in fig. 3.2 is point where $f(y) = 0$, $\dfrac{df}{dy} = 0$ and $\dfrac{d^2f}{dy^2} = 0$. Its coordinates are $\frac{\omega_H}{\omega_a} = \frac{1}{\sqrt{3}} \approx 0.58$ and $\vartheta = \arccos\frac{1}{3} \approx 70.5^o$. In stability analysis it is called codimension-2 bifurcation [80] because at this point the only node with neutral stability splits into one saddle point and two nodes with different stability.

The phase diagram (fig. 3.2) can also be found in authors article [26], where the neutral stability lines and codimension-2 bifurcation point are calculated numerically.

In experiments instead of changing angle ϑ it is easier to fix the rotating part of the field strength H_r and change only the non rotating part $H_\omega = \vec{H}\cdot\vec{e}_H$. Here $H^2 = H_r^2 + H_\omega^2$. Then the total field strength H changes and a new constant parameter $\omega_c = \omega_a\dfrac{H_r^2}{H^2}$ should be introduced. Then neutral line of stability at $\frac{1}{2\sqrt{2}} < \frac{H_\omega}{H_r} < \frac{1}{\sqrt{2}}$ ($\frac{1}{3} < \sigma < \frac{1}{\sqrt{3}}$) (3.13) changes into:

$$\frac{\omega_H}{\omega_c} = \sqrt{\frac{2\left(1+\dfrac{H_\omega^2}{H_r^2}\right)^3}{9\left(1-2\dfrac{H_\omega^2}{H_r^2}\right)}} \tag{3.17}$$

and for $0 < \frac{H_\omega}{H_r} < \frac{1}{2\sqrt{2}}$ ($0 < \sigma < \frac{1}{3}$)we have neutral stability lines (3.16) at

$$\frac{\omega_H}{\omega_c} = \sqrt{\frac{1+20\left(\dfrac{H_\omega}{H_r}\right)^2 - 8\left(\dfrac{H_\omega}{H_r}\right)^4 \pm \sqrt{\left[1-8\left(\dfrac{H_\omega}{H_r}\right)^2\right]^3}}{8}}, \tag{3.18}$$

where plus sign is for prolate particle and minus sign is for oblate particle.

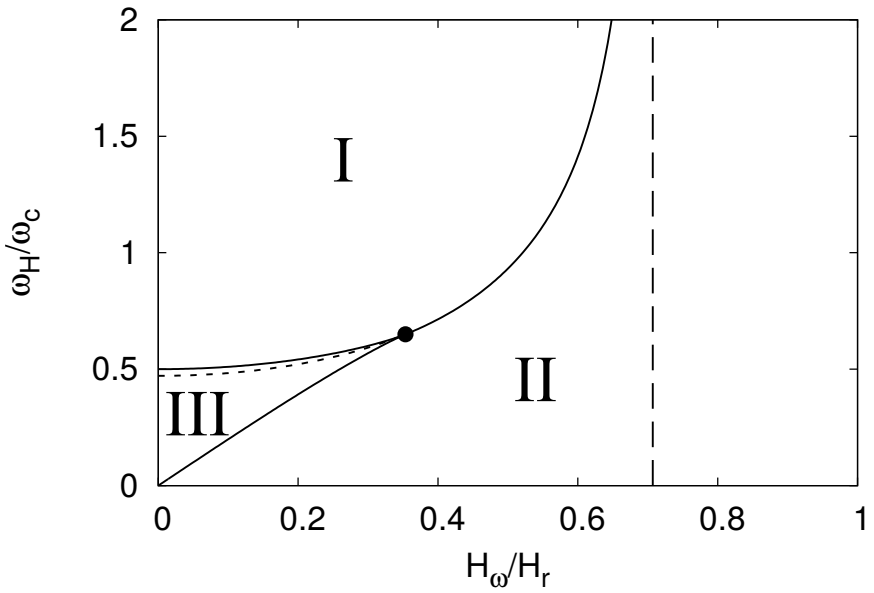

Figure 3.3: Phase diagram. The prolate particle has a stable synchronous regime in region $II \bigcup III$, and the oblate particle in region $I \bigcup III$. The regions is divided by the neutral stability (solid) line. Long dashed line is asymptote at $\frac{\omega_H}{\omega_a} \to \infty$ and short dashed line is extension of line (3.17) in the region where equation $f(y) = 0$ has three real roots. The point shows a codimension-2 bifurcation point.

The results of (3.17) and (3.18) is summarized in fig. 3.3. Fig. 3.2 and fig. 3.3 differs only by labels on the axis. In the new parameters the codimension-2 bifurcation point is at $\frac{H_\omega}{H_r} = \frac{\sqrt{2}}{4} \approx 0.35$ and $\frac{\omega_H}{\omega_c} = \frac{3\sqrt{3}}{8} \approx 0.65$.

3.6 Dipolar interaction

Here we want to calculate mean interaction energy between two identical particles rotating synchronously with the field. The interaction energy between two magnetic dipoles with magnetic moments $\vec{m}_1$ and $\vec{m}_2$ separated by the distance $\vec{r}$ is:

$$E = \frac{\vec{m}_1 \cdot \vec{m}_2}{r^3} - 3\frac{(\vec{m}_1 \cdot \vec{r})(\vec{m}_2 \cdot \vec{r})}{r^5} \tag{3.19}$$

If the particles are equally orientated then equation (3.19) can be written in form:

$$E = \frac{m^2}{r^3}(1 - 3\cos^2 \beta_{mr}) \ , \tag{3.20}$$

where β_{mr} is angle between $\vec{m}$ and $\vec{r}$. It is more convenient to use angles for $\vec{m} = (\sin\beta\cos\omega_H t, \sin\beta\sin\omega_H t, \cos\beta)$ and $\vec{r} = (\sin\psi, 0, \cos\psi)$, where

vertical direction is chosen to be $\vec{e}_H$. Equation (3.19) can be written in these angles as

$$E = \frac{m^2}{r^3}\left[1 - (\sin\psi \sin\beta \cos\omega_H t + \cos\psi\cos\beta)^2\right]$$

Averaging it over the period gives mean energy of interaction

$$E_{mean} = \frac{m^2}{r^3}(1 - 3\cos^2\beta)\left(1 - \frac{3}{2}\sin^2\psi\right) . \tag{3.21}$$

For rod like particles ($\chi_\parallel \gg \chi_\perp$) $m^2 = V^2\chi_\parallel^2 H^2(\vec{n}\cdot\vec{h})$ and $\cos\beta = (\vec{n}\cdot\vec{h})(\vec{n}\cdot\vec{e}_H) = \sigma$, but for plate like particles ($\chi_\perp \gg \chi_\parallel$) $m^2 = V^2\chi_\perp^2[1-(\vec{n}\cdot\vec{h})^2]$ and $\cos\beta = 0$.

The mean energy (3.21) has minimum at $\psi = \frac{\pi}{2}$ for plate like particles, what makes it more favourable for this type of particle to form sheets if they are in synchronous regime. The formation of sheets and other structures of magnetic Janus particles in precessing magnetic field can be found in [85].

The mean energy (3.21) for rod like particles has a minimum at $\psi = 0$, what makes it more favourable to form chains if rods are in synchronous regime.

3.7 Angular velocity and trajectory of the particle

In the experiment in addition to fact that particle is in synchronous or asynchronous regime, the dynamics of particle motion can be measured. The main parameters which can be calculated from the experiment are mean angular velocity in asynchronous regime and precession angle in synchronous regime. In this part the theoretical expressions for these parameters for the rod like particle will be obtained.

3.7.1 Synchronous regime

The precession angle of the rod in synchronous regime can be found from solution of equation $f(y) = 0$ (3.7). Then precession angle of the rod $\vartheta_{\vec{n}}$ is calculated as

$$\vartheta_{\vec{n}} = \arccos\left(\frac{\sigma}{\sqrt{y}}\right) ,$$

where y is solution of equation $f(y) = 0$ (3.7) and $\sigma = \vec{e}_H \cdot \vec{h}$.

In experiment the change of the observable length of the rod can be measured, which is equal to $L = L_0\sqrt{1-(\vec{e}_H\cdot\vec{n})^2}$, where L_0 is true length of the rod and $\vec{e}_H$ is perpendicular to the plane of observation.

Theoretically calculated values of $\frac{L}{L_0}$ are shown in fig. 3.4. The theoretical values are found from solution of cubic equation $f(y) = 0$ (3.7)

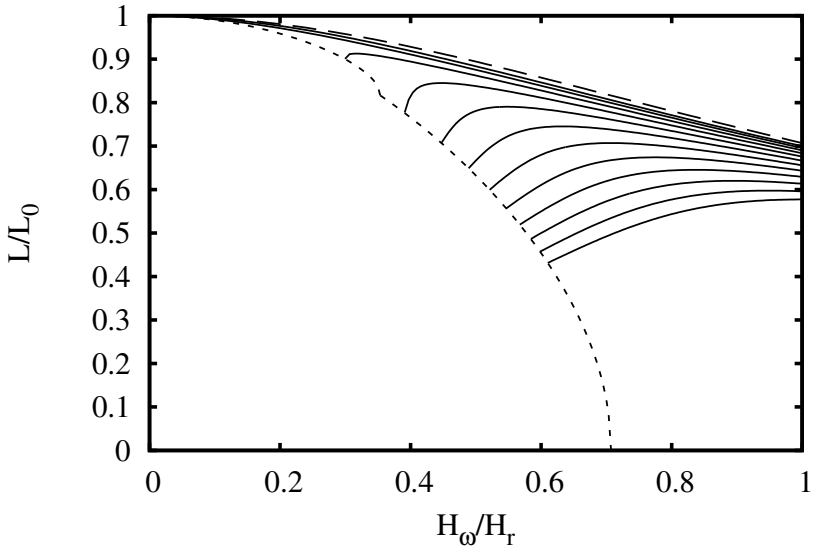

Figure 3.4: Observable length of the rod L in dependence of magnetic field strength ratio $\frac{H_\omega}{H_r}$ for field frequencies $\frac{\omega_H}{\omega_c}$ form 0.4 till 1.5 with step 0.1 (solid lines). Field frequency is increasing in downward direction. Long dashed line is situation if rod is orientated in the direction of the magnetic field. Below short dashed line synchronous regime becomes unstable.

with $\sigma = \dfrac{\frac{H_\omega}{H_r}}{\sqrt{1+\left(\frac{H_\omega}{H_r}\right)^2}}$ and $\omega = \dfrac{\omega_H}{\omega_c}\dfrac{1}{1+\left(\frac{H_\omega}{H_r}\right)^2}$. When y is found then $\frac{L}{L_0} = \sqrt{1-\frac{\sigma^2}{y}}$.

In fig. 3.4 can be seen that for slow fields $\omega_H \ll \omega_c$ the rod aligns with the external magnetic field (long dashed line). If the field frequency is increased, the rod stands steeper then the magnetic field is, therefore reducing velocity of the tip of the rod and dissipation due to viscous drag. The steeper the rod is the smaller it will look. The depart from magnetic field direction is connected with the lag of the rod from the magnetic field. And at some point the depart and therefore the lag becomes large enough and rod goes into asynchronous regime (short dashed line). The short dashed line has a deflection at $\frac{H_\omega}{H_r} = \frac{\sqrt{2}}{4}$, because at this point changes condition of neutral stability.

In the synchronous regime rod rotates with the same angular frequency ω_H than magnetic field.

3.7.2 Asynchronous regime

The asynchronous regime is too complicated to calculate it analytically directly from equation (3.1), therefore some assumptions about the particle movement should be made and the validity of the assumptions can be tested numerically by solving (3.1).

We will assume that rod in the asynchronous regime, when the regime is stabilized, in the frame rotating with the magnetic field forms disk. In other words, $\vec{n}$ stays in the plane which rotates with angular frequency ω_H around $\vec{e}_H$. We will call this plane the plane of lag and the corresponding normal vector of this plane would be $\vec{e}_L$. Therefore rotational velocity of the rod $\omega_{\vec{n}}$ can be divided into two parts: rotation around $\vec{e}_H$ with velocity ω_H and rotation around $\vec{e}_L$ with velocity $-\omega_L$. Therefore $\vec{e}_L$ can be found from relation:

$$\omega_H \left[\vec{e}_H - (\vec{e}_H \cdot \vec{n})\vec{n}\right] - \omega_a(\vec{n} \cdot \vec{h})[\vec{h} \times \vec{n}] = \omega_L \vec{e}_L \ , \tag{3.22}$$

where first term of the left hand side is synchronous rotation with the external field, second term is true rotation of the particle $\vec{n}$ and term on the right hand side gives the lag angular velocity, where

$$\omega_L = \left|\omega_H \left[\vec{e}_H - (\vec{e}_H \cdot \vec{n})\vec{n}\right] - \omega_a(\vec{n} \cdot \vec{h})[\vec{h} \times \vec{n}]\right|$$

From equation (3.22) the $\vec{e}_L$ can be calculated. It was checked for wide range of variables ω and σ of asynchronous regime that $\vec{e}_L$ reaches some constant value after some time. In the synchronous regime $\omega_L \vec{e}_L = 0$ and no lag occur. But in asynchronous regime ω_L changes in time.

As we know, in the region, where the synchronous regime of the rod is unstable, the synchronous regime of the plate like particle is stable and, as we just assumed, the rod in asynchronous regime forms something similar to synchronously rotating disk. Therefore we assume that normal of the plane of lag $\vec{e}_L$ moves equally to $\vec{n}$ of the corresponding oblate particle (with negative ω_a). This can be proved numerically.

Now we know what is the trajectory of the rod in asynchronous regime and we can calculate the mean rotational frequency of the rod in the asynchronous regime. To do so we introduce one more unit vector $\vec{k}$, which in the direction of the projection of the $\vec{h}$ onto plane of lag. Therefore $\vec{h} = (\vec{k} \cdot \vec{h})\vec{k} + (\vec{e}_L \cdot \vec{h})\vec{e}_L$, where $\vec{k} \perp \vec{e}_L$. This gives that

$$\vec{n} \cdot \vec{h} = (\vec{n} \cdot \vec{k})(\vec{k} \cdot \vec{h})$$

because $\vec{n} \cdot \vec{e}_L = 0$. Examination the change of $\vec{k} \cdot \vec{n}$ in time gives:

$$\frac{d(\vec{n} \cdot \vec{k})}{dt} = \frac{d\vec{n}}{dt} \cdot \vec{k} + \frac{d\vec{k}}{dt} \cdot \vec{n}$$

$\vec{k}$ rotates with $\vec{h}$ and plane of lag therefore $\frac{d\vec{k}}{dt} = \omega_H \vec{e}_H \times \vec{k}$ and previous expression is rewritten in form:

$$\frac{d(\vec{n}\cdot\vec{k})}{dt} = \omega_a(\vec{k}\cdot\vec{h})^2(\vec{n}\cdot\vec{k})\left(1-(\vec{n}\cdot\vec{k})^2\right) - \omega_H \vec{e}_H \cdot [\vec{n}\times\vec{k}] \tag{3.23}$$

This equation can be solved analytically introducing angle $\phi_{\vec{k}}$ between $\vec{k}$ and $\vec{n}$, then $\vec{n}\cdot\vec{k} = \cos\phi_{\vec{k}}$ and $\vec{n}\times\vec{k} = \sin\phi_{\vec{k}}\vec{e}_L$. In the angle form equation (3.23) looks:

$$\frac{d\phi_{\vec{k}}}{dt} = \omega_H(\vec{e}_L\cdot\vec{e}_H) - \omega_a(\vec{k}\cdot\vec{h})^2\cos\phi_{\vec{k}}\sin\phi_{\vec{k}} \tag{3.24}$$

From the definition and proved assumptions of $\vec{e}_L$ and $\vec{k}$ the quantities $(\vec{e}_L\cdot\vec{e}_H)$ and $(\vec{k}\cdot\vec{h})$ does not change if the trajectory of the rod is stabilized. Therefore equation (3.24) can be integrated analytically. Separation of the variables and integration over period gives:

$$T_L = \frac{2\pi}{\sqrt{\omega_H^2(\vec{e}_L\cdot\vec{e}_H)^2 - \frac{\omega_a^2}{4}(\vec{k}\cdot\vec{h})^4}}\,, \tag{3.25}$$

where T_L is period of the lag, when rod lags behind magnetic field one full period. Remembering that $\vec{e}_L$ is the same as $\vec{n}$ for the corresponding oblate particle, the $(\vec{e}_L\cdot\vec{h})^2 = y$ can be calculated from equation $f(y) = 0$ (3.7). Knowing y we can calculate $(\vec{e}_L\cdot\vec{e}_H)^2 = \frac{\sigma^2}{y}$ and knowing that $\vec{k}$ is orthogonal to $\vec{e}_L$ and $\vec{h}$ is between $\vec{k}$ and $\vec{e}_L$ gives that $(\vec{k}\cdot\vec{h})^2 = 1-y$. These relations give us average rotational frequency of the rod, which consists of synchronous rotation with the field and periodic lag:

$$\langle\omega_{\vec{n}}\rangle = \omega_H - \sqrt{\omega_H^2\frac{\sigma^2}{y} - \frac{\omega_a^2}{4}(1-y)^2}$$

Using equation (3.7) it can be written in form:

$$\langle\omega_{\vec{n}}\rangle = \omega_H - \sqrt{\omega_H^2 - \frac{\omega_a^2}{4} - \omega_a^2\left(\frac{y}{2} - \frac{3y^2}{4}\right)}\,, \tag{3.26}$$

where $\langle\omega_{\vec{n}}\rangle$ is average angular velocity when he regime is stabilized and y is solution of the cubic equation (3.7). If the magnetic field rotates in the plane , not precesses, then $\sigma = 0$ and in asynchronous regime of the rod the only real solution of the cubic equation (3.7) is $y = 0$ and we get known formula [33]:

$$\langle\omega_{\vec{n}}\rangle = \omega_H - \sqrt{\omega_H^2 - \frac{\omega_a^2}{4}} \tag{3.27}$$

But if $\sigma \neq 0$ the cubic equation (3.7) does not have solution $y = 0$ (if $\omega > 0$). From section 3.4 we know that rod like particle is in asynchronous regime only if $y < \frac{1}{3}$ is the only solution of the equation (3.7). This gives that $\left(\frac{y}{2} - \frac{3y^2}{4}\right) > 0$ and the average angular frequency of the rod is larger in the precessing field than in the rotating field if magnetic field strength is kept constant.

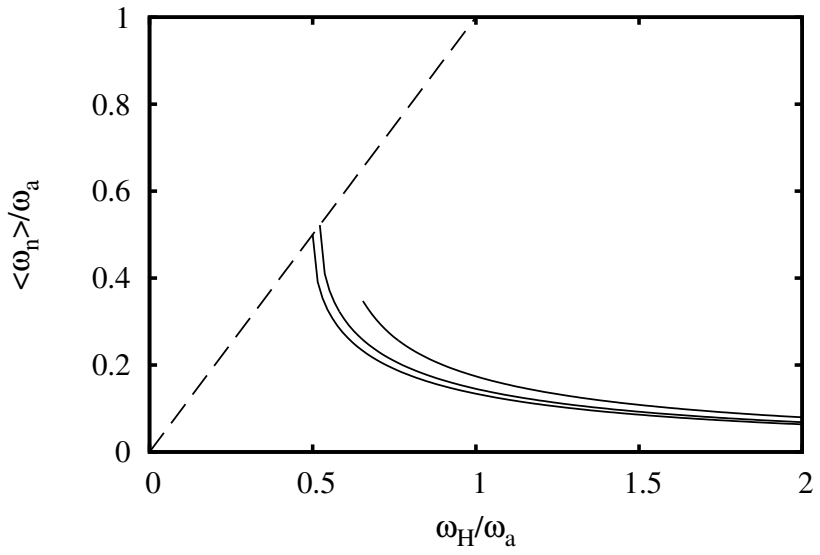

Figure 3.5: Average rotation frequency $\langle\omega_{\vec{n}}\rangle$ in dependence of field frequency ω_H for angles of the field $\sigma = (\vec{e}_H \cdot \vec{h})$ equal to 0; 0.2; and 0.4;. Solid lines are values in asynchronous regime, where σ increases in upward direction. Dashed line is synchronous rotation with the field frequency.

The calculated values of average angular velocity (3.26) is shown in fig. 3.5. As can be seen, the average rotational frequency in precessing field only slightly differs from the situation in rotating field with the same field strength H. It should be mentioned that for $\sigma > \frac{1}{3}$ the graph of $\langle\omega_{\vec{n}}\rangle$ has discontinuity between synchronous and asynchronous regime. This can be seen in the fig. 3.5 for $\sigma = 0.4$. For $\sigma < \frac{1}{3}$ the stable node disappears in saddle node bifurcation, what means that the place, were the stable node is, is still attractive and the plane of lag should go through this point. But for $\sigma > \frac{1}{3}$ the change of the stability of the regime changes the stability of the node. That means that, when the synchronous regime becomes unstable, rod should move to orthogonal plane to get stabilized in asynchronous regime, which could have completely different rotational frequency.

As we remember from section 3.4, for $\sigma > \frac{1}{3}$, the stability changes at

$y = \frac{1}{3}$ and average frequency of asynchronous rotation in this situation is

$$\langle \omega_{\vec{n}} \rangle = \omega_H - \sqrt{\omega_H^2 - \frac{\omega_a^2}{3}} = \omega_H \left(1 - \sqrt{\frac{9}{2}\sigma^2 - \frac{1}{2}} \right) ,$$

which is unusable for $\sigma < \frac{1}{3}$ and gives jump of average rotation frequency of the rod equal to $\frac{\omega_a}{3}\sqrt{\frac{9\sigma^2-1}{1-3\sigma^2}}$, when the particle goes from synchronous to asynchronous regime or vice versa.

3.8 Experiment

To test provided theory, the experiment was made. The experiment was made in Laboratory of Magnetic Soft Materials in University of Latvia by Artis Brasovs and Kaspars Ērglis. In the experiment superparamagnetic rods, which were synthesized according to the method detailed in [35], were used. Technical details about used setup can be found in appendix B. The superparamagnetic rod dynamics in synchronous and asynchronous regime were studied using rotating field with field strength $H_r = 54\,Oe$ and fixed field frequencies in the range $0.05\,Hz - 2\,Hz$ and the constant field H_ω was increased in step like manner. Experimentally obtained angles of one rod and corresponding magnetic field for one field frequency are shown in fig. 3.6. In this experiment mixture of glycerol and water in volume fractions 3:7 were used.

In fig. 3.6 it can be seen, that for small constant field strengths H_ω rod rotates slower, because it is in asynchronous regime, but, when the constant field strength H_ω is increased, at one moment rod starts to rotate much faster (with the field frequency). The transition from asynchronous regime to synchronous regime is not smooth. This can be seen as distortion of angle graph at $t \approx 300\,s$. The reverse process, when rod moves from synchronous to asynchronous state, can be seen at right end of the graph fig. 3.6, where the rod rotates with field frequency or near to it even when the field strength is below critical value and particle should be in asynchronous state.

To compare experimental results with theory the average rotational frequency form obtained angles for each field strength ration $\frac{H_\omega}{H_r}$ were calculated. First $10\,s$ for each field strength is omitted in the calculation of average frequency, in order to reduce influence of the previous state of superparamagnetic rod. The experimentally obtained results of average angular velocity is seen in fig. 3.7.

As was seen in fig. 3.6 the transition from asynchronous regime to the synchronous and vice versa took long time therefore in fig. 3.7 points, where transition between stable and unstable regime was observed, is omitted. In fig. 3.7 can bee seen that approximation goes a bit above experimental values. This is done because it is assumed that rod is not fully stabilized in

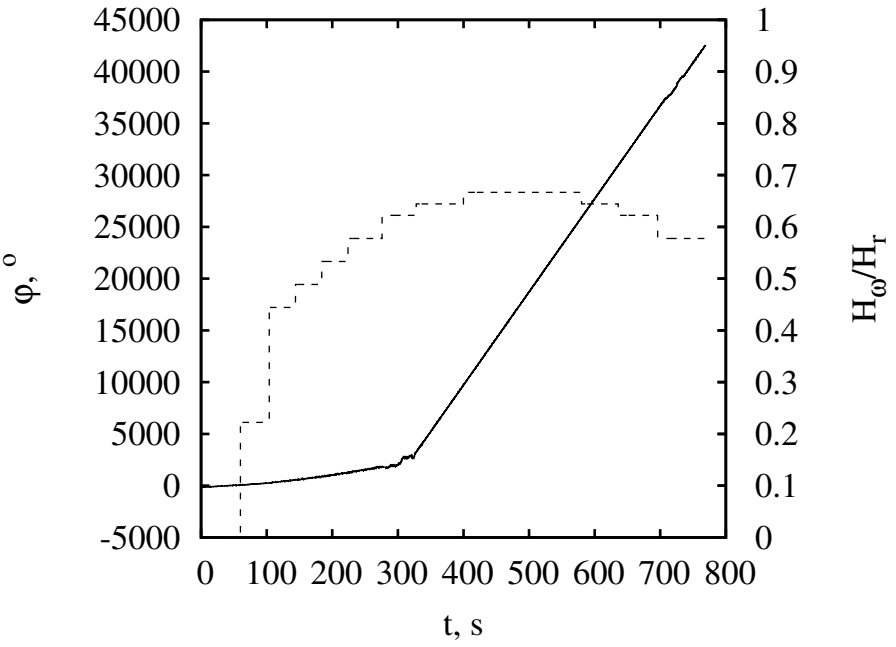

Figure 3.6: Experimentally measured orientation angle φ of the superparamagnetic rod (solid line and left axis) for different constant field strengths H_ω (dashed line and right axis) change in time. Rotating field frequency is $0.25\,Hz$

the new state and rotates closer to the previous state, which in increasing field strength is slower than new state. We could chose smaller ω_c, which makes approximation go through majority of the points of fig. 3.7. But in that case critical value of H_ω, where transition from asynchronous to synchronous regime occurs, would increase and we will get that first (or more) point of the synchronous regime would fall in asynchronous regime of the approximation.

Experimentally 15 particles each for 2 or 3 different frequencies were observed. Approximation of the experimental results gives ω_c in the range between $0.4\,\frac{1}{s}$ and $1.3\,\frac{1}{s}$ with mean value $\omega_c = 0.8\frac{1}{s}$. To compare it with other experiments, form-factor

$$F = \frac{\Delta\chi}{8\pi\Gamma} = \frac{\omega_c \eta}{H_r^2}$$

of the rod should be calculated, which is characteristic property of the rod. We get that form-factor F of the rods used in experiment is between $3.7{\cdot}10^{-5}$ and $1.2 \cdot 10^{-4}$ with mean value $7.1 \cdot 10^{-5}$. Here the viscosity is calculated according to [23] in temperature 25^oC using volume fraction of water and glycerol as 3:7. This gives $\eta = 0.27\,P$ large viscosity. Calculated form-factor

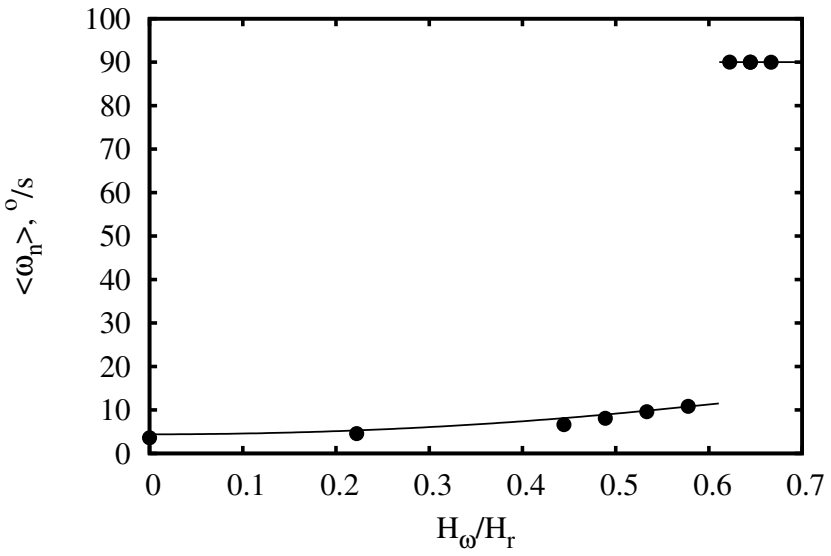

Figure 3.7: Experimentally measured average angular velocity $\langle \omega_{\vec{n}} \rangle$ of the superparamagnetic rod (filled circles) in dependence of constant field strength H_ω. Rotating field frequency is $0.25\,Hz$. Solid line is ω_H in the synchronous regime (upper circles) and approximation with equation (3.26) using $\omega_c = 0.97\,\frac{1}{s}$ in the asynchronous regime (lower circles).

is less than theoretical value $F = 8.1 \cdot 10^{-4}$ [14] but more then measured value $F = 4.7 \cdot 10^{-5}$ in the same paper. The difference between theoretical and measured value can be explained by finite size of the measurement cell, which increases drag due to nearness of the walls, and is not taken into account in theory.

In the precessing magnetic field the asynchronous rotation of the rod besides back and forth [37] motion also has as swinging motion. The dynamics of rod with $\omega_c = 0.4\frac{1}{s}$ in precessing with field frequency $0.075\,Hz$ and constant field strength $H_\omega = 31.2\,Oe$ is shown in fig. 3.8. There can be seen that at some time one end of the rod is sharp (in the focus) and after some time the other end of the rod is sharp. And the visible length of the rod is also changing. Only one end of the rod is sharp because rod is not perpendicular to the plane of observation, but is tilted. In the asynchronous regime rod lags from the rotating field and after some time the other end of the particle is closer to the magnetic field. Therefore the other end of the rod tries to align with the field, what looks like swing and other end of the particle gets into focus (and becomes sharp).

The observable length of the particle is not compared with theoretical result because in many pictures like at $t = 16\,s$ in fig. 3.8 it is hard to define observable length. In synchronous regime particles is steeper than in

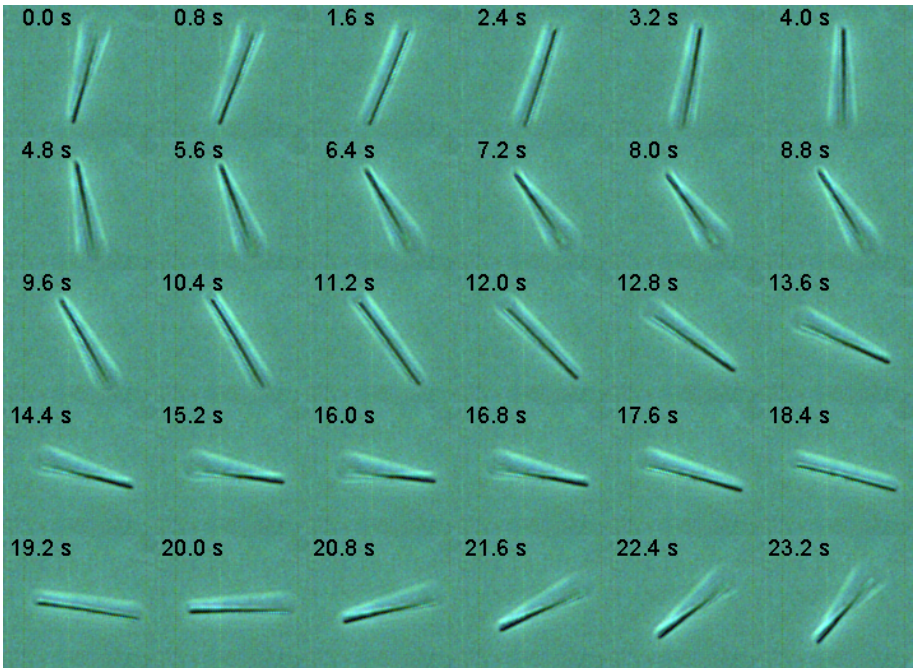

Figure 3.8: Dynamics of the rod in asynchronous regime

asynchronous regime which makes it almost impossible to measure visible length of the rod right. In order to measure angle of the rod in synchronous regime, the camera with higher depth of field should be used or the direction of observation should be changed which is impossible for used setup.

Chapter 4

Superparamagnetic particle in microrheological measurements

4.1 Motivation and contents

Possible usages of magnetic rods for microrheology are interested by scientists [24, 9]. We wanted to try use method described long time ago by Crick [31, 30] for measuring viscoelastic properties.

In this chapter in order to measure form-factor of the rods configuration of crossed AC and DC magnetic fields is used. The possible stable regimes in crossed AC and DC magnetic fields will be shown and stability of these regimes will be calculated numerically for general case. Dynamics of the rod in slow field and fast field limit will be calculated. It will be shown how experimental data is processed for form-factor and microrheological measurements.

4.2 Model

In this chapter the superparamagnetic particle is used, therefore here similar equations to chapter 3 will be used. The equation of motion of the particle is taken from chapter 3 (3.1):

$$\frac{d\vec{n}}{dt} = \frac{V\Delta\chi}{\xi}(\vec{n}\cdot\vec{H})\left[\vec{H} - (\vec{n}\cdot\vec{H})\vec{n}\right] \ , \tag{4.1}$$

Here elongated particles will be used, therefore $\Delta\chi > 0$

In this chapter crossed AC and DC magnetic fields will be used $\vec{H} = \big(H_\perp \cos(\omega_H t), 0, H_\parallel\big)$. Since magnetic field is two dimensional, the particle will rotate in the same plane as magnetic field is, therefore particle motion

can be expressed using only one angle φ: $\vec{n} = (\sin\varphi, 0, \cos\varphi)$. The equation (4.1) in the angle representation looks:

$$2\dot{\varphi} = \omega_c \left[\frac{1}{2} h_\perp^2 \cos(2\omega_H t) \sin(2\varphi) + \left(\frac{1}{2} h_\perp^2 - 1 \right) \sin(2\varphi) + \right. \\ \left. + 2h_\perp \cos(\omega_H t) \cos(2\varphi) \right], \tag{4.2}$$

where $\omega_c = \dfrac{V \Delta\chi H_\parallel^2}{\xi}$ and $h_\perp = \dfrac{H_\perp}{H_\parallel}$.

4.3 Possible regimes

In the limit $t \to \infty$ particle can oscillate around DC magnetic field $\langle\varphi\rangle = 0$ or around AC magnetic field $\langle\varphi\rangle = \frac{\pi}{2}$, where

$$\langle\varphi\rangle = \frac{1}{T} \int_t^{t+T} \varphi(s) ds$$

is the average value over the period T. This is because in the limit $t \to \infty$ $\langle\varphi\rangle$ should not change and we demand that $\dot{\varphi}(t + \frac{T}{2}) = -\dot{\varphi}(t)$, what will give that $\langle\dot{\varphi}\rangle = 0$. This condition is possible only if $\varphi(t + \frac{T}{2}) = -\dot{\varphi}(t)$ or $\varphi(t + \frac{T}{2}) = \pi - \varphi(t)$ (equivalently $\varphi(t + \frac{T}{2}) - \frac{\pi}{2} = \frac{\pi}{2} - \varphi(t)$), what gives that $\langle\varphi\rangle = 0$ or $\langle\varphi\rangle = \frac{\pi}{2}$ in the stabilized regime where $\langle\varphi\rangle$ does not change over period. To both of the found results $k\pi$ can be added, where $k \in \mathbb{Z}$, because $\vec{n}$ is equivalent to $-\vec{n}$.

Around which of the magnetic fields AC or DC will particle fluctuate depends on field frequency $\dfrac{\omega_H}{\omega_c}$ and field strength ratio $h_\perp = \dfrac{H_\perp}{H_\parallel}$ and can be found numerically. In order to do numerical calculations we should prove that both regimes $\langle\varphi\rangle = 0$ and $\langle\varphi\rangle$ can not be stable simultaneously. We can see in equation (4.2) that $\dot{\varphi}$ depends linearly on $\sin(2\varphi)$ and $\cos(2\varphi)$, therefore time derivative of small perturbation around state φ will also depend linearly on $\sin(2\varphi)$ and $\cos(2\varphi)$, which for transformation $\varphi \to \varphi + \frac{\pi}{2}$ will change sign. Therefore if the state with values φ is stable then state with values $\varphi + \frac{\pi}{2}$ is unstable and vice versa. What means that only one of the two possible states is stable and it is sufficient to calculate $\varphi(t+T) - \varphi(t)$ and $\langle\varphi\rangle$ to know which of the states is stable. For example, if $0 < \langle\varphi\rangle < \frac{\pi}{2}$ and $\varphi(t+T) - \varphi(t) < 0$ then stable is state $\langle\varphi\rangle = 0$, but if $\varphi(t+T) - \varphi(t) > 0$ then stable is state $\langle\varphi\rangle = \frac{\pi}{2}$. For better accuracy it is better to choose φ around $\frac{\pi}{4}$ to increase $\varphi(t+T) - \varphi(t)$ values. The numerical results for line of neutral stability is shown in fig. 4.1.

In fig. 4.1 can be seen that for slow fields or field with strong DC magnetic field, stable is fluctuation of the particle around DC magnetic

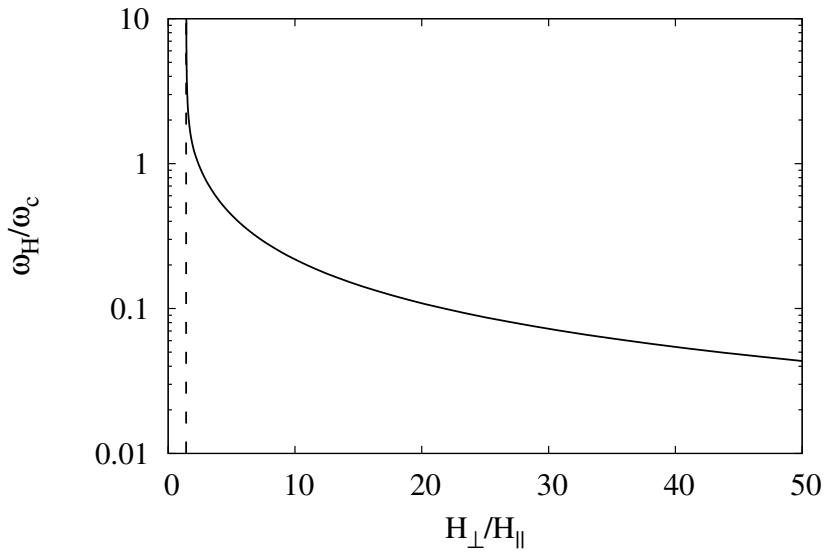

Figure 4.1: Phase diagram. Solid line is line of neutral stability. In the region I oscillation of the particle around DC magnetic field is stable, in the region II oscillation of the particle around AC magnetic field is stable. Dashed line is asymptote $\frac{H_\perp}{H_\parallel} = \sqrt{2}$ of solid line in the limit $\omega_H \to \infty$.

field. But if the field frequency is high or AC magnetic field is strong, the particle prefer to fluctuate around AC field. The asymptote $h_\perp = \sqrt{2}$ will be discussed in the next section.

4.3.1 Slow field limit

Equation (4.2) can be written into form:

$$\dot{\varphi} = \omega_c p(t, \varphi) \ , \tag{4.3}$$

where

$$p(t, \varphi) = (h_\perp \cos(\omega_H t) \sin\varphi + \cos\varphi)\,(h_\perp \cos(\omega_H t) \cos\varphi - \sin\varphi)$$

At the low frequency limit $\omega_H \ll \omega_c$ particle is always aligned with magnetic field and orientation angle φ stays on one of the stable solution $p(t, \varphi) = 0$ ($\frac{\partial p(t,\varphi)}{\partial \varphi} < 0$) fig. 4.2. This solution corresponds to regime $\langle\varphi\rangle = 0$.

At the extreme values of $h_\perp \gg 1$ ($H_\perp \gg H_\parallel$) φ jumps between neighboring stable states $p(t, \varphi) = 0$ ($\frac{\partial p(t,\varphi)}{\partial \varphi} < 0$) fig. 4.3. In this situation $H_\parallel$ can be assumed as small perturbation of $H_\perp$ and particle is in pure AC magnetic

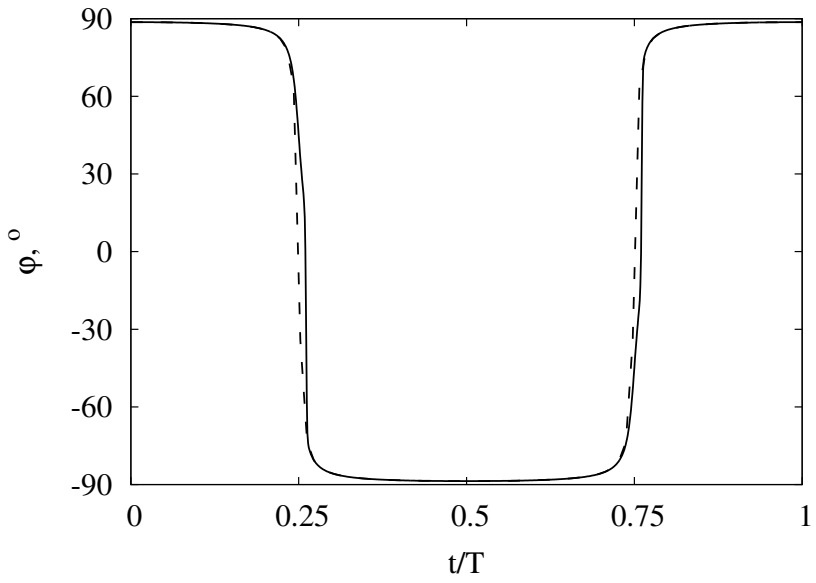

Figure 4.2: Numerical solution of particle movement (solid line) (4.2) in slow field limit $\omega_H = \frac{\omega_c}{20}$ comparison with solution (4.4) (dashed line) at $H_\perp = 43H_\parallel$ - near neutral stability line shown in fig. 4.1. $\langle\varphi\rangle = 0$ regime.

field, therefore it stays in AC field direction all the time. This corresponds to regime $\langle\varphi\rangle = \frac{\pi}{2}$.

The equation $p(t,\varphi) = 0$ has two solutions

$$\tan\varphi = h_\perp \cos(\omega_H t) \quad \& \quad \cot\varphi = -h_\perp \cos(\omega_H t)$$

and corresponding first derivatives $\frac{\partial p(t,\varphi)}{\partial\varphi}$ are

$$-\cos^2\varphi\left(h_\perp^2\cos^2(\omega_H t)+1\right) \quad \& \quad \sin^2\varphi\left(h_\perp^2\cos^2(\omega_H t)+1\right)$$

It can be seen that $\frac{\partial p(t,\varphi)}{\partial\varphi} < 0$ for solution $\tan\varphi = h_\perp\cos(\omega_H t)$ for all values of φ and t. This solution corresponds to particle which is aligned with magnetic field $\vec{n}\|\vec{H}$, but the solution $\cot\varphi = -h_\perp\cos(\omega_H t)$ corresponds to particle which is orthogonal to magnetic field $\vec{n} \perp \vec{H}$, which, also from physical point of view, is unstable. Therefore in fig. 4.2 and fig. 4.3 only solution

$$\tan\varphi = h_\perp\cos(\omega_H t) \tag{4.4}$$

is shown.

In fig. 4.2 can be seen that in slow field limit $\omega_H \ll \omega_c$ particle follows direction of magnetic field even if the $H_\perp$ is much larger then $H_\parallel$. Near neutral line of stability of fig. 4.1 particle starts to deviate from the direction of magnetic field in the range where magnetic field direction changes rapidly

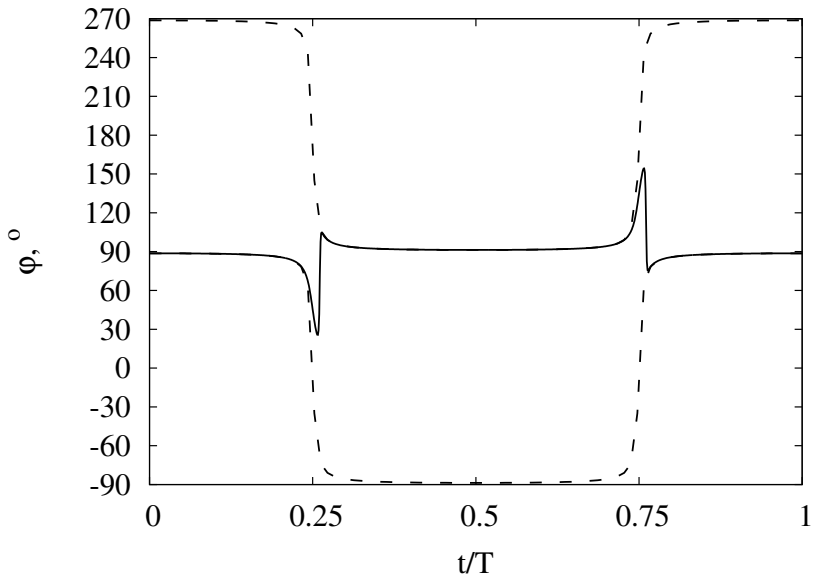

Figure 4.3: Numerical solution of particle movement (solid line) (4.2) in slow field limit $\omega_H = \frac{\omega_c}{20}$ comparison with solution (4.4) (dashed line) at $H_\perp = 44H_\parallel$ - near neutral stability line shown in fig. 4.1. $\langle\varphi\rangle = \frac{\pi}{2}$ regime.

(this can be seen in fig. 4.2 near $t = \frac{T}{4}$ and $t = \frac{3T}{4}$. If we increase magnetic field more, then deviation becomes larger until other end of the particle is closer to the field direction. Then the particle starts to jump between neighbouring states with $p(t, \varphi) = 0$ as can be seen in fig. 4.3 and particle oscillates around AC field.

4.3.2 Fast field limit

At the fast field limit $\omega_H \gg \omega_c$ there are two time scales: fast time scale ω_H corresponding to the period of the AC field, and slow time scale ω_c determined by the magnetic torque on the particle. The change of the angle φ of the particle can be divided in slow part φ_s and fast part φ_f:

$$\varphi(t) = \varphi_s(t) + \varphi_f(t)$$

In the slow time scale $\varphi_s(t)$ all the time effects, which comes from field frequency ω_H, are averaged out. Using identity $\langle\cos(\omega_H t)\rangle = 0$ the equation (4.2) for slow field is:

$$2\dot{\varphi}_s = \omega_c \left(\frac{1}{2}h_\perp^2 - 1\right) \sin(2\varphi_s) \ , \tag{4.5}$$

which gives slow relaxation to one of the stable regimes.

In the fast time scale we use that amplitude of fast oscillations is small, therefore it can be assumed that $\varphi(t) = \varphi_s(t)$ is constant. Then equation (4.2) after subtraction of (4.5) can be integrated:

$$\varphi_f = \frac{\omega_c}{\omega_H}\left(\frac{1}{8}h_\perp^2 \sin(2\omega_H t)\sin(2\varphi_s) + h_\perp \sin(\omega_H t)\cos(2\varphi_s)\right)$$

This gives fast oscillations with frequency ω_H and amplitude $\frac{\omega_c}{\omega_H}$ around particles mean orientation φ_s.

Equation (4.5) shows that for $h_\perp < \sqrt{2}$ slow orientation angle tends to value $\varphi_s = 0$ and particle relaxes to stable oscillations around DC magnetic field. For $h_\perp > \sqrt{2}$ slow orientation angle goes to $\varphi = \frac{pi}{2}$ and particle relaxes to stable oscillations around AC magnetic field. This value $h_\perp = \sqrt{2}$ is shown in fig. 4.1 by dashed line.

Equation (4.5) can be solved analytically:

$$\ln(|\tan(\varphi_s)|) = -\lambda t + C$$

or equivalently

$$\varphi_s = \arctan\left[\exp\left(-\lambda t + C\right)\right] \ , \tag{4.6}$$

where

$$\lambda = \omega_c\left(1 - \frac{h_\perp^2}{2}\right)$$

and C is arbitrary constant, which is determined by the initial conditions.

The numerical solution of equation (4.2) in the fast field limit $\omega_H \gg \omega_c$ is shown in fig. 4.4 by the grey line. The grey line looks wide because, besides slow rotation of the the particle, it also oscillates around its mean value, with much higher frequency. As we can see, the numerical results is in good agreement with solution (4.6) in the slow time scale.

4.4 Stray field

In the experiment AC magnetic field frequency was 50Hz and images was obtained at frame-rate 25 frames per second. It was seen that particle rotates slowly and is a bit smeared, what is in good agreement with found results in fast field limit. Therefore we can assume that $\omega_c \ll \omega_H$ and use equation (4.6) for approximation of experimental results.

In experiment AC and DC fields are calculated using currents in the coils (which is calibrated), but experimental results showed some deflection from theory. Without AC magnetic field, the particle aligns with DC field. Then turning on AC field with $H_\perp > \sqrt{2}H_\parallel$ and $\omega_H \gg \omega_c$ theoretically it is equal probable for particle to rotate in both directions $\varphi > 0$ and $\varphi < 0$, but in experiment it was found that one direction is more probable. And was found that in experiment particle stops moving not only at values

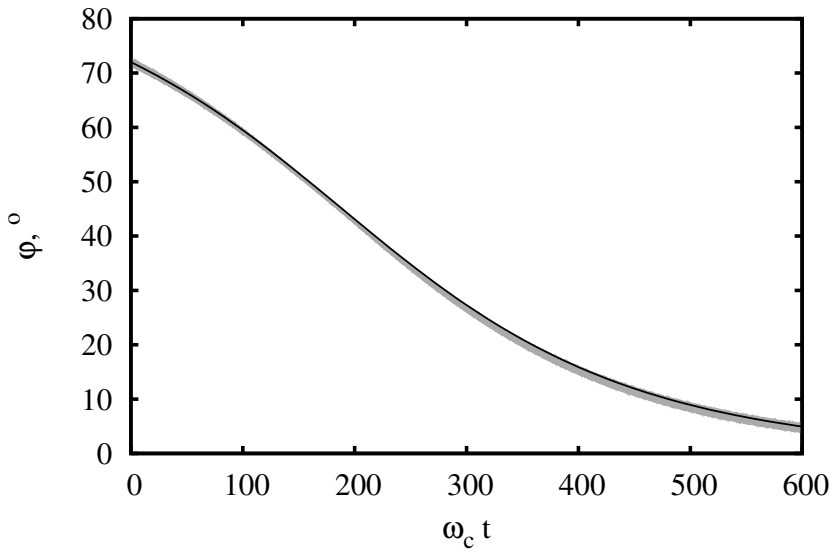

Figure 4.4: Numerical solution of particle movement (black line) (4.2) in fast field limit $\omega_H = 100\omega_c$ comparison with solution (4.6) (grey line) at $H_\perp = 1.41H_\parallel$ - near neutral stability line $H_\perp = \sqrt{2}H_\parallel$.

$\varphi = 0$ or $\varphi = \frac{\pi}{2}$, but also at some other values in between. Therefore additional stray field H_s is introduced in the direction of AC field, which theoretically explains experimentally observed behaviour. Then magnetic field is $\vec{H} = (H_\perp \cos(\omega_H t) + H_s, 0, H_\parallel)$ and equation (4.5) for the change of the angle φ in slow time scale is:

$$2\dot{\varphi}_s = \omega_c \left[\frac{1}{2} \left(\frac{H_\perp}{H_\parallel} \right)^2 + \left(\frac{H_s}{H_\parallel} \right)^2 - 1 \right] \sin(2\varphi_s) + 2\omega_c \frac{H_s}{H_\parallel} \cos(2\varphi_s) \qquad (4.7)$$

This equation can be solved analytically:

$$\ln(|\tan(\varphi_s - \varphi_c^\infty)|) = -\lambda' t + C$$

or equivalently

$$\varphi_s = \varphi_s^\infty + \arctan\left[\exp\left(-\lambda' t + C\right)\right] \ , \qquad (4.8)$$

where C is arbitrary constant, which is determined by the initial conditions and

$$\lambda' = \omega_c \sqrt{A^2 + B^2} \ , \qquad (4.9)$$

and function

$$\varphi_s^\infty = \frac{1}{2} \arccos\left(\frac{A}{\sqrt{A^2 + B^2}} \right) \ , \qquad (4.10)$$

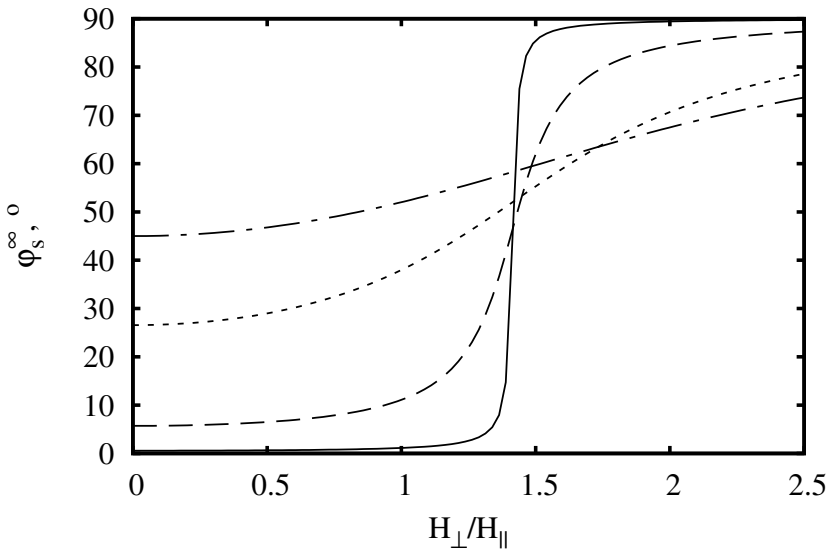

Figure 4.5: Stationary orientation angle φ_s^∞ as a function of dimensionless AC magnetic field $\frac{H_\perp}{H_\parallel}$ for different values of the stray field H_s: $H_s = 0.01H_\parallel$ - solid line, $H_s = 0.1H_\parallel$ - long dashed line, $H_s = 0.5H_\parallel$ - short dashed line and $H_s = H_\parallel$ - dash-dot line.

where

$$A = 1 - \frac{1}{2}\left(\frac{H_\perp}{H_\parallel}\right)^2 - \left(\frac{H_s}{H_\parallel}\right)^2 \qquad \& \qquad B = 2\frac{H_s}{H_\parallel}$$

φ_s^∞ is angle around which will particle oscillate after long time if the magnetic field components $H_\parallel$, $H_\perp$ and H_s are kept constant.

Here stray field is assumed only in AC field direction, firstly because stray field in DC direction would not change physically observable movement just critical values of the AC magnetic field strength. Secondly, less unknown values make approximation of noisy experimental data more robust. Thirdly stray field is observed mainly in AC field direction.

In the limit $H_s \to 0$ we get that $\lambda' = |\lambda|$ and $\varphi_s^\infty = \frac{1}{2}\arccos\left[\mathrm{sign}\,(A)\right]$, what is $\varphi_s^\infty = 0$ for $A > 0$ and $\varphi_s^\infty = \frac{\pi}{2}$ for $A < 0$. Therefore results in the limit $H_s \to 0$ are equal to results found in section 4.3.2 without stray field, what validates the found results. Therefore stray field smooths jump of φ_s^∞ graph what can be seen in fig. 4.5, where increase of stray field H_s makes graph more flat.

The relaxation constant λ' has a minimum in dependence of $\frac{H_\perp}{H_\parallel}$ at $\frac{H_\perp}{H_\parallel} = \sqrt{2\left[1 - \left(\frac{H_s}{H_\parallel}\right)^2\right]}$ and minimal value is $\lambda' = 2\omega_c\frac{H_s}{H_\parallel}$ if $\frac{H_s}{H_\parallel} < 1$. It can be seen

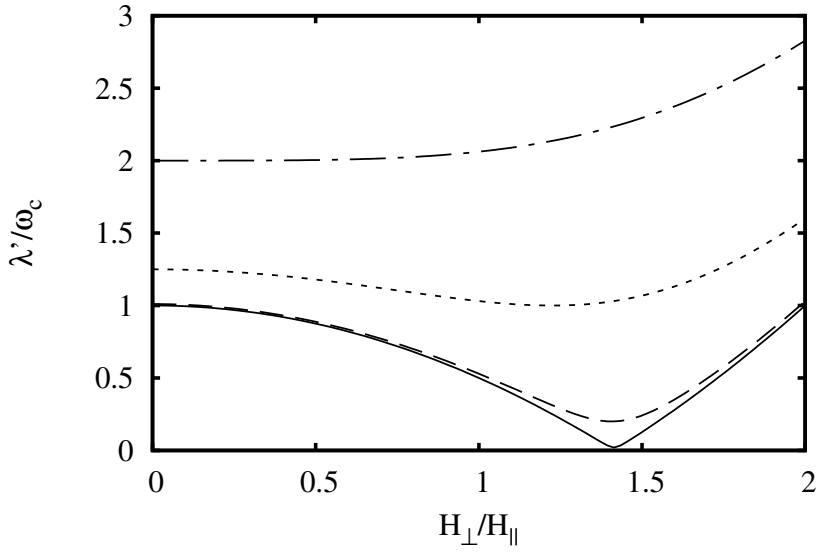

Figure 4.6: Relaxation constant λ' in dependence of AC magnetic field strength $H_\perp$ for different stray field strength H_s values. $H_s = 0.01H_\parallel$ - solid line; $H_s = 0.1H_\parallel$ - long dashed line; $H_s = 0.5H_\parallel$ - short dashed line; $H_s = H_\parallel$ - dash-dot line.

in fig. 4.6 that minimum moves to the left if $\frac{H_s}{H_\parallel}$ is increased. If $H_s \geq H_\parallel$, minimum stays at $H_\perp = 0$ and minimal value is $\lambda' = \omega_c \left[1 + \left(\frac{H_s}{H_\parallel}\right)^2\right]$. From equations (4.9) and (4.10) we see that minimum of λ' is at $A = 0$ or $\phi_s^\infty = \frac{\pi}{4}$, where both directions (AC and DC) are equal distant, if $H_s < H_\parallel$. It was found that stray field strength in experiment is around $0.1\,H_\parallel$.

4.5 Experimental results

The experiment was made in Laboratory of Magnetic Soft Materials in University of Latvia by Artis Brasovs and Kaspars Ērglis. In the experiments described in this work superparamagnetic rods were synthesized according to the method detailed in [35]. Technical details about used setup can be found in appendix B. Dynamics of the superparamagnetic rod at different values of $\frac{H_\perp}{H_\parallel}$ were studied by applying impulses of AC field with frequency 50 Hz with increasing amplitude while retaining a constant value of DC field $H_\parallel = 18\,Oe$. The orientation angle and field fraction $h_\perp = \frac{H_\perp}{H_\parallel}$ in the dependence of time for one particle are shown in fig. 4.7.

The experimental data was divided in intervals, where $h_\perp$ is constant and in each interval approximated by equation (4.8). In order to reduce

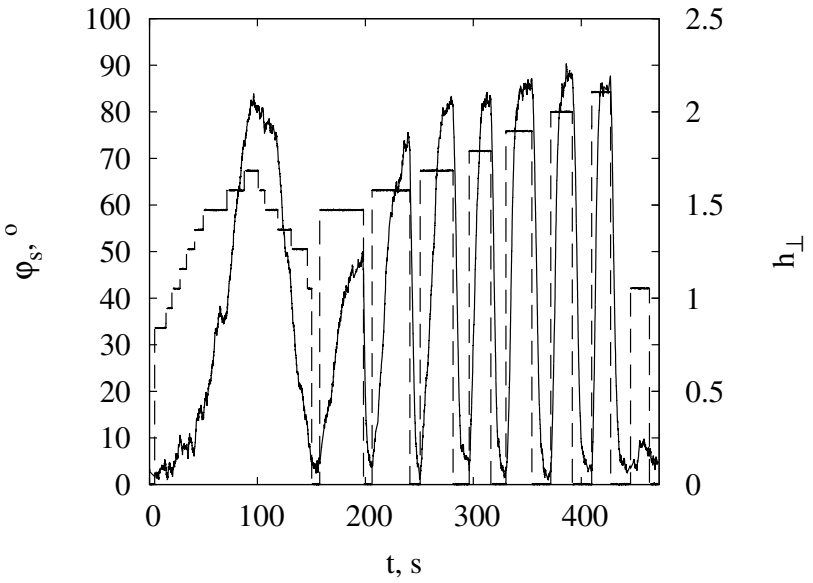

Figure 4.7: Experimentally measured mean orientation angle φ_s of the magnetic rod (solid line and left axis) for different AC field strengths h (dashed line and right axis) as a function of time.

errors, for each interval the local time is used, which is zero at beginning of the interval. The experimental data and their approximation in one of the intervals are shown in fig. 4.8. The approximation is made using (4.8) by varying φ_s^∞, λ' and C, thus in each interval φ_s^∞ and λ' are found, what give φ_s^∞ and λ' in dependence of $h_\perp$.

For each rod more than 20 intervals with significant change of φ_s were found, where less than half of them were for $h_\perp = 0$. Therefore for each particle more than 20 plausible φ_s^∞ and λ' values were found. Further for each experiment φ_s^∞ was approximated by (4.10) from which the stray field $\frac{H_s}{H_\parallel}$ was found. Experimental results of φ_s^∞ and its approximation with (4.10) for one rod can be found in fig. 4.9.

From obtained values of λ' the characteristic frequency ω_c is found using fit to (4.9), where $\frac{H_s}{H_\parallel}$ is known from fit of φ_s^∞. This fit also shows that $\frac{H_s}{H_\parallel}$ is found correctly. Experimental results of λ' and its approximation with (4.9) for one rod can be found in fig. 4.10. It was found that characteristic frequency ω_c is from $0.5\,Hz$ for the longest particle (shown in fig. 4.7, 4.8, 4.9 and 4.10) to $2.4\,Hz$ for shortest particle with mean value $1.5\,Hz$.

Lets remember that $\omega_c = \frac{V\Delta\chi H_\parallel^2}{\xi}$ and assume that particle is ellipsoidal, then from (1.24) we have $\xi = 8\pi\eta V\Gamma$. This gives us possibility to calculate

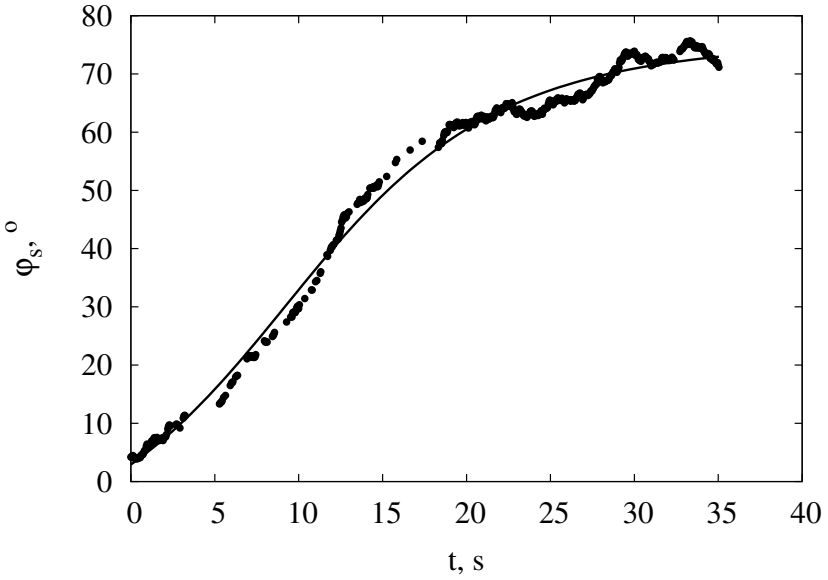

Figure 4.8: Experimentally measured mean orientation angle φ_s of the magnetic rod in the region with constant $h_\perp = 1.58$ as a function of the local time in the interval. Full circles denote the experimental data. The solid line shows the fit of experimental data with (4.8) with parameters $\varphi_s^\infty = 74.3°$, $\lambda' = 0.12 s^{-1}$ and $C = 1.15$. This interval in experiment time is $t \in (206\,s, 241\,s)$ shown in fig. 4.7.

dimensionless form-factor

$$F = \frac{\Delta\chi}{8\pi\Gamma} = \frac{\omega_c \eta}{H_\parallel^2}\ , \tag{4.11}$$

which depends on particles form and material. For used rods experimental obtained form-factor F is between $1.7 \cdot 10^{-5}$ and $7.4 \cdot 10^{-5}$ with mean value at $4.7 \cdot 10^{-5}$, where the viscosity of water at room temperature is taken $\eta = 1\,cP$.

The form-factor F can be also calculated theoretically from known values of rod. In experiment were used rods with axis ratio $\frac{a}{b} = 18$ and susceptibility $\chi = 3.4$ [24], what gives theoretical value of form-factor $F = 8.1 \cdot 10^{-4}$, which is more than 10 times larger then experimental value. Experimentally obtained value is smaller because of enhanced rotational drag on the rod due to its settlement near the bottom of the cell under action of the gravitational force.

In experiment was found that stray field is $H_0 = 1.1\,Oe$. Comparing it with horizontal component of Earth's magnetic field in Riga $H_{Riga} = 0.16\,Oe$ [61], gives that stray field comes from equipment and therefore it is called

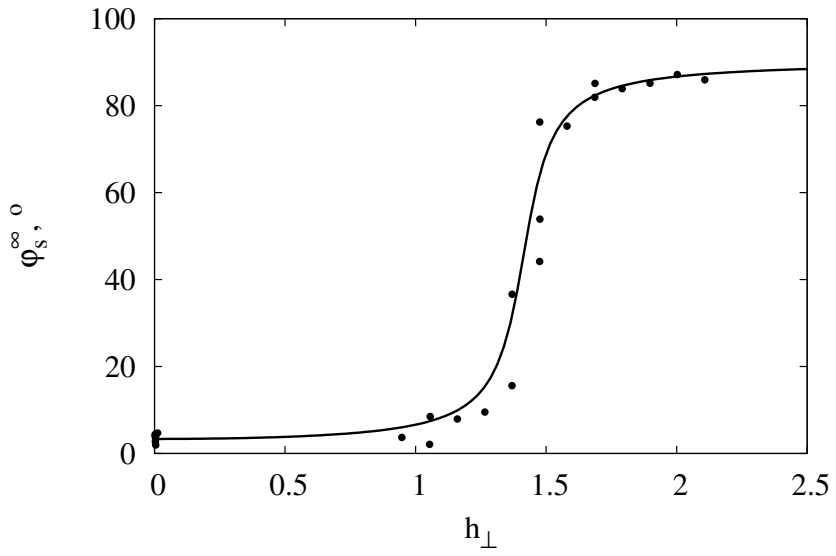

Figure 4.9: Orientation angle φ_0^∞ dependence on the parameter $h_\perp$. Full circles denote experimental data obtained from a fit to (4.8). The solid line shows a fit to (4.10), using stray field $\frac{H_s}{H_\parallel} = 0.06$.

the stray field. It was also found that this stray field is in the direction of earth magnetic field.

4.6 Magnetorheological measurements

The rods characterized in crossed AC and DC fields are used to determine the viscoelastic properties of the gel by studying the relaxation of the rod orientation after releasing the acting torque in the deformed state of the gel. The geometry and the process of the experiment are explained in fig. 4.11. Magnetic torque is applied on the particle for small time interval T. Afterwards the magnetic field is switched off and relaxation of the particle to the position near initial is registered. In experiments the magnetic field with strength $H_0 = 36\,Oe$ is used.

Magnetic torque on superparamagnetic rod in the setup shown in fig. 4.11 is calculated as (2.22):

$$\vec{M}_m = \vec{m} \times \vec{H} = V\Delta\chi(\vec{H}\cdot\vec{n})[\vec{n}\times\vec{H}]\ ,$$

which in angle representation looks like

$$M_m = \frac{V\Delta\chi H_0^2}{2}\sin\left(\frac{\pi}{2} - 2\vartheta\right)\ . \tag{4.12}$$

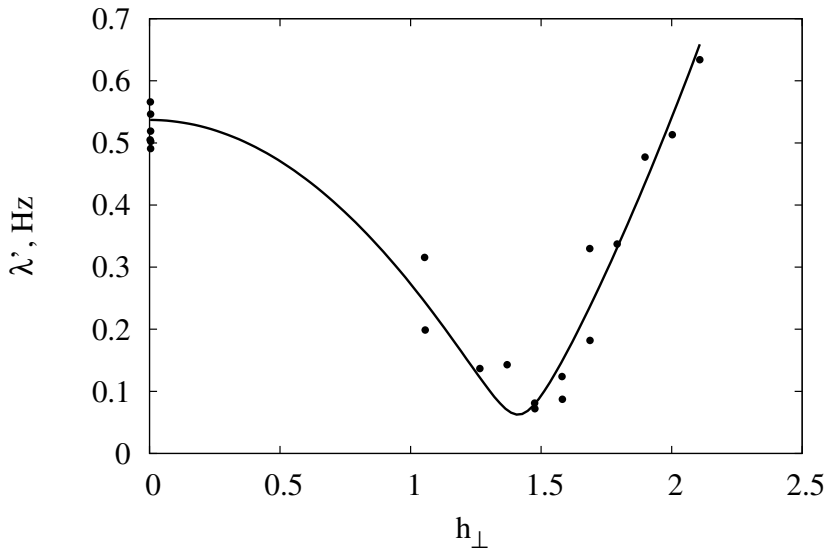

Figure 4.10: Relaxation frequency λ' dependence on the parameter $h_\perp$. Full circles denote experimental data obtained from a fit to (4.8). The solid line shows a fit to (4.9), using characteristic frequency $\omega_c = 0.5\,Hz$ and stray field $\frac{H_s}{H_\parallel} = 0.06$.

This torque is balanced by viscoelastic torque, which can be calculated from Jeffrey fluid model (1.37) giving:

$$\frac{dM_m}{dt} + \frac{M_m}{\tau_M} = \frac{\xi_V + \xi_M}{\tau_M}\frac{d\vartheta}{dt} + \xi_V \frac{d^2\vartheta}{dt^2}\ , \tag{4.13}$$

where ξ_V and ξ_M are rotational drag coefficients (1.24) of corresponding dashpots with viscosities η_V and η_M.

Since the duration of the applied magnetic field was chosen to be fairly short so the angle ϑ is close to its initial value $\frac{\pi}{2}$ all the time, it is possible to consider the case with the constant applied torque determined by the magnetic torque in the initial moment of time $\vartheta = \frac{\pi}{2}$. This assumption gives magnetic torque:

$$M_m = \frac{V\Delta\chi H_0^2}{2}\ . \tag{4.14}$$

And dynamic of the particle is defined by equation:

$$\eta_0 \frac{d\vartheta}{dt} + \eta_V \tau_M \frac{d^2\vartheta}{dt^2} = -\frac{F H_0^2}{2}\ , \tag{4.15}$$

where $\eta_0 = \eta_V + \eta_M$ and F is form factor defined in (4.11).

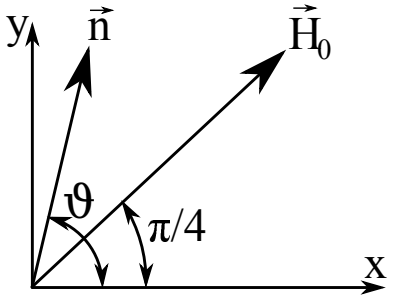

Figure 4.11: Sketch of the experiment of microrheology. Magnetic rod is initially oriened along the y axis by the application of the magnetic field. At some moment the magnetic field is swiched to a new direction making an angle $\frac{pi}{4}$ with the y axis. The time interval T of the application of the magnetic field in $\frac{\pi}{4}$ direction is chosen to be small enough to ensure that during this time interval the magnetic torque acting on the particle is practically constant. During this time the angle ϑ of the particle changes from initial $\frac{\pi}{2}$ to some value $\vartheta(T) < \pi 2$. After time interval T the magnetic field is swiched off and relaxation process of the angle ϑ to a value close to the initial is registered.

Solving (4.15) gives similar expression to (1.38)

$$\vartheta(t) = \vartheta(0) - \frac{FH_0^2}{2}\frac{1}{\eta_0}t - \tau_J\left(\dot{\vartheta}(0^+) + \frac{FH_0^2}{2}\frac{1}{\eta_0}\right)\left[1 - \exp\left(-\frac{t}{\tau_J}\right)\right] \ , \quad (4.16)$$

where $\tau_J = \dfrac{\eta_M \eta_V}{\eta_0 E}$ is Jeffrey relaxation time. Angular velocity at initial time $\vartheta(0^+)$ can be found in two equivalent ways. First, by integrating (4.13) in the time interval $[-\varepsilon, \varepsilon]$, where due to the switching of the direction of the magnetic field, the term $\dot{M}_m$ is infinity large. Taking the limit $\varepsilon \to 0$ the only terms which gives finite contribution are

$$\int_{-\varepsilon}^{\varepsilon} \frac{dM_m}{dt} dt = M_m(\varepsilon) - M_m(-\varepsilon) = -\frac{V\Delta\chi H_0^2}{2}$$

and

$$\int_{-\varepsilon}^{\varepsilon} \frac{d^2\vartheta}{dt^2} dt = \dot{\vartheta}(\varepsilon) - \dot{\vartheta}(-\varepsilon) = \dot{\varepsilon}(0^+)$$

Therefore

$$\dot{\vartheta}(0^+) = -\frac{FH_0^2}{2}\frac{1}{\eta_V} \quad (4.17)$$

Second possibility is using assumption that at initial state spring in Jeffrey model (fig. 1.5) has no strain. Therefore strain on dashpot with η_M also

must be zero, since it is in series with spring. Therefore all applied strain works on dashpot with η_V, And we get equation (4.17).

With calculated $\vartheta(0^+)$ eqrefeq:tetaexp1 can be written in form:

$$\vartheta(t) = \vartheta(0) - \frac{FH_0^2}{2}\frac{1}{\eta_0}t - \frac{FH_0^2}{2}\frac{1}{k}\left[1 - \exp\left(-\frac{t}{\tau_J}\right)\right] , \tag{4.18}$$

where $k = \frac{\eta_0^2 E}{\eta_M^2}$. In [14] is used a bit different description of Jeffrey model, but the obtained equation (4.18) is the same. Jeffrey model has three unknown parameters and the sets (η_V, η_M, E) and (η_0, k, τ_J) are equivalent to describe properties of viscoelastic fluid.

Since torque is applied only for short time, it can be assumed that $t \ll \tau_J$ and only linear part of the equation (4.18) will be used:

$$\vartheta(t) = \frac{\pi}{2} - \frac{FH_0^2}{2}\frac{1}{\eta_V}t \tag{4.19}$$

At the time moment t=T the magnetic field is switched off and the orientation angle relaxes towards the initial value due to the accumulated elastic energy in the gel. The relaxation process when $M = 0$ is described by the equation:

$$\frac{d^2\vartheta}{dt^2} + \frac{1}{\tau_J}\frac{d\vartheta}{dt} = 0 \tag{4.20}$$

The solution of the equation (4.20) is

$$\vartheta(t) = \vartheta(T) - \tau_J\dot{\vartheta}(T^+)\left[1 - \exp\left(-\frac{t-T}{\tau_J}\right)\right] \tag{4.21}$$

The angular velocity of the rod at the time moment T^+, when the field is switched off, can be found as previously by the integration of equation (4.13) in the time interval $[T-\varepsilon, T+\varepsilon]$. In the limit $\varepsilon \to 0$ we get:

$$\dot{\vartheta}(T^+) - \dot{\vartheta}(T^-) = \frac{FH_0^2}{2}\frac{1}{\eta_V}$$

and $\dot{\vartheta}(T^-)$ can be calculated from (4.18):

$$\dot{\vartheta}(T^-) = -\frac{FH_0^2}{2}\left[\frac{1}{\eta_0} + \frac{1}{\tau_J k}\exp\left(-\frac{T}{\tau_J}\right)\right]$$

Putting all this in equation (4.21) gives:

$$\vartheta(t) = \vartheta(T) - \frac{FH_0^2}{2}\frac{1}{k}\left[1 - \exp\left(-\frac{T}{\tau_J}\right)\right]\left[1 - \exp\left(-\frac{t-T}{\tau_J}\right)\right] \tag{4.22}$$

Relations (4.19) and (4.22) are further used to describe experimental results and calculate rheological parameters.

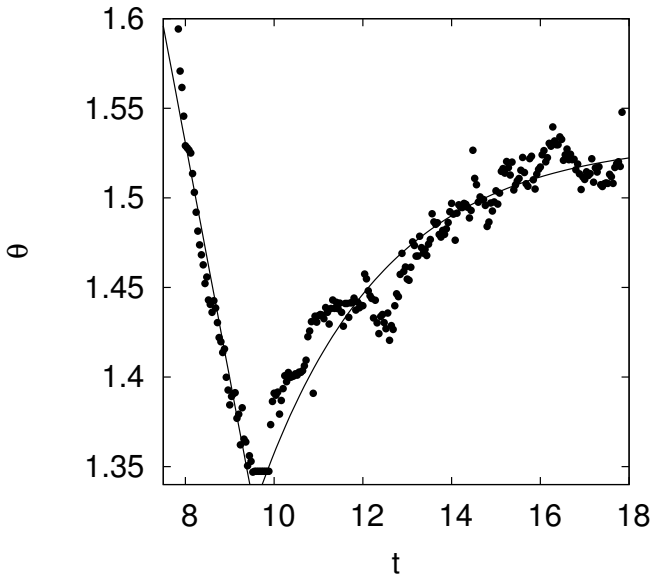

Figure 4.12: Dependence of the orientation angle of the rod if Pf1 gel when the field is on and off. Experimental data- full circle, approximation with (4.19) and (4.22) - solid lines.

In figure 4.12 can be seen experimental data obtained in Laboratory of magnetic soft materials at University of Latvia by Artis Brasovs and Kaspars Ērgis. The experimental setup is described in fig. 4.11 and particles are characterized in section 4.5.

From the approximation of experimental data when the magnetic field is switched on with the straight line (4.19) the constant η_V can be found (left part of fig. 4.12). Approximating right part of fig. 4.12 when the magnetic field is switched off with (4.22) the parameters k and τ_J can be found. Therefore viscoelastic properties of the fluid can be found. The results of viscoelastic properties of Pf1 gel with different concentration of $MgCl_2$ salt is found in [14], where in this section described method is compared with macrorheological measurements.

Chapter 5

Stochastic dynamics of hard magnetic dipole in viscoelastic fluid

5.1 Motivation and contents

Available theory for contrast agents for nuclear magnetic resonance (NMR) assumes that contrast agents are immersed in viscous fluid [57]. Liquids in human organism are mainly viscoelastic (not viscous). The aim of this chapter is to compare relaxation relation in viscous and viscoelastic fluid.

In this chapter the relaxation of particle in viscoelastic fluid without magnetic field in 2 dimensional case will be calculated analytically. Series expansion of relaxation of the particle direction in viscoelastic fluid in 3 dimensions will be derived. The numerical algorithm for calculating particle direction relaxation in 3 dimensions in static external magnetic field will be shown. Qualitative difference between relaxation of magnetic particle in viscous and viscoelastic fluid will be given.

5.2 Model

For modelling viscoelasticity we will use Jeffrey fluid model discussed in section 1.6.3. As mentioned in section 1.6.3 Jeffrey model consists of parallel connected viscous element (dashpot) and Maxwell element. Without any additional forces in inertia-free limit the equation of motion of the particle is:

$$\vec{M}^V + \vec{M}^M = 0 \tag{5.1}$$

where viscous part satisfies

$$\vec{M}^V = -\xi_V \vec{\omega} + \vec{\zeta}^V \tag{5.2}$$

and Maxwell part satisfies

$$\vec{M}^M + \tau_M \frac{d\vec{M}^M}{dt} = -\xi_M \vec{\omega} + \vec{\zeta}^M \ , \tag{5.3}$$

where $\xi_{V,M} = 8\pi V \eta_{V,M} \Gamma$ is drag coefficient of corresponding dashpot in Jeffrey model (fig. 1.5), $\tau_M = \frac{\eta_M}{E}$ is Maxwell relaxation time and $\zeta^{V,M}$ is corresponding white noise terms with $\langle \zeta_i^{V,M}(t) \rangle = 0$ and

$$\langle \zeta_i^{V,M}(t) \zeta_k^{V,M}(t') \rangle = 2\delta_{ik} \xi_{V,M} k_B T \delta(t - t')$$

Combining equations (5.1), (5.2) and (5.3) give system of stochastic differential equations:

$$\begin{cases} \vec{\omega} = \dfrac{\vec{M}^M}{\xi_V} + \dfrac{\vec{\zeta}^V}{\xi_V} \\ \dfrac{d\vec{M}^M}{dt} = -\dfrac{\vec{M}^M}{\tau_J} - \dfrac{\vec{\zeta}^V}{\tau_V} + \dfrac{\vec{\zeta}^M}{\tau_M} \end{cases} , \tag{5.4}$$

where $\tau_J = \frac{\xi_V \tau_M}{\xi_V + \xi_M} = \frac{\tau_M \tau_V}{\tau_V + \tau_M}$ and $\tau_V = \frac{\xi_V \tau_M}{\xi_M} = \frac{\eta_V}{E}$

5.3 Two-dimensional case

In two-dimensional (2D) case, when particle can rotate only in the plane, equation (5.4) can be written in form, where $\vec{\omega}$ and $\vec{M}^M$ have only one nonzero component. Then angular velocity $\vec{\omega}$ is time derivative of angle ϕ between particle direction $\vec{n}$ and some static axis $\vec{e}_H$ in the plane of rotation of particle. Then we have system of stochastic equations for the angle ϕ:

$$\begin{cases} \dfrac{d\phi}{dt} = \omega = \dfrac{M^M}{\xi_V} + \dfrac{\zeta^V}{\xi_V} \\ \dfrac{dM^M}{dt} = -\dfrac{M^M}{\tau_J} - \dfrac{\zeta^V}{\tau_V} + \dfrac{\zeta^M}{\tau_M} \end{cases} \tag{5.5}$$

The second equation of (5.5) can be solved giving:

$$M^M(t) = M^M(0) \exp\left(-\frac{t}{\tau_J}\right) - \int_0^t \exp\left(-\frac{t-\tau}{\tau_J}\right) \left(\frac{\zeta^V(\tau)}{\tau_V} - \frac{\zeta^M(\tau)}{\tau_M}\right) d\tau \tag{5.6}$$

Equipartition gives that in equilibrium mean energy on the spring in Jeffrey model $\frac{\langle M^M(t) m^M(t) \rangle}{2k}$ is equal to $\frac{k_B T}{2}$, where $k = 8\pi V \Gamma E = \frac{\xi_M}{\tau_M}$ is stiffness of the spring. This gives that

$$\langle M^M(t) M^M(t) \rangle = \frac{k_B T \xi_M \xi_V}{(\xi_M + \xi_V)\tau_J}$$

$\langle M^M(t)M^M(t)\rangle$ should stay constant all the time and mean value $\langle M^M(t)\rangle = 0$. Then, using that both white noise generators are independent of M^M ($\langle M^M(t)\zeta^{M,V}(t')\rangle = 0$) and independent between themselves ($\langle \zeta^V(t)\zeta^M(t')\rangle = 0$), the correlation of M^M can be calculated analytically:

$$\langle M^M(t)M^M(t')\rangle = \frac{k_B T \xi_M \xi_V}{(\xi_M + \xi_V)\tau_J} \exp\left(-\frac{|t-t'|}{\tau_J}\right) \tag{5.7}$$

This result gives us possibility to calculate correlation of ω:

$$\langle \omega(t)\omega(t')\rangle = \frac{2k_B T}{\xi_V}\delta(t-t') - \frac{k_B T \xi_M}{(\xi_M + \xi_V)\xi_V \tau_J} \exp\left(-\frac{|t-t'|}{\tau_J}\right) \tag{5.8}$$

and $\langle \omega(t)\rangle = 0$.

In 2D we can simply calculate average value of change of the angle ϕ:

$$\langle \phi(t) - \phi(t')\rangle = \int_{t'}^{t} \langle \omega(\tau)\rangle \, d\tau = 0$$

and mean square rotation is

$$\begin{aligned} \langle [\phi(t) - \phi(t')]^2\rangle &= \int_{t'}^{t}\int_{t'}^{t} \langle \omega(\tau)\omega(\tau')\rangle \, d\tau d\tau' = \\ &= 2D\left\{|t-t'| + \tau_J \frac{\xi_M}{\xi_V}\left[1 - \exp\left(-\frac{|t-t'|}{\tau_J}\right)\right]\right\} \end{aligned} , \tag{5.9}$$

where $D = \frac{k_B T}{\xi_V + \xi_M}$ is rotational diffusion coefficient. This result coincide with results found by Raikher and Rusakov [72], [73]. For simplicity we will use that $t' = 0$ and $t > 0$, then (5.9) can be written for new parameter $\Delta\phi = \phi(t) - \phi(0)$ in form:

$$\langle (\Delta\phi)^2\rangle = 2D\left\{t + \tau_J \frac{\xi_M}{\xi_V}\left[1 - \exp\left(-\frac{t}{\tau_J}\right)\right]\right\} \tag{5.10}$$

Equation (5.10) shows two diffusion processes. Expanding (5.10) in the limit $t \ll \tau_J$ we get fast diffusion:

$$\langle (\Delta\phi)^2\rangle = 2D\frac{\xi_M + \xi_V}{\xi_V} t = \frac{2k_B T}{\xi_V} t \tag{5.11}$$

and in the limit $t \gg \tau_J$ we get slow diffusion:

$$\langle (\Delta\phi)^2\rangle = 2D\left(t + \tau_J \frac{\xi_M}{\xi_V}\right) \tag{5.12}$$

The difference between (5.11) and (5.12) becomes notable if $\xi_M \gg \xi_V$.

The Jeffrey fluid in the limit $\xi_M \gg \xi_V$ becomes equivalent to Maxwell fluid model discussed in section 1.6.1. The main advantage of Jeffrey fluid is that diffusion in short times $t \ll \tau_J$ is large but finite (5.11), where in Maxwell model it becomes infinite what is non-physical. For the long time interval $t \gg \tau_J$ both models give similar result (5.12).

The Jeffrey fluid in the limit $\xi_M \ll \xi_V$ becomes equivalent to Voigt-Kelvin fluid model discussed in section 1.6.2. This situation is not interesting for further analysis because it gives same result as viscous fluid:

$$\langle(\Delta\phi)^2\rangle = 2Dt$$

for all values of t.

Since ω consists of independent and identically distributed random beats, then, according to central limit theorem, ω is normally distributed. Since $\Delta\phi$ is infinite sum (integral) of normally distributed variables ω, then $\Delta\phi$ is also normally distributed. Exponent of normally distributed variables is log-normally distributed with mean value [69]:

$$\langle\exp(i\Delta\phi)\rangle = \exp\left(-\frac{\langle(\Delta\phi)^2\rangle}{2}\right) \tag{5.13}$$

since mean value $\langle\Delta\phi\rangle = 0$

On the other hand

$$\begin{aligned}\exp(i\Delta\phi) &= \exp(i[\phi(t) - \phi(0)]) = \\ &= \cos(\phi(t))\cos(\phi(0)) + \sin(\phi(t))\sin(\phi(0)) - \\ &\quad - i[\sin(\phi(t))\cos(\phi(0)) + \cos(\phi(t))\sin(\phi(0))]\end{aligned}$$

Taking average of both sides gives that complex part on right hand side is zero. After averaging the equation should not depend on starting value $\phi(0)$, but only on time t, therefore we can add arbitrary constant to ϕ, what shows that $\langle\cos(\phi(t))\cos(\phi(0))\rangle$ should be equal to $\langle\sin(\phi(t))\sin(\phi(0))\rangle$. Comparing it with (5.13) and knowing that $\langle\cos^2(\phi(0))\rangle + \langle\sin^2(\phi(0))\rangle = 1$ gives that:

$$\begin{aligned}\langle\cos(\phi(t))\cos(\phi(0))\rangle &= \langle\sin(\phi(t))\sin(\phi(0))\rangle = \\ &= \frac{1}{2}\exp\left\{-Dt - D\tau_J\frac{\xi_M}{\xi_V}\left[1 - \exp\left(-\frac{t}{\tau_J}\right)\right]\right\}\end{aligned} \tag{5.14}$$

5.4 Three-dimensional case

In the 3-dimensional (3D) case solutions for $M^M(t)$ and $\omega(t)$ does not change their appearance, just they are expanded to the 3D, where they are vectors $\vec{M}^M$ and $\vec{\omega}$. For the components of the vector $\vec{\omega}$ we can write:

$$\langle\omega_i(t)\omega_k(t')\rangle = \delta_{ik}\left[\frac{2k_BT}{\xi_V}\delta(t-t') - \frac{k_BT\xi_M}{(\xi_M+\xi_V)\xi_V\tau_J}\exp\left(-\frac{|t-t'|}{\tau_J}\right)\right] \tag{5.15}$$

The main difference between 2D and 3D case is that in 3D total rotation depends on order of simple rotations. In general:

$$\vec{\omega}_1 \times [\vec{\omega}_2 \times \vec{n}] \neq \vec{\omega}_2 \times [\vec{\omega}_1 \times \vec{n}] \ ,$$

where $\vec{n}$ denotes direction of the particle and satisfies equation

$$\frac{d\vec{n}}{dt} = \vec{\omega} \times \vec{n} \ , \tag{5.16}$$

where $\vec{\omega}$ is coloured noise with zero mean and correlation defined in (5.15).

For further analysis it is necessary to introduce rotation matrix $\vec{\vec{U}}(t, t_0)$ with property

$$\vec{n}(t) = \vec{\vec{U}} \cdot \vec{n}(t_0)$$

in component form it looks:

$$n_i(t) = U_{ik}(t, t_0) n_k(t_0)$$

From the definition of $\vec{\vec{U}}$ follows that

- $\vec{\vec{U}}(t, t) = \vec{\vec{I}}$, where $\vec{\vec{I}}$ is unit matrix.
- $\vec{\vec{U}}(t, t_0) \cdot \vec{\vec{U}}(t_0, t_1) = \vec{\vec{U}}(t, t_1)$
- $\vec{\vec{U}}^{-1}(t, t_0) = \vec{\vec{U}}(t_0, t)$

And from fact that $\vec{\vec{U}}$ preserves length of $\vec{n}$ follows that $\vec{\vec{U}}$ is orthogonal matrix with

- $\vec{\vec{U}}^T(t, t_0) = \vec{\vec{U}}^{-1}(t, t_0)$

The equation (5.16) for rotation matrix can be written as:

$$\frac{d\vec{\vec{U}}(t, t_0)}{dt} = \vec{\vec{W}}(t) \cdot \vec{\vec{U}}(t, t_0) \ , \tag{5.17}$$

where product of angular velocity $\vec{\omega}\times$ is replaced with skew-symmetric angular velocity tensor $\vec{\vec{W}}$, which in component form looks like:

$$W_{ik} = \varepsilon_{ijk} \omega_j \ ,$$

where ε_{ijk} is totally antisymmetric Levi-Civita symbol.

Integrating both sides of (5.17) gives:

$$\vec{\vec{U}}(t, t_0) = \vec{\vec{I}} + \int_{t_0}^{t} \vec{\vec{W}}(\tau) \cdot \vec{\vec{U}}(\tau, t_0) \, d\tau$$

Putting in last expression into itself gives so called Dyson-Chen [10] series:

$$\vec{\vec{U}}(t,t_0) = \sum_{n=0}^{\infty} \vec{\vec{U}}_n(t,t_0) \ , \tag{5.18}$$

where

$$\vec{\vec{U}}_n(t,t_0) = \int_{t_0}^{t} d\tau_1 \int_{t_0}^{\tau_1} d\tau_2 \cdots \int_{t_0}^{\tau_{n-1}} d\tau_n \vec{\vec{W}}(\tau_1)\cdot\vec{\vec{W}}(\tau_2)\cdots\vec{\vec{W}}(\tau_n)$$

It also can be written using time-ordering operator $\mathcal{T}$ on exponent [10]

$$\vec{\vec{U}}(t,t_0) = \mathcal{T}\exp\left(\int_{t_0}^{t} \vec{\vec{W}}(\tau)\,d\tau\right) \tag{5.19}$$

In order to find relaxation of $\vec{n}$ it is necessary to know mean value of $\vec{\vec{U}}(t,t_0)$ calculated by (5.18) or (5.19). We will use (5.18), which reduces problems with time-ordering.

$$\langle\vec{\vec{U}}(t,t_0)\rangle = \sum_{n=0}^{\infty}\langle\vec{\vec{U}}_n(t,t_0)\rangle \tag{5.20}$$

Since $\vec{\omega}$ is normally distributed with zero mean, all mean values of odd powers (odd moments) of $\vec{\omega}$ is zero, therefore

$$\langle\vec{\vec{U}}_{2k+1}(t,t_0)\rangle = 0 \ \forall k \in \mathbb{N}$$

Whereas for mean values of even powers (even moments) of $\vec{\omega}$ we can write

$$\langle\vec{\vec{U}}_{2k}(t,t_0)\rangle = \vec{\vec{C}}_{i_1\cdots i_n}\int_{t_0}^{t} d\tau_1 \int_{t_0}^{\tau_1} d\tau_2 \cdots \int_{t_0}^{\tau_{n-1}} d\tau_n \langle\omega_{i_1}(\tau_1)\omega_{i_2}(\tau_2)\cdots\omega_{i_n}(\tau_n)\rangle \ , \tag{5.21}$$

where $\vec{\vec{C}}_{i_1\cdots i_n} = \prod_{j=1}^{n}\vec{\vec{\ell}}_{i_j}$ and $\vec{\vec{\ell}}_j$ is matrix with coordinates $\left(\vec{\vec{\ell}}_j\right)_{ik} = \varepsilon_{ijk}$. Since $\vec{\omega}$ is normally distributed, then $\langle\omega_{i_1}(\tau_1)\cdots\omega_{i_n}(\tau_n)\rangle$ can be expressed using Isserlis' theorem [64]:

$$\langle\omega_{i_1}(\tau_1)\cdots\omega_{i_n}(\tau_n)\rangle = \sum\prod\langle\omega_{i_j}(\tau_j)\omega_{i_m}(\tau_m)\rangle \ ,$$

where the notation $\sum\prod$ means summing over all distinct ways of partitioning $\omega_{i_1}(\tau_1)$, $\omega_{i_2}(\tau_2)$, …, $\omega_{i_n}(\tau_n)$ into pairs. This sum consists of $(2k-1)!!$ terms.

As we remember $\langle\omega_{i_j}(\tau_j)\omega_{i_m}(\tau_m)\rangle$ contains $\delta_{i_j i_m}$ and $\vec{\vec{C}}_{i_1\dots i_n}$ contains sum of multiplications of $\delta_{i_j i_m}$, because of identity of Levi-Civita symbol $\varepsilon_{ijl}\varepsilon_{lmk} = \delta_{im}\delta_{jk} - \delta_{ik}\delta_{jm}$. Since all indexes i_k is summed out, then $\langle\vec{\vec{U}}_{2k}(t,t_0)\rangle$ is some function of $t-t_0$ multiplied by identity matrix $\vec{\vec{I}}$, what means that all directions is equivalent and they do not interact with each other.

In order to calculate $\langle\vec{\vec{U}}_{2k}(t,t_0)\rangle$ we will divide $\vec{\omega}$ into two non-cross-correlated noises [69]:

$$\vec{\omega} = \vec{\omega}^V + \vec{\omega}^M$$

where

$$\langle\omega_i^V(t)\omega_j^V(t')\rangle = \delta_{ij}2D(1+q)\delta(t-t')$$

and

$$\langle\omega_i^M(t)\omega_j^M(t')\rangle = -\delta_{ij}\frac{Dq}{\tau_J}\exp\left(-\frac{|t-t'|}{\tau_J}\right)] \ ,$$

where we introduced new dimensionless parameter $q = \frac{\xi_M}{\xi_V}$ as in [73, 72]. Then

$$\langle\vec{\vec{U}}\rangle = \langle\vec{\vec{U}}^V\rangle\cdot\langle\vec{\vec{U}}^M\rangle = \langle\vec{\vec{U}}^M\rangle\cdot\langle\vec{\vec{U}}^V\rangle \ , \tag{5.22}$$

where $\vec{\vec{U}}^{M,V}$ is calculated using accordingly $\vec{\omega}^{M,V}$. Equation(5.22) can be proved using that $\vec{\omega}^M$ influence only $\vec{\vec{U}}^M$ and $\vec{\omega}^V$ influence only $\vec{\vec{U}}^V$. Then on the one hand

$$\left\langle\frac{d\vec{\vec{U}}}{dt}\right\rangle = \langle\vec{\vec{W}}\cdot\vec{\vec{U}}\rangle = \langle\vec{\vec{W}}^M\cdot\vec{\vec{U}}^M\rangle\cdot\langle\vec{\vec{U}}^V\rangle + \langle\vec{\vec{U}}^M\rangle\cdot\langle\vec{\vec{W}}^V\cdot\vec{\vec{U}}^V\rangle$$

on the other hand

$$\left\langle\frac{d\vec{\vec{U}}}{dt}\right\rangle = \left\langle\frac{d\vec{\vec{U}}^M}{dt}\right\rangle\cdot\langle\vec{\vec{U}}^V\rangle + \langle\vec{\vec{U}}^M\rangle\cdot\left\langle\frac{d\vec{\vec{U}}^V}{dt}\right\rangle \ ,$$

what proves the validity of (5.22).

For the $\vec{\vec{U}}^V_{2k}$ the only non-zero integral in (5.21) is the one where all $\delta(\tau_{i_j}-\tau_{i_k})$ has subsequent τ_i. This is possible only if $i_1\dots i_n$ is progressive and then integral is

$$\int_0^t d\tau_1\int_0^{\tau_1}d\tau_2\cdots\int_0^{\tau_{n-1}}d\tau_n\delta(\tau_1-\tau_2)\dots\delta(\tau_{n-1}-\tau_n) = \frac{1}{2^k}\frac{1}{k!}t^k \ ,$$

where first multiplier comes from the delta function, which is non-zero only at the limit of the integral, second multiplier comes from multiple integration of τ_i.

For progressive $i_1 \dots i_n$ the matrix multiplier consists of k equal elements

$$\varepsilon_{ri_1j_1}\varepsilon_{j_1i_2s}\delta_{i_1}i_2 = -2\delta_{rs}$$

therefore matrix multiplier is

$$\vec{\vec{C}}_{i_1\cdots_n}\delta_{i_1i_2}\dots\delta_{i_{n-1}i_n} = (-2)^k\vec{\vec{I}}$$

and we get that

$$\langle\vec{\vec{U}}^V_{2k}(t,0)\rangle = \frac{[-2D(q+1)]^k}{k!}t^k\vec{\vec{I}}$$

Sum of $\langle\vec{\vec{U}}^V_{2k}\rangle$ gives exponent:

$$\langle\vec{\vec{U}}^V(t,0)\rangle = \exp\left(-2D(q+1)t\right)\vec{\vec{I}}$$

We should emphasize that $t > 0$, otherwise we should use $|t|$ instead of t.

The situation becomes more complicated with $\langle\vec{\vec{U}}^M(t,0)\rangle$, because integral (5.21) is non-zero for all combinations of $i_1 \dots i_n$ and these integrals has different multipliers, which comes from $\vec{\vec{C}}_{i_1\dots i_n}$. Therefore this situation is calculated explicitly using Wolfram Mathematica©. The Mathematica© code is available in appendix C.2. Computational time increases more than exponentially therefore only first six terms (not counting zeroth term) are calculated of expansion of $\langle\vec{\vec{U}}^M\rangle$. Further we will leave $\langle\vec{\vec{U}}^M\rangle$ unexpanded but keeping in mind that this is series which numerically can be calculated to certain accuracy.

For further analysis we will need to calculate correlation of particle direction $\vec{n}$. This can easily be done knowing correlation of rotation matrix $\langle\vec{\vec{U}}(t,t_0)\rangle$.

$$\langle n_i(t)n_j(t')\rangle = \langle U_{ik}(t,t')n_k(t')n_j(t')\rangle$$

and $U_{ik}(t,t')$ is independent of starting position $n_k(t')$, therefore

$$\langle n_i(t)n_j(t')\rangle = \langle U_{ik}(t,t')\rangle\langle n_k(t')n_j(t')\rangle \ .$$

Since all directions are equal, uncorrelated and $n_i(t)n_i(t) = 1$, then

$$\langle n_k(t)n_j(t)\rangle = \frac{1}{3}\delta_{kj} \ .$$

This gives that correlation of $\vec{n}$ is

$$\langle n_i(t)n_j(0)\rangle = \frac{1}{3}\langle U_{ij}(t,0)\rangle = \frac{1}{3}\exp\left(-2D(q+1)t\right)\langle U^M_{ij}(t,0)\rangle \qquad (5.23)$$

If we assume that result for $\langle \vec{\vec{U}}(t,0)\rangle$ is in form $\exp(\lambda(t))$, where $\lambda(t)$ is some function of t, and use only first term of the expansion to compare $\exp(\lambda(t))$ with (5.20) we get similar result to 2D case (5.14):

$$\langle \vec{\vec{U}}(t,0)\rangle = \exp\left\{-2Dt - 2D\tau_J \frac{\xi_M}{\xi_V}\left[1-\exp\left(-\frac{t}{\tau_J}\right)\right]\right\}\vec{\vec{I}} \tag{5.24}$$

Comparison of series expansion and approximate result (5.24) with numerical results is shown in fig. 5.1.

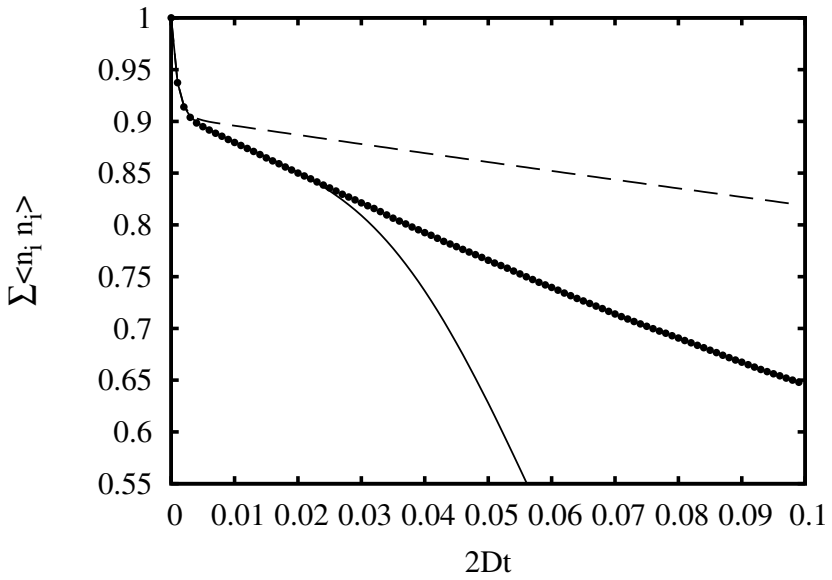

Figure 5.1: Comparison of results obtained by Dyson series with six terms (solid line), approximated result (5.24) (dashed line) and numerical results obtained by algorithm explained in section 5.6 (full circles). $q = 100$, $2D\tau_J = 0.001$ and averaged in numerical experiment over $N = 10^7$ samples.

In figure 5.1 summation is outside averaging sign $\langle\rangle$ to make maximal value equal to 1 and reduce error of numerical calculations. In fig. 5.1 as true relaxation relation we will assume numerical result. As can be seen in fig. 5.1 approximate formula (5.24) gives wrong exponential decay for $t > \tau_J$. The approximate result gives comparable result to numerical calculations only for small values of q. Whereas result (5.23) with Dyson-Chen expansion in fig. 5.1 gives reasonable result, but too few terms in expansion makes it to depart from numerical result for larger times. Only six terms in Dyson-Chen expansion are calculated because calculation time for terms increases more than exponentially.

5.5 Relaxation in external magnetic field

If we put this particle in the static magnetic field with magnetic field strength $\vec{H} = H\vec{h}$ then in the equation (5.1) additional therm $\vec{M}^H$ should be added. We assume that magnetic moment $\vec{m}$ of the particle is in the same direction as particle direction $\vec{n}$ which match hydrodynamic anisotropy axis (for spherical particle all directions are equal). Therefore $\vec{m} = m\vec{n}$ and

$$\vec{M}^H = mH\vec{n} \times \vec{h} \tag{5.25}$$

Then equation of angular velocity is similar to (5.4):

$$\begin{cases} \vec{\omega} = \dfrac{\vec{M}^M}{\xi_V} + \dfrac{\vec{\zeta}^V + mH\vec{n} \times \vec{h}}{\xi_V} \\ \dfrac{d\vec{M}^M}{dt} = -\dfrac{\vec{M}^M}{\tau_J} - \dfrac{\vec{\zeta}^V + mH\vec{n} \times \vec{h}}{\tau_V} + \dfrac{\zeta^M}{\tau_M} \end{cases} \tag{5.26}$$

As can be seen, we can divide angular velocity $\vec{\omega}$ and Maxwell torque $\vec{M}^M$ into random part $\vec{\omega}^R$, $\vec{M}^R$ and deterministic part which depends on particle orientation $\vec{n}$: $\vec{\omega}^D$ and $\vec{M}^D$, where

$$\vec{\omega} = \vec{\omega}^R + \vec{\omega}^D$$

$$\vec{\omega}^D = \frac{\vec{M}^D}{\xi_V} + \frac{mH\vec{n} \times \vec{h}}{\xi_V}$$

$$\frac{d\vec{M}^D}{dt} = -\frac{\vec{M}^D}{\tau_J} - \frac{mH\vec{n} \times \vec{h}}{\tau_V}$$

and properties of the random angular velocity $\vec{\omega}^R$ are the same as in the situation without magnetic field discussed in previous sections 5.3 and 5.4. Solving equation for $\vec{\omega}^D$ gives:

$$\vec{\omega}^D(t) = \int_0^t \left[\frac{2mH}{\xi_V}\delta(t-\tau) - \frac{mHq}{(\xi_M + \xi_V)\tau_J} \exp\left(-\frac{t-\tau}{\tau_J}\right) \right] [\vec{n}(\tau) \times \vec{h}]\, d\tau \tag{5.27}$$

It was assumed that $\vec{\omega}^D(0) = \vec{M}^D(0) = 0$. In the equation (5.27) the first term on the right hand side has been putted under integral sign to make this equation look similar to (5.8).

For the rotation of the vector $\vec{n}$ we have equation:

$$\frac{d\vec{n}}{dt} = \vec{\omega}^R \times \vec{n} + \vec{\omega}^D \times \vec{n}$$

Taking average of both sides gives:

$$\frac{d\langle\vec{n}\rangle}{dt} = \langle\vec{\omega}^R \times \vec{n}\rangle + \langle\vec{\omega}^D \times \vec{n}\rangle\ , \tag{5.28}$$

where first term on the right hand side can be found from equation without magnetic field (5.23). If we assume that for situation without magnetic field we had

$$\langle n_i(t)n_j(0)\rangle = \exp(F(t))\langle n_i(0)n_j(0)\rangle \ ,$$

where $\exp(F(t))$ is relaxation function calculated in (5.23). For some starting state $\langle\vec{n}(0)\rangle$, which is not in equilibrium, particles will relax to equilibrium as

$$\langle\vec{n}(t)\rangle = \exp(F(t))\langle\vec{n}(0)\rangle$$

and without magnetic field $\langle\vec{\omega}^R\times\vec{n}\rangle$ should be equal to $\frac{d\langle\vec{n}\rangle}{dt}$ what gives that:

$$\langle\vec{\omega}^R(t)\times\vec{n}(t)\rangle = \dot{F}(t)\langle\vec{n}(t)\rangle \ , \tag{5.29}$$

where $\dot{F}(t)$ is time derivative of $F(t)$.

Looking at deterministic part separately, we should calculate:

$$\frac{d\vec{n}(t)}{dt} = \int_0^t f^D(t-\tau)[\vec{n}(\tau)\times\vec{h}]\times\vec{n}(t)\,d\tau \ ,$$

where $f^D(t-\tau)$ is function found under integral sign in (5.27). Solution of this equation is

$$\vec{n}(t) = \vec{n}(0) + \int_0^t\int_0^{\tau_1} f^D(\tau_1-\tau_2)[\vec{n}(\tau_2)\times\vec{h}]\times\vec{n}(\tau_1)\,d\tau_1\,d\tau_2$$

Putting this solution into itself we will get different from (5.18) Dyson-Chen series, what makes further analysis complicated.

Mean values in viscoelastic fluid coincide with mean values in viscous fluid. The evolution of mean value $\langle n_\parallel\rangle$ and other in viscoelastic fluid can be found in appendix A.5. Therefore relaxation in the direction of the magnetic field $\vec{h}$ is:

$$\langle n_\parallel(t)\rangle = (\langle n_\parallel(0)\rangle - \langle n_\parallel\rangle)F_\parallel(t) + \langle n_\parallel\rangle \tag{5.30}$$

and relaxation of the component perpendicular to magnetic field direction:

$$\langle n_\perp(t)\rangle = \langle n_\perp(0)\rangle F_\perp(t) \ , \tag{5.31}$$

where $\langle n_\parallel\rangle = L(\nu)$ is average value of the $n_\parallel$ in the equilibrium [7]:

$$L(x) = \coth(x) - \frac{1}{x}$$

called Langevin function and $F_\perp(t)$ and $F_\parallel(t)$ is corresponding relaxation relations.

In viscous fluid $F_i(t) = \exp\left(-\frac{t}{\tau_i}\right)$, where i stands for $\perp$ or $\parallel$ and corresponding τ_i can be calculated using effective field method [59]:

$$2D\tau_{\parallel} = \frac{\nu}{L(\nu)}\frac{dL(\nu)}{d\nu} \qquad 2D\tau_{\perp} = \frac{2L(\nu)}{\nu - L(\nu)} \ . \tag{5.32}$$

But relaxation relation in viscoelastic fluid is more complicated and will be calculated numerically.

5.6 Numerical calculations

For the numerical calculations the equation (5.26) is used, which is written in form:

$$\begin{cases} \vec{\omega} = \dfrac{\vec{M}^M}{\xi_V} + \dfrac{mH}{\xi_V}\vec{n}\times\vec{h} + \dfrac{\vec{\zeta}^V}{\xi_V} \\ \dfrac{d\vec{M}^M}{dt} = -\dfrac{\vec{M}^M}{\tau_M} - \dfrac{\xi_M\vec{\omega}}{\tau_M} + \dfrac{\vec{\zeta}^M}{\tau_M} \\ \dfrac{d\vec{n}}{dt} = \vec{\omega}\times\vec{n} \end{cases} \tag{5.33}$$

Further we will write this equation in dimensionless form using dimensionless variables:

$$\hat{\vec{\omega}} = \frac{\vec{\omega}}{2D} \qquad \hat{\vec{M}}^M = \frac{\vec{M}^M}{2k_BT} \qquad \hat{\vec{\zeta}}^{V,M} = 2k_BT\sqrt{\frac{\xi_{V,M}}{\xi_V+\xi_M}}\zeta^{V,M}$$

and dimensionless parameters

$$q = \frac{\xi_M}{\xi_V} \qquad \hat{\tau}_J = \frac{2D\xi_V\tau_M}{\xi_M+\xi_V} \qquad \nu = \frac{mH}{k_BT} \ ,$$

where $D = \dfrac{\xi_V+\xi_M}{k_BT}$ and dimensionless time is $\hat{t} = Dt$. Dimensionless form of the equation (5.33) then is (hats further in this section will be omitted):

$$\begin{cases} \vec{\omega} = (1+q)\left(\vec{M}^M + \nu\vec{n}\times\vec{h}\right) + \sqrt{1+q}\vec{\zeta}^V \\ \dfrac{d\vec{M}^M}{dt} = -\dfrac{1}{(1+q)\tau_J}\left(\vec{M}^M + \dfrac{q}{1+q}\vec{\omega} - \sqrt{\dfrac{q}{1+q}}\vec{\zeta}^M\right) \\ \dfrac{d\vec{n}}{dt} = \vec{\omega}\times\vec{n} \end{cases} \ , \tag{5.34}$$

where dimensionless noise $\vec{\zeta}^{V,M}$ has zero mean value and correlation is delta function $\langle\zeta_i^V(t)\zeta_k^V(t')\rangle = \langle\zeta_i^M(t)\zeta_k^M(t')\rangle = \delta(t-t')$.

These equations are solved numerically using Euler-Maruyama method [51], where white noise part is replaced by normally distributed random

variable with zero mean and variance equal to time step Δt. The numerical algorithm will look like:

$$\begin{cases} \vec{\omega}(t)\Delta t = (1+q)\left(\vec{M}^M(t) + \nu\vec{n}(t)\times\vec{h}\right)\Delta t + \sqrt{(1+q)\Delta t}\vec{N}(0,1) \\ \vec{M}^M((t+\Delta t) = \vec{M}^M(t) - \dfrac{1}{(1+q)\tau_J}\cdot \\ \qquad\qquad \cdot\left(\vec{M}^M(t)\Delta t + \dfrac{q}{1+q}\vec{\omega}(t)\Delta t + \sqrt{\dfrac{q\Delta t}{1+q}}\vec{N}(0,1)\right) \\ \vec{n}(t+\Delta t) = \vec{n}(t) + [\vec{\omega}(t)\Delta t]\times\vec{n}(t) \end{cases}, \tag{5.35}$$

where $\vec{N}(0,1)$ is vector whose coordinates are independent normally distributed random variables with zero mean and unit variance.

We should take into account that equation (5.35) contains multiplicative noise. According to [55] the equation in the form:

$$\frac{dx_i}{dt} = f_i(\vec{x}) + g_{ij}(\vec{x})\hat{\zeta}_j(t) \tag{5.36}$$

contains multiplicative noise if $g_{ij}(\vec{x})$ depends on $\vec{x}$, where $\zeta_j(t)$ is white noise term and $f_i(\vec{x})$ does not contain noise. In the case of multiplicative noise, additional drift term [55]

$$f_i^1(\vec{x}) = \frac{1}{2}\frac{\partial(g_{il}g_{jl})}{\partial x_j} - \alpha\frac{\partial g_{ij}}{\partial x_l}g_{lj} \tag{5.37}$$

should be added to the equation (5.36), where α depends on the discretization scheme used. If $g_{ij}(\vec{x})$ is calculated at the beginning of the time interval $(t, t+\Delta t)$ then $\alpha = 0$ and it is called Ito convention. Taking $g_{ij}(\vec{x})$ from (5.34) and calculating drift term according to (5.37) gives two drift terms:

$$f_i^{1M}(\vec{n}, \vec{M}^M) = 0 \qquad\qquad f_i^{1n}(\vec{n}, \vec{M}^M) = (1-2\alpha)n_i \tag{5.38}$$

where f_i^{1n} is drift term which should be added to $\vec{n}(t+\Delta t)$ and f_i^{1M} is drift term which should be added to $\vec{M}^M((t+\Delta t)$. Drift term f_i^{1M} is zero because noise in $\frac{d\vec{M}^M}{dt}$ is not multiplicative. The drift term f_i^{1n} will increase the length of the unit vector $\vec{n}$ and can be neglected if the vector $\vec{n}$ is normalized to unit after each time step.

In order to calculate numerically relaxation relations (5.30) and (5.31), first of all we multiply $n_i(t)$ by $n_i(0)$ and after averaging we get that:

$$\langle n_\parallel(t)n_\parallel(0)\rangle = (\langle n_\parallel^2\rangle - \langle n_\parallel\rangle^2)F_\parallel(t) + \langle n_\parallel\rangle^2 \tag{5.39}$$

and

$$\langle n_\perp(t)n_\perp(0)\rangle = \langle n_\perp^2\rangle F_\perp(t)\ . \tag{5.40}$$

We assumed that particles are in equilibrium state at the beginning ($\langle n_i(0)\rangle = \langle n_i\rangle$ and $\langle n_i^2(0)\rangle = \langle n_i^2\rangle$, here i stands for $\parallel$ or $\perp$). Equations (5.39) and (5.40) give us possibility to calculate relaxation functions in equilibrium state, where $\langle n_i\rangle$ and $\langle n_i^2\rangle$ stays constant.

Secondly we use Ergodic hypothesis [66] assuming that average of the process over the statistical ensemble is the same as average over time for long enough observation times. Then average $\langle n_i(t)n_i(0)\rangle$ is calculated as

$$\frac{1}{N}\sum_{j=1}^{N} n_i(t+t_j)n_i(t_j)\ .$$

Averaging part implementation in C++ programming language with GSL package is shown in appendix C.3

5.7 Numerical results

In this section we will check some properties of relaxation in viscoelastic fluid in field which differs from viscous fluid. The analysis will be based on direction $\perp$, but similar results can be obtained in $\parallel$.

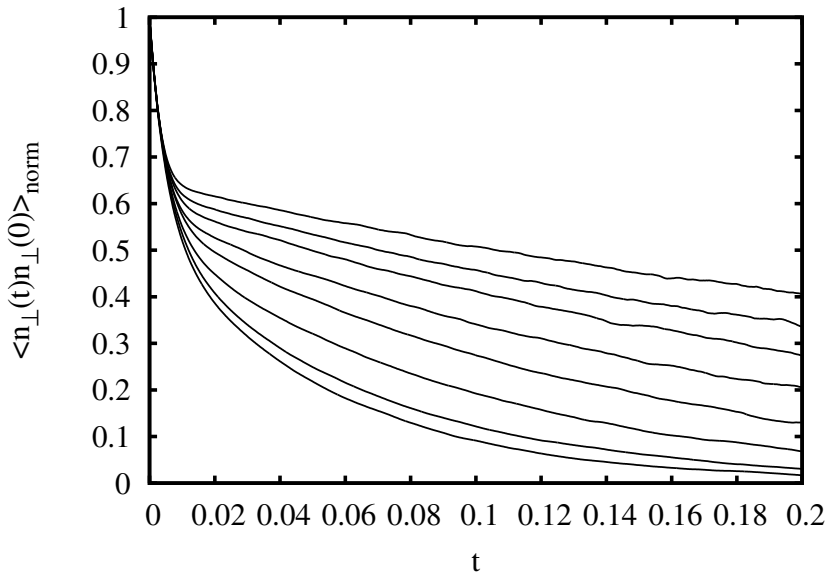

Figure 5.2: Normalized relaxation function $\langle n_\perp(t)n_\perp(0)\rangle_{norm}$ (5.41) for dimensionless magnetic field strength $\xi = 0; 1; 2; 3; 4; 5; 6; 7$. Field strength is increasing in upward direction. Viscoelastic fluid parameters: $q = 100$, $\tau_J = 0.01$. Averaging is made over 10^8 samples for each line.

Numerical computations using implementation of algorithm (5.35) in C++ programming language show that there are two time scales in vis-

coelastic fluid as was predicted. In the short time scale $t \ll \tau_J$ particle behaves as it were in viscous fluid with viscosity η_V. This is because in this limit $\exp\left(-\frac{t}{\tau_J}\right) \to 0$ and relaxation is determined by the delta function relation in $\langle \omega_i(t)\omega_j(0)\rangle$ (5.8). This can be seen in fig. 5.2. In this section dimensionless parameters introduced in previous section are used.

In fig. 5.2 normalized relaxation function is used:

$$\langle n_\perp(t)n_\perp(0)\rangle_{norm} = \exp\left[\ln\left(\frac{\langle n_\perp(t)n_\perp(0)\rangle}{\langle n_\perp^2\rangle}\right)\tau_\perp\right] , \tag{5.41}$$

where $\tau_\perp$ and $\langle n_\perp^2\rangle$ depend on ξ and are calculated according to (5.32) and (A.17). This shows that in short time scale $t \ll \tau_J$ viscoelastic particle dynamics scale similar to viscous fluid, but, as can be seen, for large time scale $t \gg \tau_J$ viscoelastic behaviour is important and scales different from viscous fluid. How $\langle n_\perp(t)n_\perp(0)\rangle$ depends on ξ in the large time scale $t \gg \tau_J$ is left open for further work.

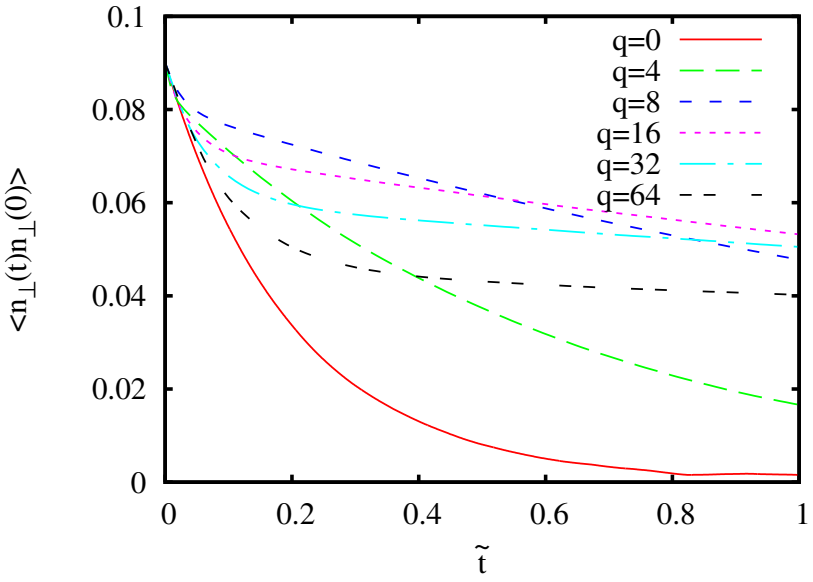

Figure 5.3: Relaxation function $\langle n_\perp(t)n_\perp(0)\rangle$ in for different values of viscoelastic parameter q in magnetic field with dimensionless strength $\xi = 10$. Viscoelastic fluid parameter $\tau_J = 0.003$. Averaging is made over 10^8 samples for each line.

In fig. 5.3 different time scale is used, which is fixed when q changes:

$$\tilde{t} = (1+q)t \ . \tag{5.42}$$

In fig. 5.3 can be seen that increase in viscoelasticity by increasing q sharpens the difference between short time behaviour and long time behaviour. It can

also be seen in fig. 5.3 that increase of q decreases exponential decay at large time scale. It can be seen in fig. 5.3 that if viscoelasticity is not pronounced (small q), the relaxation graph can be approximated by single exponential decay similar to viscous fluid but for large values of q viscoelasticity becomes notable and should be taken into account.

Chapter 6

Results and conclusions

- For the first time it is shown that single-domain particle with uniaxial anisotropy in rotating magnetic field has three possible stable regimes: synchronous planar rotation, synchronous precession and asynchronous planar rotation.
- The stable regimes for defined parameters of the rotating magnetic field are given by the calculated phase diagram.
- It is shown that for defined range of the field strength and frequency irreversible magnetic moment "jumps" occur, which increase the energy dissipation.
- The transformation map which connects prolate and oblate superparamagnetic particle in precessing magnetic field is found.
- There exists jump in mean rotational frequency of the superparamagnetic particle in precessing magnetic field if particle goes from synchronous to asynchronous regime or vice versa. This jump exists in definite range of precession angle
- Superparamagnetic particle in crossed AC and DC magnetic fields can oscillate around AC or DC field in dependence of magnetic field strength.
- Stochastic rotational relaxation of magnetic particle in viscoelastic fluid has two time scales and which of the time scales will be determinative depends on magnetic field strength.

6.1 Thesis

- Magnetic moment jumps is important for dissipated energy of single domain particle in asynchronous rotation.

- Superparamagnetic particle rotation dynamics in magnetic field can be used as a tool for microrheological measurements.
- Viscoelastic properties of the fluid are important in relaxation spectrum in nuclear magnetic resonance.

Bibliography

[1] M. Abramowitz and I. A. Stegun, editors. *Handbook of Mathematical Functions with Formulas, Graphs, and Mathematical Tables*. Dover publications, Inc., New York, 1965.

[2] A. Aharoni. Thermal agitation of single domain particles. *Phys. Rev.*, 135(2A):A447–A449, 1964.

[3] A. Aharoni. Effect of a magnetic field on the superparamagnetic relaxation time. *Phys. Rev.*, 177(2):793–796, 1969.

[4] A. Aharoni. Relaxation time of superparamagnetic particles with cubic anisotropy. *Phys. Rev. B*, 7(3):1103–1107, 1973.

[5] A. Aharoni. Elongated superparamagnetic particles. *J. Appl. Phys.*, 75(10):5891–5893, 1994.

[6] A. Aharoni. Brown's "fundamental theorem" revisited. *J. Appl. Phys.*, 90:4645, 2001.

[7] A. Aharoni. *Introduction to the Ferromagnetism*. International Series of Monographs on Physics. Oxford University Press Inc., Oxford, 2nd edition, 2007.

[8] A. Aharoni and I. Eisenstein. Theoretical relaxation times of large superparamagnetic particles with cubic anisotropy. *Phys. Rev. B*, 11(1):514–519, 1975.

[9] D. B. Allan, D. M. Firester, V. P. Allard, D. H. Reich, K. J. Stebe, and R. L. Leheny. Linear and nonlinear microrheology of lysozyme layers forming at the air–water interface. *Soft Matter*, 10, 2014.

[10] M. Bauer, R. Chetrite, K. Ebrahimi-Fard, and F. Patras. Time-ordering and a generalized magnus expansion. *Lett. Math. Phys.*, 103:331–350, 2013.

[11] D. A. Bazylinski and R. B. Frankel. Magnetosome formation in prokaryotes. *Nat. Rev. Microbiol.*, 2:217–230, 2004.

[12] C. P. Bean and J. D. Livingston. Superparamagnetism. *J. Appl. Phys.*, 30(4), 1959.

[13] E. Blūms, A. Cēbers, and M. M. Maiorovs. *Magnetic Fluids*. Walter de Gruyter, 1997.

[14] A. Brasovs, J. Cīmurs, K. Ērglis, A. Zeltiņš, J.-F. Berret, and A. Cēbers. Magnetic microrods as a tool for microrheology. *Soft Matter*, 11:2563–2569, 2015.

[15] W. F. Brown Jr. Thermal fluctuations of a single-domain particle. *Phys. Rev.*, 130(5):1677–1686, 1963.

[16] W. F. Brown Jr. *Magnetoelastic Interactions*, volume 9 of *Springer Tracts in Natural Philosophy*. Springer-Verlag Berlin Heidelberg GmbH, 1966.

[17] W. F. Brown Jr. The fundamental theorem of the theory of fine ferromagnetic particles. *Ann. N. Y. Acad. Sci.*, 147:463–488, June 1969.

[18] W. F. Brown Jr. Time constants of superparamagnetic particles. *Physica B*, 86-88:1423–1424, 1977.

[19] W. F. Brown Jr. Tutorial paper on dimensions and units. *IEEE Trans. Magn.*, 20(1):112–117, 1984.

[20] R. F. Butler and S. K. Banerjee. Theoretical single-domain grain size range in magnetite and titanomagnetite. *J. Geophys. Res.*, 80(29):4049–4058, 1975.

[21] C. Caroli and P. Pincus. Response of an isolated magnetic grain suspended in a liquid to a rotating field. *Z. Phys. B Con. Mat.*, 9:311–319, 1969.

[22] P. M. Chaikin and T.C. Lubensky. *Principles of Condensed Matter Physics*. Press Syndicate of the University of Cambridge, 1995.

[23] N.-S. Cheng. Formula for the viscosity of a glycerol−water mixture. *Ind. Eng. Chem. Res.*, 47:3285–3288, 2008.

[24] L. Chevry, N. K. Sampathkumar, A. Cēbers, and J.-F. Berret. Magnetic wire-based sensors for the microrheology of complex fluids. *Phys. Rev. E*, 88:062306, 2013.

[25] R. M. Christensen. *Theory of Viscoelasticity*. Academic Press, Inc., 2nd edition, 1982.

[26] J. Cīmurs and A. Cēbers. Dynamics of anisotropic superparamagnetic particles in a precessing magnetic field. *Phys. Rev. E*, 87:062318, June 2013.

[27] W. T. Coffey, P. J. Cregg, D. S. F. Crothers, J. T. Waldron, and A. W. Wickstead. Simple approximate formulae for the magnetic relaxation time of single domain ferromagnetic particles with uniaxial anisotropy. *Journal of Magnetism and Magnetic Materials*, 131(3):L301 – L303, 1994.

[28] W. T. Coffey, Yu. P. Kalmykov, and J. T. Waldron. *The Langevin Equation*. World Scientific Publishing, 2nd edition, 2004.

[29] N. Coq, S. Nago, O. du Rouge, M. Fermigier, and D. Bartolo. Three-dimensional beating of magnetic microrods. *Phys. Rev. E*, 82:041503, 2010.

[30] F. H. C. Crick. The physical properties of cytoplasm: A study by means of the magnetic particle method, part ii. theoretical treatment. *Exp. Cell Res.*, 1:505–533, 1950.

[31] F. H. C. Crick and A. F. W. Hughes. The physical properties of cytoplasm: A study by means of the magnetic particle method, part i. experimental. *Exp. Cell Res.*, 1(1):37–80, 1950.

[32] B. D. Cullity and C. D. Graham. *Introduction to Magnetic Materials*. Wiley-IEEE Press, 2nd edition, December 2008.

[33] K. Ērglis, Qi Wen, V. Ose, A. Zeltiņš, A. Sharipo, P. A. Janmey, and A. Cēbers. Dynamics of magnetotactic bacteria in a rotating magnetic field. *Biophys. J.*, 93(4):1402 – 1412, 2007.

[34] G. Di Fratta, C. Serpico, and M. d'Aquino. A generalization of the fundamental theorem of brown for fine ferromagnetic particles. *Physica B*, 407:1368–1371, 2012.

[35] J. Fresnais, J.-F. Berret, B. Frka-Petesic, O. Sandre, and R. Perzynski. Electrostatic co-assembly of iron oxide nanoparticles and polymers: Towards the generation of highly persistent superparamagnetic nanorod. *Adv. Mater.*, 20:3877–3881, 2008.

[36] J. Frick, L. Yao, T. C. Elston, and M. G. Forest. Time-domain methods for diffusive transport in soft matter. *SIAM J. Appl. Math.*, 69(5):1277–1308, 2009.

[37] B. Frka-Petesic, K. Ērglis, J.-F. Berret, A. Cēbers, V. Dupuis, J. Fresnais, O. Sandre, and R. Perzynski. Dynamics of paramagnetic nanostructured rods under rotating field. *J. Magn. Magn. Mater.*, 323:1309–1313, 2011.

[38] H. C. Fu, C. W. Wolgemuth, and T. R. Powers. Beating patterns of filaments in viscoelastic fluids. *Phys. Rev. E*, 78(4):041913+, October 2008.

[39] T. L. Gilbert. A phenomenological theory of damping in ferromagnetic materials. *IEEE Trans. Magn.*, 40(6):3443–3449, 2004. Originaly publiced in Gilbert, T.L. (1955), "A Lagrangian formulation of the gyromagnetic equation of the magnetic field", Physical Review 100: 1243, which is only an abstract of unpublised work.

[40] J. B. Goodenough. *Magnetism and the Chemical Bond*. John Wiley & Sons, Inc., 1963.

[41] S. R. Gorodkin, B. E. Kashevskii, V. I. Kordonskii, and I. V. Prokhorov. Energy dissipation and heat exchange in magnetorheological suspensions in a rotating magnetic field. *J. Eng. Phys. Thermophys.*, 52:44–48, 1987.

[42] S. R. Gorodkin, B. E. Kashevskii, I. V. Prokhorov, and V. I. Kordonskii. Rotational moment and hysteresis in suspensions of ferromagnetic particles. *Pis'ma Zh. Tekh. Fiz.*, 10(2):94–98, 1984. Russian.

[43] G. F. Goya, E. Lima Jr., A. D. Arelaro, T. Torres, H. R. Rechenberg, L. Rossi, C. Marquina, and M. R. Ibarra. Magnetic hyperthermia with fe3o4 nanoparticles: The influence of particle size on energy absorption. *IEEE Trans. Magn.*, 44(11 Part 2), 2008.

[44] J. D. Jackson. *Classical Electrodynamics*. John Wiley & Sons, Inc., 1962.

[45] I. S. Jacobs and F. E. Luborsky. Magnetic anisotropy and rotational hysteresis in elongated fine-particle magnets. *J. Appl. Phys.*, 28(4):467–473, 1957.

[46] A. Jordan, R. Scholz, P. Wust, H. Fahling, and R. Felix. Magnetic fluid hyperthermia (mfh): Cancer treatment with ac magnetic field induced excitation of biocompatible superparamagnetic nanoparticles. *J. Magn. Magn. Mater.*, 201:413–419, 1999.

[47] B. E. Kashevskii. Torque and rotational hysteresis in a suspension of single-domain ferromagnetic particles. *Magnetohydrodynamics*, 22(2):161–168, 1986.

[48] R. Kikuchi. On the minimum of magnetization reversal time. *J. Appl. Phys.*, 27(11):1352–1357, 1956.

[49] C. Kittel. Fifty years of ferromagnetic single-domain theory. *J. Geophys. Res.*, 103(B12):30533–30533, 1998.

[50] C. Kittel, J. K. Galt, and W. E. Campbell. Crucial experiment demonstrating single domain property of ferromagnetic powders. *Phys. Rev.*, 77:725, March 1950.

[51] P. E. Kloeden and E. Platen. *Numerical Solution of Stochastic Differential Equation*. Springer-Verlag Berlin, 1995.

[52] S. H. Koenig. Brownian motion of an ellipsoid. a correction to perrin's results. *Biopolymers*, 14(11):2421–2423, 1975.

[53] L. D. Landau and E. M. Lifshitz. Theory of the dispersion of magnetic permeability in ferromagnetic bodies. *Phys. Z. Sowietunion*, 8:153–169, 1935.

[54] L. D. Landau, E. M. Lifshitz, and L. P. Pitaevskiĭ. *Electrodynamics of continuous media*. Course of theoretical physics. Butterworth-Heinemann, 1995.

[55] A. W. C. Lau and T. C. Lubensky. State-dependent diffusion: Thermodynamic consistency and its path integral formulation. *Phys. Rev. E*, 76:011123, 2007.

[56] E. W. Lee and J. E. L. Bishop. Magnetic behaviour of single-domain particles. *Proc. Physiol. Soc.*, 89, 1966.

[57] M. Levy. *Nanostructures Magnetiques pour le Diagnostic et la Therapie: Hyperthermie, Relaxation Magnetique et Devenir dans L'organisme*. PhD thesis, Paris Diderot University, 2011.

[58] J. C. Mallinson. On damped gyromagnetic precession. *IEEE Trans. Magn.*, Mag-23(4):2003–2004, 1987.

[59] M. A. Martsenyuk, Y. L. Raikher, and M. I. Shliomis. On the kinetics of magnetization of suspensions of ferromagnetic particles. *J. Exp. Theor. Phys.*, 38:413, February 1974.

[60] G. A. Maugin. A continuum theory of deformable ferrimagnetic bodies. i. field equations & ii. thermodynamics, constitutive theory. *J. Math. Phys.*, 17:1727–1751, 1976.

[61] S. Maus, S. Macmillan, S. McLean, B. Hamilton, A. Thomson, M. Nair, and C. Rollins. The us/uk world magnetic model for 2010-2015. Noaa technical report nesdis/ngdc, NOAA National Geophysical Data Center, 2010.

[62] J. C. Maxwell. *A Treatise on Electricity and Magnetism*, volume 2 of *Clarendon Press Series*. The Clarendon Press, Oxford, 1873.

[63] T. Meidav. Viscolestic properties of the standard linear solid. *Geophysical Prospecting*, 12:80–99, 1964.

[64] J. V. Michalowicz, J. M. Nichols, F. Bucholtz, and C. C. Olson. An isserlis' theorem for mixed gaussian variables: Application to the auto-bispectral density. *J. Stat. Phys.*, 136:89–102, 2009.

[65] N. Mori. Calculation of ferromagnetic anisotropy energies for ni and fe metals. *J. Phys. Soc. Jpn.*, 27:307–312, 1969.

[66] J. V. Neumann. Physical applications of the ergodic hypothesis. *Proc. Natl. Acad. Sci. U. S. A.*, 18(3):263–266, 1932.

[67] L. Néel. Théorie du traînage magnétique des ferromagnétiques en grains fins avec applications aux terres cuites. *Ann. Géophys.*, 5:99–136, 1949.

[68] J. A. Osborn. Demagnetizing factors of the general ellipsoid. *Phys. Rev.*, 67(11):351–357, 1945.

[69] J. K. Patel and C. B. Read. *Handbook of the Normal Distribution.* Marcel Deckker, 1982.

[70] F. Perrin. Mouvement brownien d'un ellipsoide - i. dispersion diélectrique pour des molécules ellipsoidales. *J. Phys. Radium*, 5(10):497–411, 1934.

[71] F. Perrin. Mouvement brownien d'un ellipsoide (ii). rotation libre et dépolarisation des fluorescences. translation et diffusion de molécules ellipsoidales. *J. Phys. Radium*, 7(1):1–11, 1936.

[72] Yu. L. Raikher and V. V. Rusakov. Theory of brownian motion in a jeffreys fluid. *J. Exp. Theor. Phys.*, 111(5):883–889, 2010.

[73] Yu. L. Raikher, V. V. Rusakov, and R.Perzynski. Brownian motion in a viscoelastic medium modelled by the jeffreys fluid. *Soft Matter*, 9:10857–10865, 2013.

[74] V. Rubakov. *Classical Theory of Gauge Fields.* Princeton University Press, 1999.

[75] M. I. Shliomis and V. I. Stepanov. Frequency dependence and long time relaxation of the susceptibility of the magnetic fluids. *J. Magn. Magn. Mater.*, 133:176–181, 1993.

[76] M. I. Shliomis and V. I. Stepanov. Rotational viscosity of magnetic fluids: contribution of the brownian and néel relaxational processes. *J. Magn. Magn. Mater.*, 122:196–199, 1993.

[77] D. V. Sivukhin. The international system of physical units. *Sov. Phys. Usp.*, 22:834–836, 1979.

[78] E. C. Stoner. The demagnetizing factors for ellipoids. *Philos. Mag.*, 36:803–821, 1945.

[79] E. C. Stoner and E. P. Wohlfarth. A mechanism of magnetic hysteresis in heterogeneous alloys. *Phil. Trans. R. Soc. A*, 240(826):599–642, 1948.

[80] S. H. Strogatz. *Nonlinear Dynamics and Chaos.* Perseus Books, 1994.

[81] P. Tierno. Recent advances in anisotropic magnetic colloids: realization, assembly and applications. *Phys. Chem. Chem. Phys.*, 16, 2014.

[82] P. Tierno, J. Claret, F. Sagués, and A. Cēbers. Overdamped dynamics of paramagnetic ellipsoids in a precessing magnetic field. *Phys. Rev. E*, 79:021501, Feb 2009.

[83] J. Vincent. *Structural Biomaterials.* Princeton University Press, third edition, 2012.

[84] T. O. Woods. Standards for medical devices in mri: Present and future. *J. Magn. Reson. Imaging*, 26:1186–1189, 2007.

[85] Jing Yan, Moses Bloom, Sung Chul Bae, Erik Luijten, and Steve Granick. Linking synchronization to self-assembly using magnetic janus colloids. *Nature*, 491, 2012.

Appendix A

Derivations

A.1 Rotation of magnetic rod in Maxwell fluid

Let us look at magnetic dipole with dipole moment $\vec{m}$ in Maxwell fluid (introduced in section 1.6.1), which tries to align with external magnetic field $\vec{H}$. In inertialess limit sum of all mechanical moments should be zero:

$$\vec{M}_{ve} + \vec{M}_H = 0 \ , \tag{A.1}$$

where $\vec{M}_H = \vec{m} \times \vec{H}$ is magnetic torque and $\vec{M}_{ve}$ is viscoelastic torque, which should satisfy (1.35), (1.34)

$$\vec{M}_{ve} + \tau_M \dot{\vec{M}}_{ve} = -\xi \vec{\omega} \ , \tag{A.2}$$

where $\vec{\omega}$ is rotation frequency of particle with its magnetic moment $\dot{\vec{m}} = \vec{\omega} \times \vec{m}$ and ξ is viscous drag (1.24). Expressing $\dot{\vec{M}}_{ve}$ from (A.1) and putting it in (A.2) gives:

$$\xi \vec{\omega} - \tau_M [\vec{\omega} \times \vec{m}] \times \vec{H} = \vec{m} \times \vec{H} \tag{A.3}$$

In component form it can be written as:

$$\left[\delta_{ij} \left(1 + \frac{\tau_M}{\xi} \vec{m} \cdot \vec{H} \right) - \frac{\tau_M}{\xi} m_i H_j \right] \omega_j = \frac{1}{\xi} \varepsilon_{ijk} m_j H_k \ ,$$

where ε_{ijk} gives vector cross product as $(\vec{m} \times \vec{H})_i = \varepsilon_{ijk} m_j H_k$.

Using Neumann series we get that:

$$\left[\delta_{ij} \left(1 + \frac{\tau_M}{\xi} \vec{m} \cdot \vec{H} \right) - \frac{\tau_M}{\xi} m_i H_j \right]^{-1} = \frac{\delta_{ij} + \frac{\tau_M}{\xi} m_i H_j}{1 + \frac{\tau_M}{\xi} \vec{m} \cdot \vec{H}} \ ,$$

what gives equation for rotational velocity components:

$$\omega_i = \frac{\varepsilon_{ijk} m_j H_k}{\xi + \tau_M \vec{m} \cdot \vec{H}}$$

therefore equation of motion of the particle is

$$\frac{d\vec{m}}{dt} = \frac{\vec{H} - (\vec{m}\cdot\vec{H})\vec{m}}{\xi + \tau_M \vec{m}\cdot\vec{H}} \ . \tag{A.4}$$

In all fluids $\vec{m}$ should try to align with external magnetic field $\vec{H}$ or $\vec{m}\cdot\vec{H}$ tries to become maximal. In Maxwell fluid it looks like:

$$\frac{d(\vec{m}\cdot\vec{H})}{dt} = \frac{\vec{H}^2 - (\vec{m}\cdot\vec{H})^2}{\xi + \tau_M(\vec{m}\cdot\vec{H})}$$

and it should be positive for all values of $(\vec{m}\cdot\vec{H})$, but for $\tau_M > \xi$ there exist values $(\vec{m}\cdot\vec{H}) < 0$, where $\frac{d(\vec{m}\cdot\vec{H})}{dt} < 0$, which is non-physical. Therefore it is preferred not to use Maxwell model in computation, but take Jeffery model instead which gives positive $\frac{d(\vec{m}\cdot\vec{H})}{dt}$ for all starting values of $(\vec{m}\cdot\vec{H})$.

A.2 Stability analysis

Stability [80] of regime $\dot{\alpha} = f_\alpha(\alpha,\gamma) = 0$ and $\dot{\gamma} = f_\gamma(\alpha,\gamma) = 0$ depends on the sign of the eigenvalues of Jacobi matrix

$$\begin{pmatrix} \frac{\partial f_\alpha}{\partial \alpha} & \frac{\partial f_\alpha}{\partial \gamma} \\ \frac{\partial f_\gamma}{\partial \alpha} & \frac{\partial f_\gamma}{\partial \gamma} \end{pmatrix}$$

These eigenvalues are:

$$\lambda_{1,2} = \frac{\tau \pm \sqrt{D}}{2} \ , \tag{A.5}$$

where $\tau = \frac{\partial f_\alpha}{\partial \alpha} + \frac{\partial f_\gamma}{\partial \gamma}$ and $D = \tau^2 - 4\Delta$, where $\Delta = \frac{\partial f_\alpha}{\partial \alpha}\frac{\partial f_\gamma}{\partial \gamma} - \frac{\partial f_\alpha}{\partial \gamma}\frac{\partial f_\gamma}{\partial \alpha}$.

A.3 Energy dissipation due magnetic moment movement

At the beginning of the magnetic moment "jump" $\vec{e}$ is not in equilibrium therefore (from (2.23) and (1.19))

$$\frac{d\vec{e}}{dt}\cdot\left(-mH\vec{h} - KV(\vec{e}\cdot\vec{n})\vec{n}\right) = \frac{d\vec{e}}{dt}\cdot\frac{\partial E}{\partial \vec{e}} \neq 0 \tag{A.6}$$

If we assume some finite drag coefficient for magnetic moment $\xi_{mag} \neq 0$ then magnetic moment movement is described by equation $\vec{J}_{\vec{e}}E = -\xi_{mag}\vec{\omega}_{\vec{e}}$. It is assumed that particle movement is much slower than magnetic moment

movement so particle can be considered stationary. $\vec{\omega}_{\vec{e}}$ is angular velocity of magnetic moment relaxation (same as $\vec{\omega}_R$ in (1.22)). Therefore

$$\vec{\omega}_{\vec{e}} = -\frac{1}{\xi_{mag}}\vec{e} \times \frac{\partial E}{\partial \vec{e}} \quad \text{, where} \quad \frac{d\vec{e}}{dt} = \vec{\omega}_{\vec{e}} \times \vec{e}$$

Putting this in (A.6) we can see that in (A.6) calculated variable is viscous dissipation of magnetic moment:

$$\frac{d\vec{e}}{dt} \cdot \frac{\partial E}{\partial \vec{e}} = \vec{\omega}_{\vec{e}} \cdot \left[\vec{e} \times \frac{\partial E}{\partial \vec{e}}\right] = -\xi_{mag}\vec{\omega}_{\vec{e}}^2 = -\frac{\vec{J}_{\vec{e}}E}{\xi_{mag}} \tag{A.7}$$

In equilibrium $\vec{J}_{\vec{e}}E = 0$ therefore dissipation in magnetic moment movement is zero, but before magnetic moment "jump" is disbalance and $\vec{J}_{\vec{e}}E \neq 0$ which gives infinite instantaneous dissipation, because $\xi_{mag} \to 0$. In order to calculate all dissipated energy in magnetic moment "jump" the equation (A.6) or (A.7) should be integrated, which gives:

$$Q_E = \int \frac{d\vec{e}}{dt} \cdot \frac{\partial E}{\partial \vec{e}}\, dt = -\Delta E \ ,$$

where ΔE is energy difference between magnetic moment energy before and after "jump". Here $\Delta E > 0$ therefore minus sign is added because energy before "jump" is higher than after "jump".

A.4 Perturbation of synchronous regime of superparamagnetic particle in precessing field

Giving small perturbation $\vec{\varepsilon}$ to (3.1) gives equation for perturbation in the linear form:

$$\frac{d\vec{\varepsilon}}{dt} = \omega_a(\vec{\varepsilon} \cdot \vec{h})(\vec{h} - \vec{n}(\vec{n} \cdot \vec{h})) - \omega_a\vec{\varepsilon}(\vec{n} \cdot \vec{h})^2 - \omega_a\vec{n}(\vec{\varepsilon} \cdot \vec{h})(\vec{n} \cdot \vec{h}) \tag{A.8}$$

Expressing $\vec{\varepsilon}$ in the component form gives (3.8):

$$\vec{\varepsilon} = \varepsilon_1[\vec{n} \times \vec{h}] + \varepsilon_2[\vec{e}_H \times \vec{n}]$$

In further computations we should take into account that $[\vec{n} \times \vec{h}]$ and $[\vec{e}_H \times \vec{n}]$ are not unit vectors. Since $\vec{n}$ and $\vec{h}$ rotate with angular frequency $\omega_H\vec{e}_H$, then we can write:

$$\frac{d\vec{\varepsilon}}{dt} = \frac{d\varepsilon_1}{dt}[\vec{n} \times \vec{h}] + \frac{d\varepsilon_2}{dt}[\vec{e}_H \times \vec{n}] + \varepsilon_1\omega_H\left[\vec{e}_H \times [\vec{n} \times \vec{h}]\right] + \varepsilon_2\omega_H\left[\vec{e}_H \times [\vec{e}_H \times \vec{n}]\right] \tag{A.9}$$

Before we can go further, some relations should be computed, which comes from (3.2) and its consequences (3.3), (3.4) un (3.5):

$$(\vec{\varepsilon}\cdot\vec{h}) = \varepsilon_2(\vec{e}_H\cdot[\vec{n}\times\vec{h}]) \overset{(3.4)}{=} \varepsilon_2\frac{\omega_a}{\omega_H}(\vec{n}\cdot\vec{h})(1-(\vec{n}\cdot\vec{h})^2)$$

$$\omega_a(\vec{h}-\vec{n}(\vec{n}\cdot\vec{h})) \overset{(3.2)}{=} \frac{\omega_H}{(\vec{n}\cdot\vec{h})}[\vec{e}_H\times\vec{n}]$$

$$\Big[\vec{e}_H\times[\vec{n}\times\vec{h}]\Big] = \Big(\vec{n}(\vec{e}_H\cdot\vec{h})-\vec{h}(\vec{e}_H\cdot\vec{n})\Big) \overset{(3.3)}{=}$$

$$\overset{(3.3)}{=} \Big(\vec{n}(\vec{e}_H\cdot\vec{n})(\vec{n}\cdot\vec{h})-\vec{h}(\vec{e}_H\cdot\vec{n})\Big) \overset{(3.2)}{=}$$

$$\overset{(3.2)}{=} -\frac{\omega_H}{\omega_a}\frac{(\vec{e}_H\cdot\vec{n})}{\vec{n}\cdot\vec{h}}[\vec{e}_H\times\vec{n}]$$

$$\omega_a\vec{n}(\vec{\varepsilon}\cdot\vec{h})(\vec{n}\cdot\vec{h}) + \varepsilon_2\omega_H\Big[\vec{e}_H\times[\vec{e}_H\times\vec{n}]\Big] \overset{(3.5)}{=}$$

$$\overset{(3.5)}{=} \vec{n}\varepsilon_2\omega_H(1-(\vec{n}\cdot\vec{e}_H)^2)+\varepsilon_2\omega_H(\vec{e}_H(\vec{e}_H\cdot\vec{n})-\vec{n}) =$$

$$= \varepsilon_2\omega_H(\vec{e}_H\cdot\vec{n})(\vec{e}_H-\vec{n}(\vec{e}_H\cdot\vec{n})) =$$

$$= \varepsilon_2\omega_H(\vec{e}_H\cdot\vec{n})\Big[\vec{n}\times[\vec{e}_H\times\vec{n}]\Big] \overset{(3.2)}{=}$$

$$\overset{(3.2)}{=} \varepsilon_2\omega_a(\vec{e}_H\cdot\vec{n})(\vec{n}\cdot\vec{h})[\vec{n}\times\vec{h}]$$

From equations (A.8) and (A.9) using just calculated relations we can separate terms with $[\vec{n}\times\vec{h}]$ and $[\vec{e}_H\times\vec{n}]$. And we get equations for ε_1 and ε_2 time derivatives:

$$\begin{cases} \dfrac{d\varepsilon_1}{dt} = -\omega_a(\vec{n}\cdot\vec{h})^2\varepsilon_1 - \omega_a(\vec{e}_H\cdot\vec{n})(\vec{n}\cdot\vec{h})\varepsilon_2 \\ \dfrac{d\varepsilon_2}{dt} = \dfrac{\omega_H^2}{\omega_a}\dfrac{(\vec{e}_H\cdot\vec{n})}{(\vec{n}\cdot\vec{h})}\varepsilon_1 + \omega_a\left(1-2(\vec{n}\cdot\vec{h})^2\right)\varepsilon_2 \end{cases} \tag{A.10}$$

Further analysis are given in section 3.4.

A.5 Mean values of magnetic moment in external field

In thermal equilibrium the probability of finding particle in state $\vec{n}$ is determined by Boltzmann distribution with probability density:

$$p(\vec{n}) = \frac{1}{Z_{\vec{n}}}\exp\left(-\frac{E(\vec{n})}{k_BT}\right), \tag{A.11}$$

where $Z_{\vec{n}}$ is scaling constant. Unfortunately energy of the particle in viscoelastic fluid depends not only on magnetic moment direction $\vec{n}$ but also

on elastic component of viscoelastic fluid. Energy of the particle in Jeffrey viscoelastic fluid is written as

$$E(\vec{n}, \vec{M}^M) = -mH(\vec{n} \cdot \vec{h}) + \frac{(\vec{M}^M)^2}{k} \ , \tag{A.12}$$

where k is stiffness of the spring in Jeffrey model for rotation. Energy $E(\vec{n}, \vec{M}^M)$ can be divided into two disconnected parts $E(\vec{n}, \vec{M}^M) = E(\vec{n}) + E(\vec{M}^M)$ since $\vec{n}$ value is independent of $\vec{M}^M$ value. Then probability density of the particle is product of probability densities of each variable:

$$p(\vec{n}, \vec{M}^M) = p(\vec{n})p(\vec{M}^M) = \frac{1}{Z_{\vec{n}}} \exp\left(-\frac{E(\vec{n})}{k_B T}\right) \frac{1}{Z_{\vec{M}^M}} \exp\left(-\frac{E(\vec{M}^M)}{k_B T}\right) \ , \tag{A.13}$$

where

$$E(\vec{n}) = -mH(\vec{n} \cdot \vec{h}) \qquad E(\vec{M}^M) = \frac{(\vec{M}^M)^2}{k} \ .$$

Since we are interested only in mean values of $\vec{n}$ and integration of probability density function $p(\vec{M}^M)$ over all possible values $\vec{M}^M$ should give one, then the $\vec{M}^M$ part in (A.13) can be neglected (because integral of it will always give 1) and in Jeffrey fluid we can use equation (A.11) for probability density.

To calculate moments of $\vec{n}$ we use spherical coordinates:

$$\begin{cases} n_x = \sin\phi\cos\beta \\ n_y = \sin\phi\sin\beta \\ n_z = \cos\phi \end{cases}$$

and choose magnetic moment $\vec{h}$ into direction $\vec{e}_H$, therefore $n_z = n_{\parallel}$ and both n_x or n_y can be chosen as $n_{\perp}$. Since length of $\vec{n}$ should not change all possible values of $\vec{n}$ are on the unit sphere and integration is made over surface with surface element in spherical coordinates $dS = \sin\phi\, d\phi\, d\beta$. Probability of finding $\vec{n}$ on the unit sphere is 1, what gives that

$$Z = Z_{\vec{n}} = \int_0^{\pi} \exp(\nu\cos\phi)\sin\phi\, d\phi \int_0^{2\pi} d\beta = \frac{4\pi\sinh\nu}{\nu} \ , \tag{A.14}$$

where $\nu = \frac{mH}{k_B T}$. This give us possibility to calculate some mean values using probability density function (A.11)

$$\begin{aligned} \langle n_z \rangle &= \frac{1}{Z}\int_0^{\pi} \cos\phi \exp(\nu\cos\phi)\sin\phi\, d\phi \int_0^{2\pi} d\beta = \frac{4\pi}{Z}\left(\frac{\cosh\nu}{\nu} - \frac{\sinh\nu}{\nu^2}\right) = \\ &= \tanh\nu - \frac{1}{\nu} = L(\nu) \end{aligned} \ , \tag{A.15}$$

where $L(\nu)$ is Langevin function. Similar can be calculated other mean values

$$\langle n_x \rangle = \langle n_y \rangle = \langle n_\perp \rangle = 0 \tag{A.16}$$

and higher moments

$$\langle n_x^2 \rangle = \langle n_y^2 \rangle = \langle n_\perp^2 \rangle = \frac{L(\nu)}{\nu} \ , \tag{A.17}$$

$$\langle n_z^2 \rangle = \langle n_\parallel^2 \rangle = 1 - 2\frac{L(\nu)}{\nu} \tag{A.18}$$

Appendix B

Materials and methods

B.1 Rods

For microrheological measurements superparamagnetic rods in the length range $10 - 25\,\mu m$ and diameter range $0.5 - 1.5\,\mu m$ were synthesized as described in [35]. The solution of superparamagnetic rods was diluted to sufficiently low concentration to ensure approximately one rod on average per area of sight in the microscope Leica DMI3000 B with an oil immersion objective of 100× magnification. High resolution images were obtained with a MIK-ROTRON MC1363 camera at 25 frames per second. Images were processed using MatLab, obtaining dimension and mean orientation angle of the rod as a function of time.

B.2 Magnetic field

An external magnetic field was applied using a custom made setup featuring five water-cooled coils with a power supply Kepco BOP 20-10M, managed with a controller NI DAQ card.

Appendix C

Codes

C.1 Octave code for finding zero stability line of asynchronous planar regime

```
clear all;
global alpha; % integration parameter
global HHa; % =H/Ha
global omega; % =omega_H/omega_a
global alpha0; % integration limit, where "jump" occur
global theta0; % where magnetic moment should be found

HHa= 0.5; % in [0.5, 1/sqrt(2))

function rez=E(x) % energy/mHa
global alpha;
global HHa;
  rez=-HHa*cos(alpha-x)-1/2*cos(x)*cos(x);
endfunction

function rez=f1(x)
global HHa;
  rez=(cos(x)**2)**(1/3)+(sin(x)**2)**(1/3)-HHa**(-2/3);
endfunction

function rez = I(x)
global omega;
global alpha;
global HHa;
global theta0;
  alpha=x;
  theta=fminbnd(@E,theta0-pi,theta0);
```

```
   f=cos(theta)**2/(cos(alpha)+cos(theta)/HHa);
   rez=f*cos(alpha)/(omega-f*sin(alpha));
endfunction

alpha0=fzero(@f1,[-pi/2,-pi/4])
theta0=atan((-tan(alpha0))**(1/3))

function rez=I0(x)
global omega
global alpha0
omega=x;
   if (x<=0.5)
     rez=-inf;
   else
     rez=quadv("I",alpha0,alpha0+pi);
   endif
endfunction

domega=0.00001; % because omega=0.5 gives -inf
fzero(@I0,[0.5+domega,1])
```

C.2 Mathematica code for calculating Dyson series

```
fmain[x_]:=-d*q/tJ*Exp[-x/tJ]

Kr[i_]:=
 If[i==1,{{0,0,0},{0,0,-1},{0,1,0}},
  If[i==2,{{0,0, 1},{0,0,0},{-1,0,0}},
   If[i==3,{{0,-1,0},{1,0,0},{0,0,0}},0]]]

pairs[l_]:=Module[{i,j,k1,k2,l2,n,m1,m2,m3,res},
  l2=(l-1)!!;
  res=Table[j,{i,l2},{j,l}];
  For[j=1,j<l/2,j++,
   n = 2*j;
   For[i = 1,i<=l-n,i++,
    m1=(l-n-1)!!;
    m3=m1*(l-n+1);
    m2=l2/m3;
    For[k1=1,k1<=m1,k1++,
     For[k2=0,k2<m2,k2++,
```

```
        {res[[i*m1+k1+k2*m3,n]],
          res[[i*m1+k1+k2*m3,n+i]]}={res[[i*m1+k1+k2*m3,
            n+i]],res[[i*m1+k1+k2*m3,n]]};
        ];
      ];
     ];
    ];
  For[i=1,i<=l2,i++,
   For[j=1,j<=l/2,j++,
     If[res[[i,2*j-1]]>res[[i,2*j]],
       {res[[i,2*j-1]],res[[i,2*j]]}={res[[i,2*j]],
         res[[i,2*j-1]]};
       ,{}
       ];
     ];
   ];
  res
  ]
pairs1[l_]:=Module[{i,j,k,l2,res},
  l2 = l*(l-2)/8+1;
  res = Table[j,{i,l2},{j,l}];
  For[i=2,i<l2+1,i++,
   For[j=l/2+1,j<l+1,j++,
    res[[i,j]]=res[[i-1,j]];
    ];
   For[j=l/2,j>0,j--,
    res[[i,j]]=res[[i-1,j]];
    If[res[[i-1,j]]<2*j-1,
     k=l/2+1;
     While[res[[i,k]]!=res[[i-1,j]]+1,
      k++
      ];
     {res[[i,k]],res[[i,j]]}={res[[i,j]],res[[i-1,j]]+1};
     Break[]
     ];
    ];
   ];
  res
  ]

func[set_]:=Module[{l,i,j,k,f,matrix,res,fKr,fKr1,l1,n},
  l=Length[set];
  If[l==0,Return[1],If[OddQ[l],Return[0],
    n=l*(l-2)/8+1;
```

```
        f=ConstantArray[1,n];
        matrix=pairs1[l];
        For[j=1,j<n+1,j++,
65       For[i=0,i<l/2,i++,
           f[[j]]*=
             fmain[set[[matrix[[j,i+1]]]] -
               set[[matrix[[j,i+1+l/2]]]]];
           ];
70       ];
        For[j=1,j<n+1,j++,
         For[i=0,i<l-1,i++,
          f[[j]]=
            FullSimplify[
75           Integrate[f[[j]],{set[[l-i]],0,set[[l-i-1]]}],
             set[[l-i-1]]>0];
          ];
         f[[j]]=
           FullSimplify[
80          Integrate[f[[j]],{set[[1]],0,t}],t>0];
         ];
        matrix=pairs[l];
        res=0;
        For[j=1,j<=(l-1)!!,j++,
85       fKr=IdentityMatrix[3];
         For[i=1,i<=l,i++,
          fKr=fKr.Kr[set[[i]]];
          ];
         For[i=0,i<l/2,i++,
90        fKr*=
            KroneckerDelta[set[[matrix[[j,2*i+1]]]],
              set[[matrix[[j,2*i+2]]]]];
          ];
         For[i=1,i<=l,i++,
95        fKr1=0;
          For[k=1,k<=3,k++,
           fKr1+=fKr/.set[[i]]->k;
           ];
          fKr=fKr1;
100       ];
         n=0;
         For[i=0,i<l/2,i++,
          n+=matrix[[j,2*i+1]];
          ];
105      n=n-l*(l+2)/8+1;
```

```
        res+=f[[n]]*fKr[[1,1]];
        ];
       ];];
   Return[res]
   ]

f1=func[Array[a,2]] // Simplify
f2=func[Array[a,4]] // Simplify
f3=func[Array[a,6]] // Simplify
f4=func[Array[a,8]] // Simplify
f5=func[Array[a,10]] // Simplify
f6=func[Array[a,12]] // Simplify
main=1+f1+f2+f3+f4+f5+f6;

Out[1]=-2 d q (-t+tJ - E^(-(t/tJ)) tJ)

Out[2]=1/2 d^2 E^(-((2 t)/
  tJ)) q^2 (4 E^(t/tJ) (t-3 tJ) tJ+3 tJ^2 +
   E^((2 t)/tJ) (4 t^2-10 t tJ+9 tJ^2))

Out[3]= 1/18 d^3 E^(-((3 t)/
  tJ)) q^3 (9 E^(t/tJ) (t-10 tJ) tJ^2+10 tJ^3 +
   18 E^((2 t)/tJ) tJ (t^2-6 t tJ+15 tJ^2) +
   E^((3 t)/tJ) (24 t^3-108 t^2 tJ+219 t tJ^2-190 tJ^3))

Out[4]=1/432 d^4 E^(-((4 t)/
  tJ)) q^4 (4 E^(t/tJ) (60 t-73 tJ) tJ^3+75 tJ^4 -
   54 E^((2 t)/tJ) tJ^2 (40 t^2+434 t tJ+1219 tJ^2)+
   12 E^((3 t)/tJ)
     tJ (-312 t^3+378 t^2 tJ-5586 t tJ^2+1499 tJ^3)+
   E^((4 t)/
    tJ)(288 t^4-2016 t^3 tJ+7812 t^2 tJ^2-24012 t tJ^3+
      48055 tJ^4))

Out[5]=(1/2160)d^5 E^(-((5 t)/
 tJ)) q^5 (25 E^(t/tJ) (9 t-25 tJ) tJ^4+84 tJ^5-
 10 E^((2 t)/tJ) tJ^3 (900 t^2+7940 t tJ+19287 tJ^2)-
 30 E^((3 t)/tJ)tJ^3 (639 t^2+23361 t tJ+59140 tJ^2)+
 10 E^((4 t)/tJ)
 tJ (2448 t^4+6588 t^3 tJ+131346 t^2 tJ^2+160926 t tJ^3+
      687253 tJ^4)+
 E^((5 t)/
 tJ)(576 t^5-5760 t^4 tJ+41760 t^3 tJ^2-330990 t^2 tJ^3+
      1914185 t tJ^4-4904919 tJ^5))
```

```
150
Out[6]=(1/194400)d^6 E^(-((6 t)/
 tJ)) q^6 (1470 tJ^6+504 E^(t/tJ) tJ^5 (15 t+14 tJ)-
 375 E^((2t)/tJ)tJ^4 (1008 t^2+8142 t tJ+19337 tJ^2)-
100 E^((3t)/tJ)tJ^4 (15660 t^2+261009 t tJ+496682 tJ^2)-
155 450 E^((4t)/tJ)tJ^4 (-14211t^2+374652t tJ+1241102 tJ^2)-
    60 E^((5t)/tJ)
      tJ (27648 t^5+204930 t^4 tJ+3608370 t^3 tJ^2+
       15179670 t^2 tJ^3+74388915 t tJ^4+102436342 tJ^5)+
    E^((6 t)/
160   tJ) (17280 t^6-233280 t^5 tJ+3056400 t^4 tJ^2-
 46737900 t^3 tJ^3+486814950 t^2 tJ^4-2780063430 t tJ^5+
      6761587469 tJ^6))

d1 = 1;
165 tJ1 = 0.001;
q1 = 100;
Plot[{main*Exp[-2*d*(1+q)*t]/.{d->d1,tJ->tJ1,q->q1},
  Exp[-2*d*t-2*d*tJ*q*(1-Exp[-t/tJ])]/.{d->d1,tJ->tJ1,
    q -> q1}}, {t, 0, 0.1}]
```

C.3 C++ code for averaging

```
0  void compute()
   {
   // Some parameters are defined outside this function
   // they are:
   // dt=  Size of the time step
5  // delta=       Interval between neighboring
   // correlation function points
   // nCorr=       Number of points in correlation function
   // nN=  Number of points for averaging

10     int i, j, dn, k1, k2;
       int dt_n=round(delta/dt); // Number of time steps
   // between neighboring correlation function points

       for(i=0; i<nCorr; i++)
15         trange[i]=(double)i*delta;

       // Initialize size of buffer
       int n_buff=max(nCorr,100000);
```

```
    int nx = nN / n_buff; // Number of buffers used
    nN = nx * n_buff; // nN will be a multiple of N_BUF

    // Initialize buffers
    gsl_matrix *buff1;
    gsl_matrix *buff2;
    buff1=gsl_matrix_alloc(3,n_buff);
    buff2=gsl_matrix_alloc(3,n_buff);

    // Correlation function placeholders
    double tmp1_nx, tmp1_ny, tmp1_nz;
    double tmp2_nx, tmp2_ny, tmp2_nz;

    // Initialize correlation function placeholders
    for (i=0; i<nCorr; i++)
    {
        corr_nx[i]=0.;
        corr_ny[i]=0.;
        corr_nz[i]=0.;
    }

    // Wait till n goes to equilibrium state
    for (i=0; i<n_buff; i++)
        new_n();

    // Fill first buffer
    for (i=0; i<n_buff; i++)
    {
        new_n();
        gsl_matrix_set_col (buff1, i, n);
    }

    for (i=0; i<nx; i++)
    {
      // Fill second buffer
      for (j=0; j<n_buff; j++)
      {
          new_n();
          gsl_matrix_set_col (buff2, j, n);
      }
      // Calculate correlation function
      for (j=0; j<nCorr; j++)
      {
        dn = j*dt_n; // Time steps in interval j*delta
```

```
            for (k1=0; k1<n_buff; k1++)
            {
65            k2=k1+dn;
              tmp1_nx=gsl_matrix_get(buff1,0,k1);
              tmp1_ny=gsl_matrix_get(buff1,1,k1);
              tmp1_nz=gsl_matrix_get(buff1,2,k1);
              if (k2/n_buff) // If k2>=n_buff
70            {
                  tmp2_nx=gsl_matrix_get(buff2,0,k2%n_buff);
                  tmp2_ny=gsl_matrix_get(buff2,1,k2%n_buff);
                  tmp2_nz=gsl_matrix_get(buff2,2,k2%n_buff);
              }
75            else  //If k2<n_buff
              {
                  tmp2_nx=gsl_matrix_get(buff1,0,k2);
                  tmp2_ny=gsl_matrix_get(buff1,1,k2);
                  tmp2_nz=gsl_matrix_get(buff1,2,k2);
80            }
              corr_nx[j]+=tmp1_nx*tmp2_nx;
              corr_ny[j]+=tmp1_ny*tmp2_ny;
              corr_nz[j]+=tmp1_nz*tmp2_nz;
            }
85        }
          // Second buffer becomes first
          gsl_matrix_swap(buff1, buff2);
      }
      // Normalization
90    for(i=0; i<nCorr; i++)
      {
          corr_nx[i]/=(double)nN;
          corr_ny[i]/=(double)nN;
          corr_nz[i]/=(double)nN;
95    }

      // Plots calculated results
      plot(trange,corr_nx,corr_ny,corr_nz,nCorr);
  }
```